Design and Demonstration of a DAB Based RadCom System

Prepared by:
Grant Norrie

Prepared for:
Dr. Stephen Paine

MSc in Radar and Electronic Defence

December 18, 2022

Declaration

1. I know that plagiarism is wrong. Plagiarism is to use another's work and pretend that it is one's own.
2. I have used the IEEE convention for citation and referencing. Each contribution to, and quotation in, this report from the work(s) of other people has been attributed, and has been cited and referenced.
3. This report is my own work.
4. I have not allowed, and will not allow, anyone to copy my work with the intention of passing it off as their own work or part thereof.

Signed by candidate

27-March-2022

Grant Norrie

Date

Acknowledgements

'You don't see the world as it is - you see the world as you are'

— *Rabbi Shemuel ben Nachmani*

This dissertation allowed me to investigate concepts that as child I would have never dreamt possible. I feel so grateful and lucky that I was afforded the opportunity to work with such incredible people and on such interesting projects during the course of its completion.

To my supervisor Dr Stephen Paine: Thank you for everything, the time and guidance have been so valuable to the completion of this dissertation and my development as an engineer. I cannot thank you enough.

To my parents: Mom and Dad, only ever wanting the best for me. I will never be able to adequately express how much I appreciate your unwavering support in this endeavour. Thank you for reminding me that when it is time to celebrate, celebrate and when it is time to work, work.

Hayden and Eron: Your ability to drop what you are doing to help complete those field tests which I would inevitably need to repeat. Thank you, your faith that it would eventually work encouraged me to try, try, and try again.

Stuart and Martine: thank you too, it is rare to find people as willing to go above and beyond as you. You truly set a fine example that I can only try emulate.

To those friends in and out of the lab. Your company and support proved invaluable. Aaron, Heinrich, Justin, Josh, Tom and Zac: The time we spent in the lab, the calls figuring out those impossible projects, and the coffees we grabbed are valuable memories.

Abstract

The electromagnetic spectrum is becoming increasingly congested due to the growing demand for telecommunications and remote sensing applications. This poses the risk of spectrum bands being reallocated from radar to these applications with organisations such as telecommunication companies willing to pay billions of dollars to use particular bands. Traditionally, this limitation is overcome by the use of passive radar that leverages off of existing communication based transmitters for radar based applications. This passive radar approach to sharing the spectrum is a commensal approach with communications first and radar second. But these increasingly narrow bands allocated for radar and the complications of commensal systems provide the motivation to merge the traditionally separate communication and radar systems into a single radar first radar-communications or 'RadCom' system. The goal of this system is to use a single hardware platform to transmit a standards based waveform, that can be used for both radar and communication applications simultaneously in a symbiotic nature. The development of the RadCom system was therefore divided into four sub-systems. This includes the development of the signal generation, communications, and radar processing chains while the final sub-system developed was the software-defined-hardware testbed.

Development began with the adjustment of the Digital Audio Broadcasting signal. These DAB signals are described by the DAB mode structure, defining their time and frequency domain characteristics. This structure was generalised to describe the RadCom signal and used by the signal generation chain to facilitate the generation of Orthogonal Frequency Division Multiplexed signals. The same generation chain provided the ability to simultaneously encode bitstreams onto OFDM signals. The communication processing chain was developed to demodulate and decode the RadCom signal, thereby extracting the encoded bitstream. The radar processing chain was designed to implement clutter map removal, pulse cancellation and channel alignment procedures to complete range Doppler map processing. Finally, the testbed was developed using two Ettus USRP N210 SDR devices with SBX daughterboards as well as two 2.4 GHz antennas. This ensured that the system was able to simultaneously transmit and receive signals. Each subsystem was individually verified for correct operation prior to the completion of field tests. These verification procedures included bit error rate calculations, FERS simulations and controlled loopback tests.

Field tests were conducted once these validation tests were completed. This involved the completion of a communications test, a static range test and moving target tests. Tests contained validation mechanisms such as reference bitstreams, GPS measurements and equivalent FERS simulations. These provided measurements to judge system performance against. Results included a bit error rate of 0 % for a close range direct link communications test, an expected 100 m static range measurement and GPS verified range doppler measurements. These results demonstrated the correct operation of the system and therefore completed the design and demonstration of the RadCom system.

Contents

List of Figures

Abbreviations

8-DPSK Differential 8-Phase Shift Keying

AF Ambiguity Function

BER Bit Error Rate

bps Bit Per Second

DAB Digital Audio Broadcasting

DBPSK Differential Bi-Phase Shift Keying

DPSK Differential Phase Shift Keying

DQPSK Differential Quadrature Phase Shift Keying

DVBT Digital Video Broadcasting — Terrestrial

EM Electromagnetic

ETSI European Telecommunications Standards Institute

FDM Frequency Division Multiplexing

FERS Flexible Extensible Radar Simulator

FMCW Frequency-Modulated Continuous-Wave

IOO Illuminators of Opportunity

ISI Intersymbol Interference

LFM Linear Frequency Modulation

MIMO Multiple-input and Multiple-output

NS Null Symbol

OFDM Orthogonal Frequency Division Multiplexing

PRS Phase Reference Symbol

PRT Pulse Repetition Time

QPSK Quadrature Phase-Shift Keying

RadCom Radar Communications

RCS Radar Cross Section

RF Radio Frequency

SDR Software Defined Radio

SNR Singal to Noise Ratio

TDM Time Division Multiplexing

UHF Ultra High Frequency

USRP Universal Software Radio Peripheral

VHF Very High Frequency

List of Symbols

A D-QPSK Phase Matrix

F_{iq} Hardware Sampling Rate

F_s Processing Sampling Rate

K Carriers in an OFDM signal

L Symbols in an OFDM frame

P_t Transmission Power

P Transmission Repeat Count

T_d Frame Delay Time

T_f Frame Time

T_g Guard Interval

T_s Symbol Time

T_u Integration Period

T_{null} Null Period

T Elementary time

W Frequency Weight Matrix

ω_D Doppler Frequency

τ_d Signal Delay

f_D Doppler Frequency

f_c Carrier frequency of a waveform

m Bits mapped to a phase

$s(t)$ Complex I/Q data

Chapter 1

Introduction

> 'For myself I am an optimist – it does not seem to be much use to be anything else'
>
> — *Winston Churchill*

1.1 Background

Radar as a technology found its first major application during World War Two. Both the Allies and Axis developed and deployed systems aimed at detecting approaching adversarial forces using electromagnetic or EM radiation. These systems, at the time large and bulky, may be classified into two categories: active and passive radar systems. Active radars transmit signals, detect echos and use these to determine target parameters. Passive radar takes an alternate approach taking advantage of EM transmissions from non cooperative Illuminators of Opportunity and using them to determine target parameters.

Since World War 2 the price of electronic hardware has fallen while performance has continually improved. This increase in performance and corresponding increase in accessibility has led to the broader use and integration of the EM spectrum and radio frequency or RF hardware into modern electronics. This broader use is not restricted to radar applications but is shared with increasingly prevalent communication applications. This increasing spectrum usage combined with surrounding regulations has led to the EM spectrum becoming increasingly congested.

Therefore over time novel methods for more efficient spectrum usage have been developed with increasingly efficient signal structures an active area of interest. This has led to the increased usage of Orthogonal Frequency Division Multiplexed (OFDM) signals in communications standards. As an example: FM radio transmissions are being increasingly replaced by the OFDM based Digital Audio Broadcasting (DAB) standard. Beyond the use of these increasingly efficient waveforms there is additionally an increasing focus and use of passive radar systems which aim to take advantage of Illuminators of Opportunity (IOO's). Transmitters not intended for radar applications rather transmitting for their own purposes.

An example of such a system is a previously developed passive radar processing chain based on the DAB standard [1]. Such a system has its applications but raises a relevant question. If a passive radar system is able to use a communication IOO's for radar applications, then could a system itself

not use its own communication transmissions for radar applications? Or conversely, could a system not use its own radar transmissions for communication purposes?

This open question creates space for the investigation of the design and demonstration of such dual purpose radar communications or RadCom system. Open questions surrounding such a system include the design of the RadCom signal structure, the implementation of system processing chains and how to complete a basic demonstration of such a system.

1.2 Objectives

The background of this investigation provides the context to set the following investigation objectives:

- Generalise the physical layer description of the DAB standard allowing for its implementation in RadCom applications
- Develop a signal generation chain allowing for the generation of a RadCom signal
- Generalise a DAB based passive radar communications processing chain to allow for generalised RadCom applications
- Develop a DAB based radar processing chain to facilitate generalised RadCom applications
- Complete a demonstration of a DAB based RadCom systems ability to conduct radar and communications operations

1.3 System Requirements

These objectives therefore require the development of a RadCom system which meets the following requirements:

- The RadCom signal should be configurable and allow for variable radar or communications performance
- The RadCom signal structure should provide the ability to encode a bitstream
- The communications chain should demodulate and decode the RadCom signal into the encoded bitstream
- The radar processing chain should allow for the range Doppler processing of received signals
- The hardware tesbed should be configured to facilitate the simultaneous transmission and receival of waveforms and echoes

1.4 Scope & Limitations

The scope of this investigation is limited to the basic demonstration of the RadCom system. Therefore any robust mapping of the testbeds radar and communications performance is out of the scope of this investigation. Furthermore, the radar processing chain is limited to range Doppler processing

techniques with further processing techniques relating to consistent target detection out of the scope of this investigation.

The primary limitation of this investigation is due to the available hardware. System integration tests are therefore limited to the bounds of the hardware performance resulting in the inability to simultaneously demonstrate radar and communications performance. Tests are therefore conducted independently using the same hardware and signals.

1.5 Investigation Outline

The content of this investigation begins with Chapter 2, a literature review beginning with radar concepts relevant to this investigation. This introduces the reader the range equation, range Doppler maps and the ambiguity function. It goes on to introduce and cover the OFDM signal structure, DAB standard but is limited to the physical description of the signals. With radar and communication concepts covered an overview of RadCom system development motivations and topologies are covered.

Chapter 3 completes an overview and description of the RadCom system developed within the scope of this investigation. This includes a review of the signal, communications and radar processing chains. It additionally introduces the RadCom testbed used to complete system demonstrations.

With the functionality of the sub-systems introduced, Chapter 4 covers aspects of signal generation. This is completed through the introduction of the RadCom DAB mode followed by the quantification of its radar and communications performance. This is followed by the introduction of the bit encoding procedure as well as the validation of the signal generation chain procedures.

Chapter 5 covers the communications processing chain. This begins with a review of a previously developed DAB passive radar chain and the alterations made to this chain. These alterations are covered in detail and are followed by the validation of chain functionality.

Chapter 6 covers aspects surrounding radar processing. This includes the generation of ambiguity functions and range Doppler maps. Additional processing techniques are introduced in this chapter. Finally, simulations using FERS are completed in order to validate the processing chain for correct functionality.

With the complete chain developed, Chapter 7 covers the configuration of the hardware used to perform system integration tests. It additionally covers the complications of working with the available hardware and how they may be addressed. With the hardware configured, a set of validation tests to verify hardware functionality were completed.

Chapter 8 completed a review of the system integration tests. This included the review and the discussion of both the communications demonstration and the static range test results. Furthermore, results from moving target tests were also reviewed and discussed.

Chapter 9 is the final chapter of this dissertation. It summarised and reviewed the outcomes of

this investigation in the context of investigation objectives and requirements. Finally, it proposed recommendations for future work to both improve and expand the functionality of the developed RadCom system.

Chapter 2

Literature Review

> 'To defend a country you need an army, but to defend a civilization you need education'
>
> — *Rabbi Lord Jonathan Sacks*

2.1 Radar Overview

The following Sections' purpose is to detail the relevant radar theory such that by its completion the reader is familiar with both the signal design and radar processing aspects of the RadCom system. It will therefore begin with the brief introduction of active and passive radar. The principles of radar measurement, propagation characteristics, matched filtering and range Doppler maps will additionally be introduced. Finally, signal analysis in the form of pulse compressed waveforms, ambiguity functions and signal parameter selection in the context of a RadCom system will also be covered.

2.1.1 Active Radar v.s Passive Radar

Radar as a technology relies on the emission of EM waves from transmitters and reception of echoes at receivers. Beyond the possibility of direct propagation from transmitter to receiver one finds an important property. These emissions invariably reflect off objects in their path of propagation [2]. The detection of these reflections or echoes is the fundamental principle of radar. This, as a result of these echoes, contains range and velocity information regarding the object from which they were reflected. This section therefore aims to outline two broad approaches by which one may implement a radar system.

Active Radar

A radar system that emits these waves *itself* may be termed an active radar system. In this case the illuminator is under direct control of the radar operator giving the operator the ability not only to emit a waveform but to control the parameters of such an emission as well. In a basic mono-static configuration using matched filtering, range Doppler processing and constant false alarm rate detectors target information such as range and velocity may be derived and displayed. This will be covered in depth in the coming sections.

Passive Radar

Passive (bistatic) radar as defined by the IEEE is 'A set of techniques using broadcast, communications, radar, or radio-navigation signals as illumination sources rather than using a dedicated radar transmitter. Other terms that have been used include passive coherent location (PCL), passive and covert radar (PCR), covert radar, non-cooperative radar, broadcast radar, parasitic radar, and opportunistic radar' [3].

This takes a notably different approach to active radar. As the definition suggests, instead of using a transmitter under direct control it makes use of IOO's [4]. These illuminators of opportunity are transmitters independent of the radar systems control already transmitting for their own purposes. This configuration relies on the use of a reference signal, a signal received directly from an IOO and a surveillance signal, an echo received from any other direction. One may then determine the locations of the targets that caused these echoes [4]. This may be completed through a multistage procedure that begins with the cross correlation of the reference and surveillance signals. Using the location of the IOO and the receiver, one forms an ellipsoid of possible target locations. Extending this to multiple receivers results in the intersections of multiple ellipsoids thereby localising targets' positions with greater certainty [4]. This system configuration benefits from its silent operation but with inherent costs [4]. These surround aspects of uncontrolled signal design and its effect on parameter determination and measurement ambiguities. Aspects of signal design will be covered in the coming sections.

2.1.2 Radar Measurement Derivation

Both passive and active radar performance is largely defined by the signals they use. To begin to understand this functionality it is useful to understand the generic radar signal and gradually increase its complexity. This is completed by first defining two signal characteristics as done by [5]. These are the base band signal (the complex I/Q data) and the carrier frequency. These will be denoted as $s(t)$ and f_c by this investigation. One may therefore express the complex envelope of the transmitted signal, $s_c(t)$, as follows:

$$s_c(t) = s(t)\, exp(j2\pi f_c t) \tag{2.1}$$

Suppose this signal is transmitted and reflected off a *stationary* target at range R. At some delay time τ_d this reflection will arrive at the receiver. This scenario, shown in the Figure 2.1, visually demonstrates the time it takes for the wave to travel both to the target and *back* to the receiver [5]. Assuming the receiver is at the same location as the transmitter, a total distance of $2R$ is covered. Combining this distance with the total delay and the speed of light, one may relate the delay to range as follows $\tau_d = \frac{2R}{c}$. Rearranging this formula one arrives at the relationship between the delay, τ_d, and range as shown in Equation 2.2.

$$R = \frac{\tau_d\, c}{2} \tag{2.2}$$

Extending this scenario one may additionally derive a mathematical description of the target's *radial*

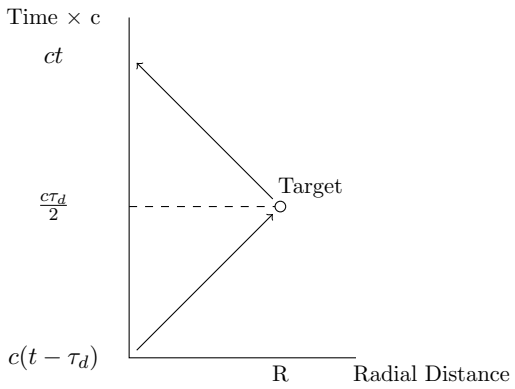

Figure 2.1: Showing the geometry used to derive the relationship for radar range and Doppler measurements

velocity. This is the proportion of the targets velocity that is either directly toward or away from the receiver. Fundamental to this derivation is the *phase relationship* between the transmitted and received waves. Or more precisely the difference between their rates of change of phase or their *angular frequencies* [5]. Importantly, phase may be described as the proportion distance to wave length ($\phi = \frac{L}{\lambda}$). Therefore the task that arises is to map the rate of change of phase to the rate of change in position. Simply put, the question is as follows: 'How does one map the derivative of the differential phase to velocity?' This may be completed by first denoting the velocity of the target as v followed by expressing the angular frequency as follows $\omega_r = \frac{d}{dt}(\omega_c\, t - \frac{\omega_c\, 2\, R}{c} - \frac{\omega_c\, 2\, v\, t}{c})$ [5]. This expression fully describes the rate of change of phase of the received echo.

Importantly, each term in this expression contributes a finite amount of absolute phase with its derivative describing the echoes angular frequency. Therefore to fully describe the expression one may examine each term independently. The first term $\omega_c\, t$ is the phase contribution of the carrier waveform. This is compared to $\frac{\omega_c\, 2\, R}{c}$ which is the phase contribution due to the distance the waveform travelled to and from the target (and is derived using $\phi = \frac{L}{\lambda}$). Finally, $\frac{\omega_c\, 2\, v\, t}{c}$ is the phase contribution due to the change in position as a result of the target's velocity over the waves interaction time. Assuming that the period of interaction between the waveform and target is short (compared to the target's velocity) allows one to simplify the velocity to a constant from $v(t)$ to v. Using this simplification and computing the derivative with respect to time produces the following expression for the resulting echo angular frequency:

$$\omega_r = \omega_c - \frac{\omega_c\, 2\, v}{c} \tag{2.3}$$

Furthermore, the Doppler frequency is defined as the *difference* between the carrier frequency ω_c and the received frequency ω_r. In doing so one is then able to define the Doppler angular frequency ω_D as follows:

$$\omega_D = \frac{-\,\omega_c\, 2\, v}{c} \tag{2.4}$$

And for completeness this may also be expressed as a frequency using $v = f\,\lambda$ where the result is the following equation:

$$f_D = \frac{-\,f_c\,2\,v}{c} \tag{2.5}$$

2.1.3 Radar Range Equation

The ability to derive target information using echoes is useful but inconsequential if one cannot *detect* the echo itself. Therefore understanding the relationship between the transmitted power and received power is a useful place to begin the discussion around echo detection methodology.

One may therefore begin with the most fundamental of parameters P_t, the transmission power. Assuming an isotropic transmitter, the power density and range R may be modelled as the total transmitted power distributed over the surface of a sphere of radius R. The resulting power density at range R is defined as $P_d = \frac{P_t}{4\pi R^2}$. Removing the isotropic radiator assumption and using an antenna gain, the proportion of power transmitted along the antennas boresight when compared to an isotropic radiator, one may adjust the power density to include this gain factor G_t. Therefore the power density at range R is described as $P_d = \frac{P_t G_t}{4\pi R^2}$ [2].

With the power density described, given a target, one may begin to model the received reflected power. Using a target's RCS (σ), a factor describing how 'electrically big' a given target is, P_r may be calculated. Notably σ has the units m^2 resulting in the unit of the reflected value being *power*. This reflected power may be described using $P_{ref} = \frac{P_t G_t \sigma}{4\pi R^2}$ [2]. As with the transmitted power, the reflected power may be modelled as being distributed across the surface of a second sphere with radius R. This therefore results in a returned power density described by $P_{rd} = \frac{P_t\,G_t\,\sigma}{(4\pi)^2\,R^4}$.

Determining the received power by the receiving antenna for a given power density relies on a similar principle to that of RCS. Instead of determining how electrically big a target is, one should consider how 'big' an antennas catchment area is and therefore how much power is received. This is known as an antennas effective aperture, A_e. The received power may therefore be described using $P_r = \frac{P_t G_t A_e}{(4\pi)^2 R^4}$. A more common representation of this equation uses the following relationship between an antennas effective aperture and gain: $A_e = \frac{G\lambda^2}{4\pi}$. The antenna gain from this equation is used to describe the total received power from a target at a range R as follows [2]:

$$P_r = \frac{P_t G_t G_r \lambda^2 \sigma}{(4\pi)^3 R^4} \tag{2.6}$$

2.1.4 Matched Filtering

Equation 2.6 should provide the reader with a sense of how to complete an estimation of the returned power. This ability to estimate the returned power should demonstrate the challenges of developing a functional radar. This is because the returned power reduces as a function of R^4. Combine this with the reality that returned echoes will be corrupted by noise results in echoes quickly becoming undetectable within the received signal. For clarification, the reflected transmission is termed an echo

while the received signal is defined as the combination of noise and echoes. The question is therefore: 'How does one detect and maximise the difference between echoes and noise in the received signal?'.

Using Equation 2.6 a basic approach may be to alter the physical parameters of a radar system. This would (not exclusively) include changing parameters such as transmission power and antenna gains [2]. More relevant is the signal processing approach to SNR optimisation, maximising the ratio of signal power to noise power in the presence of white noise. The optimisation procedure that completes this task, resulting in the maximisation of the SNR, is termed matched filtering and is defined in Equation 2.7. The derivation of the matched filter is covered in Appendix B [6].

$$y(t) = \int_{-\infty}^{\infty} h(u)s(t-u)du \tag{2.7}$$

This procedure is fundamentally convolutional. Specifically where $s(t)$ is the received waveform and $h(u)$ is a *scaled time reversed complex conjugate* of the transmitted waveform. If one assumes that the received waveform is *exactly* the transmitted waveform then the matched filter may be defined as $ks^*(-t)$ and provides a method to detect an echo amongst noise [2]. This *same* procedure may also be used to determine target range [6].

The procedure for echo detection and range determination may be described using the following scenario: Assume one transmits a signal and begins recording at time t_0 (ignoring hardware practicalities such as dead time or feed-through). Assume an echo has been received prior to the conclusion of recording at time t_1. If a matched filtering procedure is applied to the recorded signal, at some time t_n there *will* be a response above the average noise level. This is the basis for delay determination. The difference between this peak at time t_n and the start t_0 is the delay τ_d in Equation 2.2. This *delay* may therefore be converted to a *range* (from transceiver to target) using Equation 2.2.

A final consideration surrounding matched filtering relates to its practical implementation. The computation of the matched filter response described in Equation 2.7 is convolutional. This implies that the computation time grows exponentially as the length of data grows linearly. This leads to impractical processing times when conducting real world processing. Therefore the idea of frequency domain processing is introduced. This idea takes advantage of the fact that the equivalent procedure to time domain convolution is frequency domain multiplication. This offers significant computational time improvements and may be a more attractive processing technique than standard time domain processing in many applications.

2.1.5 Range Doppler Processing

The previous case only involved the processing of a single emission echo pair resulting in range determination. But processing is not constrained to a single pair when surveying a scene. One may transmit multiple pulses and record over multiple slow time periods. Observe that a slow time period consists of many fast time samples and may therefore contain multiple echoes as a result of a *single* emission being reflected by multiple targets at varying ranges. The information contained within and between the echoes in these slow time slices are used to generate range Doppler plots. These plots as

their name suggests, plot target positions as a function of their range and Doppler shifts (and therefore radial velocity) on a two dimensional plot. A generic algorithm to generate such a plot is shown by Algorithm 1:

inputs : A set of N slow time intervals, p ; The matched filter, h
output : Range Doppler map matrix, RD

begin
  while $(n < N)$ **do**
    $rd(n,:) = p(n,:) \odot h$
  end
  $RD = fft(rd, 1)$
end

Algorithm 1: Showing generic methodology to generate a range Doppler map

Using Algorithm 1 one may begin the synthesis of a range Doppler map with the set of N consecutive slow time intervals. The first procedure is the computation of the matched filter response of each slow time interval. These slow time intervals will yield range information regarding the set of targets within a given scene. This procedure is shown by the first and second plot in Figure 2.2. Matched filter response in this context is a generic procedure, meaning that it may completed in either the time or frequency domain. Each processing technique may provide different advantages when considering factors such as computation speed or further processing requirements (such as ambiguity removal). As already discussed, frequency domain processing techniques generally offer processing time improvements through the use of the FFT.

The use of the generic matched filter is noteworthy in the context of passive radar as it has useful implications. This is that as long as one knows the transmitted signal, one may still complete range Doppler processing without transmitting the signal oneself. This is the reason a passive radar system requires the previously discussed reference signal. Assuming that a reference and surveillance signal are coherent, one may form a matched filter using the reference channel. This therefore allows one to complete the generation of the range Doppler map. Not included in Algorithm 1 is how one may account for the range offset introduced by the delayed reception of the reference signal.

The specifics of range Doppler map formation require the use of a matched filter responses which are arrays of complex values. This is important as each slow time response contains phase information. As discussed in Subsection 2.1.2 this is the signal parameter of interest when attempting to discern velocity. This implies that one should be able to extract velocity information if one completes a frequency domain analysis of these phases [5]. Therefore taking an FFT across the slow time dimension will yield this information. This procedure is shown in the conversion from the center to right most image in Figure 2.2.

Given that the output of this procedure results in a 2 dimensional representation of range and velocity, a question that may arise should surround these plot limits. Specifically: ‘What would the

range and velocity limits of such a plot be?'. [5] Derives an answer to this question with its results simply stated. For the most basic pulsed radar configuration as described in Subsection 2.1.2, the minimum discernible and maximum discernible range are defined by $\frac{c\tau}{2}$ and $\frac{c\,PRT}{2}$ for a pulsed monostatic radar [5]. Notably, the minimum range bound falls away when separate transmitter and receiver antennas are used. The maximum Doppler bound, the maximum discernible velocity, is defined by $\frac{c}{4\,f_c\,PRT}$ with a velocity resolution defined by $\frac{c}{2\,f_c\,PRT\,N}$ where N is the number of slow time intervals used to generated the range Doppler plot. Note that PRT, or the pulse repetition time, is identical to the length of a slow time interval and denotes the time between successive pulses.

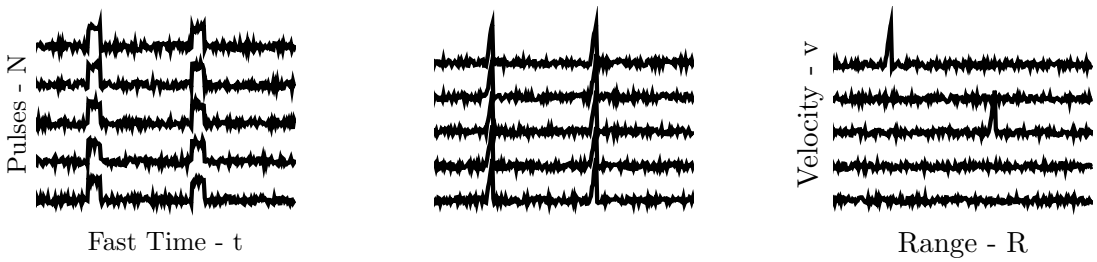

Figure 2.2: Showing a visualisation of the intermediate steps required to generate a range Doppler map involving matched filtering along rows and FFT'ing along columns

Finally, there are nuances when practically generating these plots. They are generated using discrete signals governed by their sampling rates. This implies that each sample corresponds to a discrete distance. This distance is referred to as a range bin and occur in increments of $\frac{c}{F_s}$, where is F_s is processing chain sampling rate. Furthermore, a target can therefore fall directly into a range bin if it is present at the *exact* distance. A target may not fall directly into the range bin, rather being at a range exactly halfway between two range bins. In this case the a target may appear to be partially in both bins at the same time. This effect is not limited to range bins and occurs with Doppler bins as well.

Pulse Cancellation

With the fundamentals of range doppler processing covered it is useful to introduce the reader to additional processing techniques that may be used in conjunction with standard range doppler processing. Pulse cancellation is of particular interest within the scope of this investigation.

This procedure as described by [7] involves the subtraction of slow time slice $N-1$ from slow time slice N. This procedure removes static clutter and targets from a range doppler map. On a qualitative level one may intuitively understand that this works as doppler target returns necessarily have changing phases between consecutive slow time slices.

If one considers the complex element wise subtraction between two slow time slices, static targets with the same returns in each slow time slice will be removed. This is compared to moving targets, whose changing phase results in a non zero as the outcome of the subtraction. This leaves only moving targets within pulse cancelled range doppler map.

2.1.6 Ambiguity Function Processing

Both the matched filter and range Doppler map have been introduced as signal processing techniques. This opens one up to an interesting question which can be phrased as follows: 'What would a matched filter response look like if there is mismatch between the filter and echo?'. This question has has direct implications for the range Doppler plot as its answer describes a response in terms of both delay and Doppler and therefore what a target will look like on the plot itself. This is because by definition *the ambiguity function describes the matched filter response given some Doppler range mismatch between the echo and the matched filter* [2]. The mathematical description of the ambiguity function is shown in Equation 2.8. It is important to clarify a nuance before continuing. The ambiguity function is not a processing tool in itself but rather an analysis tool and may therefore be used in the signal design procedures for radar applications or in the analysis of range Doppler plots.

$$\chi(\tau_d, f_D) = \left| \int x(\alpha)\, exp(j2\pi f_D)\, x^*(\alpha - \tau_d)\, d\alpha \right| \tag{2.8}$$

Equation 2.8 describes how one may characterize this mismatch in delay and Doppler. This is completed with the parameterisation of the Doppler and delay mismatch in terms of τ_d and f_D. To begin the analysis of Equation 2.8 observe the inclusion of $x(\alpha)$, the return of an arbitrary waveform. Next observe the inclusion of $x^*(\alpha - \tau_d)$ its matched filter, dummy integration variable α and the parameterised delay τ_d. These two components in isolation should be familiar as they form a standard matched filter. As such this portion of the ambiguity function describes the delay response of the two waveforms. Finally, after including $exp(j2\pi f_D)$, one has accounted for a Doppler shift which may be applied to the returned signal $x(\alpha)$. Where the Doppler shift is controlled by the parameter f_D. This therefore allows one to model the response of any combination of mismatch in delay and Doppler between a signal and its matched filter.

With the definition of the ambiguity function introduced, one may begin to consider an ideal ambiguity function. This may be done through a review of its meaning. Again, it is the response of a filter given some *mismatch* in either delay or Doppler. *Any* response in the region of mismatch is undesirable as it implies a non zero range and Doppler resolution. Additionally, in some cases additional ambiguity responses may present themselves as *additional* targets with range or Doppler offsets. Therefore an ideal ambiguity function will have no response except for the perfect match, zero Doppler and range. A useful visualisation is a two dimensional Dirac distribution, zero everywhere except at a zero range Doppler offset. As with most ideals, this is not realisable but offers a useful target for waveform design.

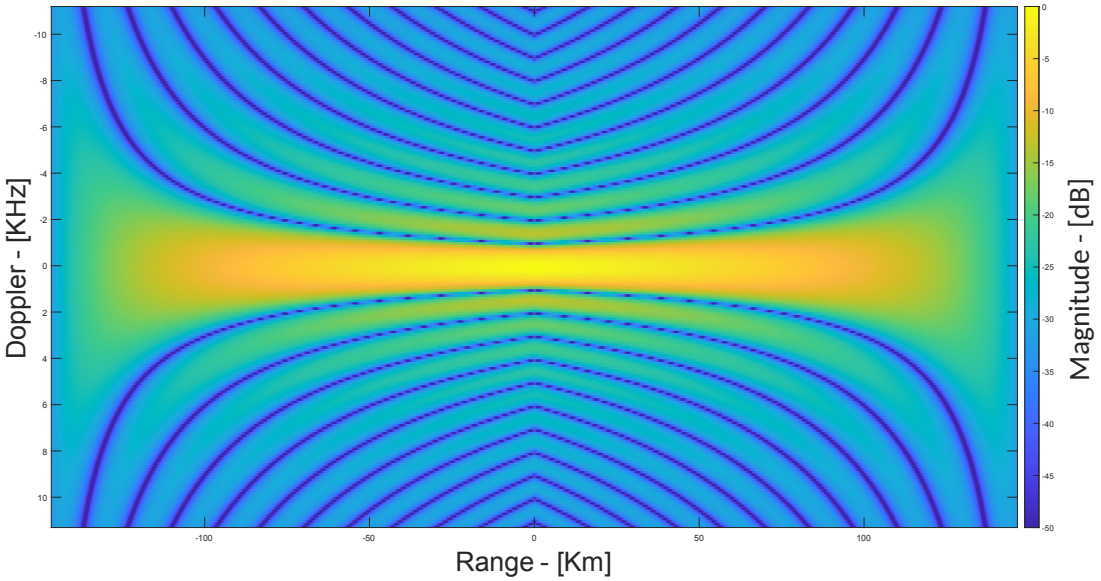

Figure 2.3: Showing the normalised ambiguity function (in decibels) of a simple 1ms *unmodulated* pulse

As an example, consider a 1 ms unmodulated pulse. The ambiguity function of this signal is shown in Figure 2.3. If one considers the response as function of delay and zero Doppler, one should observe the (decibel) matched filter response of a standard pulse. Measuring the -3 dB along the zero Doppler response defines the range resolution of the waveform. The Doppler response has a more abstract mechanism by which it is generated. As a high level overview it can the visualised as the convolution of frequency domain sinc function representation of the pulse. Moving back to the complete ambiguity function and looking at the plot itself, one should observe that the range resolution is on the order of kilometers combined with multiple Doppler responses.

2.1.7 Pulse Compressed Waveforms

Figure 2.3 is an undesirable response primarily due to its poor range resolution and Doppler ambiguities. This presents the question as to how a signal with a more useful ambiguity function may be designed. This question motivated the introduction of the of what are termed simple and complex signals. Note that complex in this case does not refer to the (IQ) signal samples but rather to the time bandwidth product of a signal. This, as its name suggests, is the multiplication of the time it takes for the signal to occur and the occupied signal bandwidth.

Before complex signal are discussed, the simple signal will be reviewed. This is a signal with a time bandwidth product close to one. The range resolution for simple signals such as the unmodulated pulse may be defined as $\Delta R = \frac{c\,\tau_p}{2}$ where τ_p within the context of this subsection is the pulse width [2]. Therefore to increase the range resolution of simple signals requires one to decrease the pulse length. This can be undesirable for many reasons. As an example: To increase range resolution while maintaining the same detection performance one is required to transmit more power in a shorter period. This increase in peak transmission power may be impossible to achieve with available radar equipment. This is another motivation into the investigation of additional methods to increase range resolution.

This resulted in the creation of pulse compressed waveforms which have time bandwidth products greater than one [2]. These complex signals have compressed matched filter mainlobe widths and in special cases allow for side lobe level reduction. This type of signal design is an area of research in itself but of interest is the method for characterising the mainlobe width or range resolution. Particularly interesting is that the range resolution of these signals are no longer defined by their pulse length but rather by their bandwidths where $\Delta R = \frac{c}{2\,BW}$. This therefore provides one with ability to increase range resolution *independent* of pulse time.

2.2 Overview of OFDM Based Signals

OFDM waveforms as complex signals will be reviewed in the context of waveform design for dual purpose radar communications systems. It will therefore begin with the introduction of OFDM signals, what they are and why they are used. Following this multipath effects, the guard interval and phase modulation schemes will be covered. Finally, a brief overview of the ambiguity functions for OFDM waveforms will also be reviewed.

2.2.1 OFDM Basics

The development of the OFDM waveform was primarily motivated by the shortcomings FDM and TDM systems [8]. During the conversion from analog to digital communications systems telecommunication companies faced issues surrounding channel fading, ISI and pulse dispersion [8]. OFDM, as a fine grained FDM technique, was investigated as a possible solution to these effects as it is able to transmit large amounts of data on narrow portions of a channel. This ability to use narrow portions of a channel is fundamental as it allows for the simplification of channel characteristics from a non constant phase amplitude channel response to a constant phase amplitude channel response [8]. OFDM achieves this by taking advantage of the ability to space sub-carriers (in the frequency domain) such that they *overlap but do not interfere*. An example of this characteristic, termed mutual orthogonality, is shown in Figure 2.4.

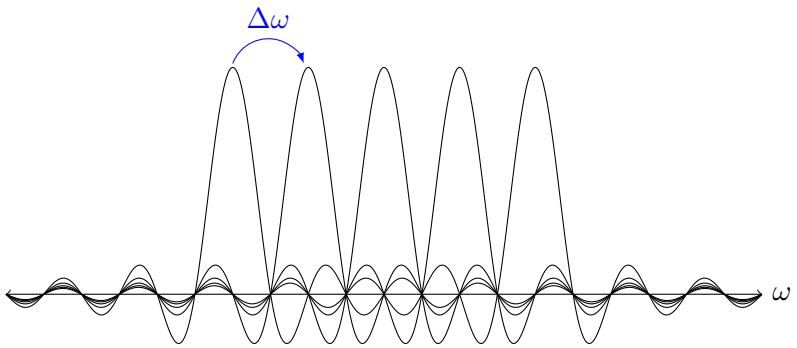

Figure 2.4: Demonstrating the OFDM mutual orthogonality where sinc function overlap but do not interfere

Figure 2.4 indicates how an OFDM signal may be constructed. Firstly, it is important to recognise the presence of multiple *sinc* functions, each representing a sub-carrier or sinusoid of a particular frequency

windowed by a rect function. Each orthogonal carrier, by definition, *must* have its peak on the null of any other sub-carrier to be orthogonal. In order to ensure this frequency spacing relationship the time over which a sub-carrier occurs, the integration period T_u, must be defined as follows:

$$\Delta\omega = \frac{2\pi}{T_u} \tag{2.9}$$

Where $\Delta\omega$ is the frequency spacing between consecutive peaks as shown in Figure 2.4. One may go on to specify a single sub-carrier at an baseband frequency $\Delta\omega k$ an arbitrary integer multiple of $\Delta\omega$ as shown in Figure 2.4. Any individual sub-carrier may also be modulated with a weight w and phase a without changing the frequency spacing. Therefore a complete description of an OFDM sub-carrier may be described as follows:

$$s_{sc}(t) = (w)(a)exp\left(\frac{j2\pi kt}{T_u}\right)rect\left(\frac{t}{T_u}\right) \tag{2.10}$$

Observing that an OFDM signal is comprised of multiple carriers, one may expand the above definition to account for K carriers. Importantly, this investigation defines the number of carriers centered around a baseband DC value. This implies that there are $\frac{K}{2}$ carriers 'above' and 'below' DC. Furthermore the frequency weights w and phase codes a are defined specifically per sub-carrier and are therefore denoted as w_k and a_k. These adjustments are shown below and fully describe the complex envelope of a single OFDM symbol that occurs for T_u units of time.

$$s(t) = \sum_{k=\frac{-K}{2}}^{k=\frac{K}{2}} (w_k)\,(a_k)\,exp\left(\frac{j2\pi kt}{T_u}\right)rect\left(\frac{t}{T_u}\right) \tag{2.11}$$

2.2.2 Multipath Effects

The motivation for the use of OFDM signals was discussed in Section 2.2.1. The signal structure addresses issues surrounding efficient channel usage and the simplification of channel modelling [8]. But this is not the full scope of challenges systems face. There are additional complications to consider when transmitting for communications purposes. When transmitting, one would ideally want only the direct path signal to arrive at the receiver. But, practically the emitted waveform will inevitably reflect off objects in the environment and will also arrive at the receiver. These reflections, travelling different distances to the direct path signal, will arrive at receiver at *different* times and are termed multipath signals.

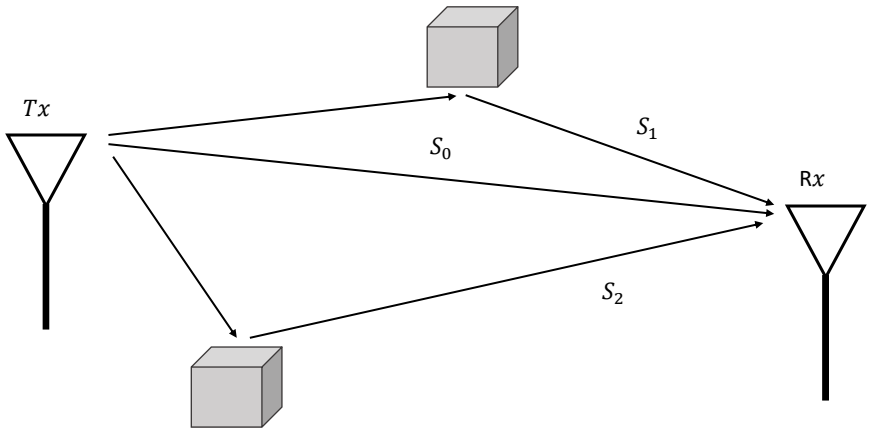

Figure 2.5: Showing the cause of multipath due to arbitrary reflectors in a given EM environment and how these reflections will arrive at the same receiver

The effects of multipath on the received signal can be clearly illustrated using Figure 2.5 and Figure 2.6. Figure 2.5 shows a transmission from the Tx antenna. After transmission this signal will propagate through the environment in the direction defined by the antenna orientation and beam pattern. But as shown in Figure 2.5 this signal may be reflected off of objects (buildings, cars, trees) in the environment. Therefore, at the receiving antenna, multiple *delayed* versions of the same signal will be received. Although Figure 2.5 shows the direct path signal S_0 and two delayed signals S_1 and S_2, for simplicity only a single delayed multipath signal, S_1, will be considered for the remainder of the explanation.

The effects on the received signal are demonstrated in Figure 2.6 with the time offset between the direct and delayed signals S_0 and S_1 shown. Importantly, the received signal is the *summation* of S_0 and S_1. This has a stark effect if one intended to demodulate and decode the received signal. Recall that for an OFDM signal to be demodulated correctly the signal needs to be considered over the course of a single integration period T_u. In the case of the signal shown below $(S_0 + S_1)$, consider an attempt to demodulate the second symbol of S_0 denoted by the green colouring. Notice that the received signal is not strictly green but rather the sum of the direct green signal *and* delayed blue signal. In this case one may not be able to demodulate the green symbol successfully due to the interference of the blue symbol. This inter symbol interference is termed ISI.

The length of T_u therefore defines important signal characteristic relating to the susceptibility to multipath delay [1]. This therefore implies that to increase resilience to multipath one would need to increase the signal length. This is because a fixed delay causes a fixed portion of a preceding symbol to overlap with the current signal. If one therefore increases the length of the symbol, the proportion of the signal that is effected by multipath is reduced. This increase in resilience comes at a cost, namely reduced data rates. Holding all other signal parameters constant allows one to attribute this to the increase in time to physically transmit a signal (and therefore a fixed number of bits).

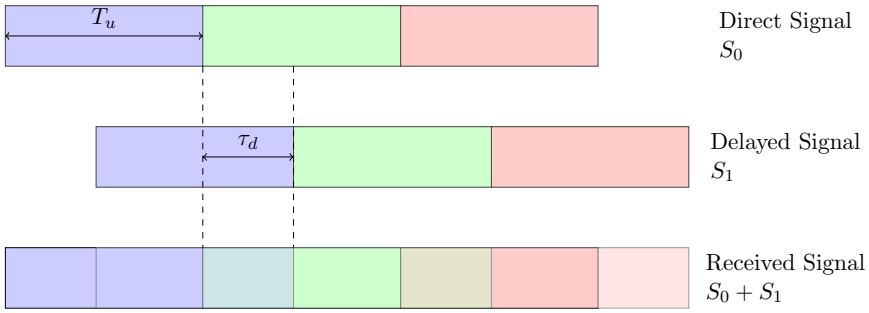

Figure 2.6: Showing the effects of multipath delayed signals on direct path signal in the form of ISI

2.2.3 The Guard Interval

Figure 2.6 raises the question as to how one can prevent ISI *without* increasing the integration period. Visually this would correspond to a reduction in the proportion of two different coloured signals overlapping in Figure 2.6. To complete this one may introduce the guard interval, a prepended portion of the signal itself using cyclic prefixing. This requires that one take the last T_g time units of the signal and place it at the front of the original symbol. The first implication of this procedure is that the symbol time has now changed. The symbol time therefore needs to be redefined as the *sum* of the guard and integration time instead of the integration interval alone.

$$T_s = T_u + T_g \tag{2.12}$$

Although the symbol time has increased, T_u, the time over which the signal is considered *remains the same*. This is important when considering the mechanism by which the guard interval reduces ISI. This is most clearly explained through a comparison of Figure 2.6 and Figure 2.7. As already discussed, without the inclusion on the guard interval one would expect prior integration periods to interfere with current integration periods (blue present in green in Figure 2.6).

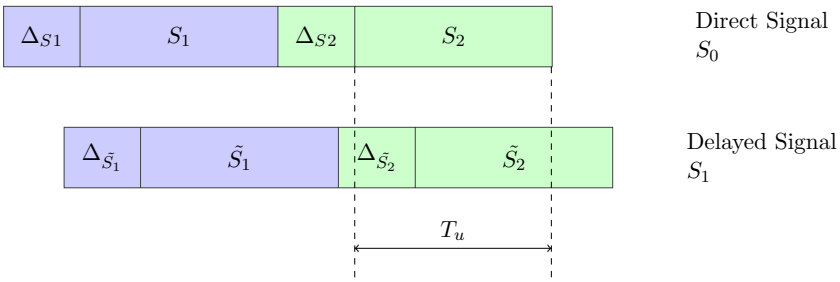

Figure 2.7: Demonstrating the reduction in ISI through the use of the guard interval

The inclusion of the guard interval prevents ISI as where one would originally expect the integration period of the previous symbol, one now finds the cyclic prefix. Stated visually: Where one would expect to originally find a blue green overlap, one now finds *only* green. This therefore implies that when demodulating, other symbols no longer interfere with the demodulation process. The guard interval therefore defines the maximum delay a signal may be subjected to before ISI begins to occur. In order to introduce this guard interval into an arbitrary OFDM signal definition, Equation 2.11 may

be adjusted as follows where T_g is the guard interval time:

$$s(t) = \sum_{k=\frac{-K}{2}}^{k=\frac{K}{2}} (w_k)\,(a_k)\, exp\left(\frac{j2\pi k(t-T_g)}{T_s}\right) rect\left(\frac{t}{T_s}\right) \tag{2.13}$$

The cyclic prefix has an equivalent frequency domain description as to how ISI is prevented. This leverages the fact that the FFT of discrete signals are cyclic. Therefore if one demodulates this signal using the prepended cyclic prefix, the OFDM results will remain the same aside from an additional phase shift in the signal[1].

2.2.4 Waveform Modulation Schemes

With the general structure of the OFDM signal (including the guard interval) introduced through Equation 2.13, the question as to how one may use an OFDM waveform to transmit information arises. There are multiple methods to encode information onto waveforms. These include techniques not specific to OFDM such as amplitude modulation and frequency modulation, where information is encoded in either the amplitude or frequency of a waveform. Techniques used within the scope of this investigation, termed phase shift keying, encode information in the complex phase coefficients a. More complicated modulation techniques (such as quadrature amplitude modulation) may be implemented through the combined use of these phase and frequency weight coefficients a and ω but are not considered within this investigation.

Phase-Shift Keying

With the phase coefficient a_k available for modulation, one may be tempted to use a simple mapping of bits to phase. As an example consider the sub-carrier described in Equation 2.10. Ignoring the rect function, one may describe this equation where the complex phase coefficient is expressed as a phase offset and $\frac{j2\pi k}{T_u}$ is an arbitrary angular frequency $\omega_{\Delta k}$. One may then express this phase offset as a function of time as shown below.

$$s_{sc}(t) = exp(\omega_{\Delta k} t + \phi(t)) \tag{2.14}$$

This is a non-trivial representation as one now has the ability to transmit usable information using $\phi(t)$. This can be done by encoding bits onto fixed phase offsets. Meaning the phase offset $\phi(t)$ is the mechanism by which information may be carried. As an example Figure 2.8 demonstrates what is termed QPSK, where the *absolute phase* of an sub-carrier maps directly onto the predefined set of bits $[\,0:00\,,\,\frac{\pi}{2}:01\,,\,\pi:10\,,\,\frac{3\pi}{4}:11\,]$. The problem of encoding information onto the waveform becomes a question of hardware implementation instead of possibility.

This method may seen attractive on first impressions but faces complications. These primarily surround the fact that the scheme uses absolute phases. This requires the transmitter and receiver to have the exact same time reference [9]. In reality this can be very challenging and makes it an unattractive option for certain use cases.

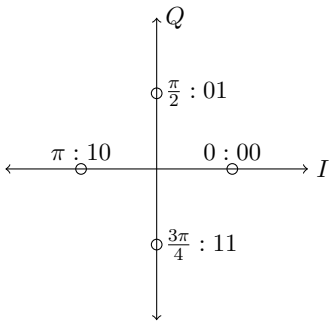

Figure 2.8: Showing the absolute phase mapping to bit sequences

Differential Quadrature Phase-Shift Keying

This motivated the development of a less stringent modulation scheme which implements differential phase shift keying or DPSK. Of particular interest is a subset of DPSK termed differential quadrature phase shift keying or DQPSK. This modulation scheme approaches encoding differently by encoding information in the *difference* between two consecutive sub-carrier phases instead of on the phase of the sub-carrier itself.

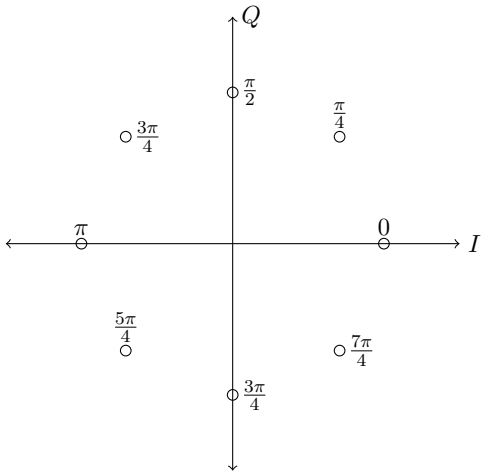

Figure 2.9: Showing the absolute phase values that may be modulated onto a sub-carrier while using DQPSK

DQPSK defines the difference between any two consecutive carriers as one of four possible phase values, namely $[\,\frac{\pi}{4}, \frac{3\pi}{4}, \frac{5\pi}{4}, \frac{7\pi}{4}\,]$. Other DPSK schemes include 8-DPSK and DBPSK but their consideration is out of the scope of this investigation. Finally, DQPSK introduces a nuance when considering the set of possible absolute sub-carrier phases. This is because the fixed difference in consecutive phases results in two alternating sets of absolute phases. These absolute phases are $[0, \frac{\pi}{2}, \pi, \frac{3\pi}{2}]$ and $[\frac{\pi}{4}, \frac{3\pi}{4}, \frac{5\pi}{4}, \frac{7\pi}{4}]$ and are shown in Figure 2.9.

2.2.5 Ambiguity Analysis

The discussion of OFDM signals thus far has surrounded its development and suitability for communications applications. But these waveforms have also demonstrated their suitability for radar applications. This is best demonstrated using an ambiguity function examination as was completed for

an unmodulated pulse in Subsection 2.1.6.

This analysis will be completed in two stages. First an OFDM signal modulated with *random* phase shift keys will be reviewed followed by the analysis of a signal modulated using the DQPSK technique. Recall that the ideal ambiguity function emulates the two dimensional Dirac distribution which therefore serves as the design objective. OFDM waveforms have an attractive AF, generally termed a thumb-tack response, similar to this ideal [10]. This makes it a useful waveform due to its narrower range and Doppler response.

Figure 2.10, demonstrates this and shows the ambiguity function of an OFDM waveform with an integration period of 1 ms, 1500 sub-carriers each separated by 1 kHz and modulated with random phase codes. This OFDM signal is a complex signal with a time bandwidth product of 1500, significantly greater than one. This therefore indicates that its range resolution should be sufficiently narrower when compared to that of a standard *rect* function. This is demonstrated when comparing Figure 2.10 and Figure 2.3. Using the $\frac{c}{2\,BW}$ and $\frac{1}{T}$ the range and Doppler resolution of the waveform may be calculated to be 100 m and 1 kHz.

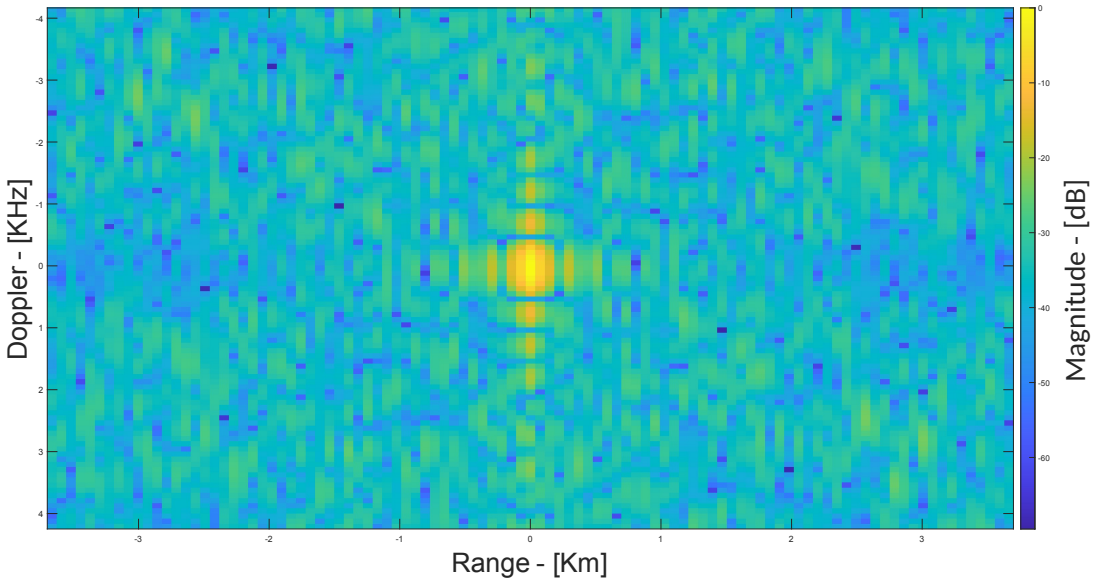

Figure 2.10: Showing the ambiguity function of an OFDM waveform sampled at 2.048 MHz, with 1500 carriers and T_u of 1ms modulated with random phase codes

This response demonstrates the usefulness of OFDM signals but does not correlate with the focus of previous subsections. Of greater importance is an OFDM waveform generated using DQPSK as the phase modulation technique. The fundamental difference is that the set of possible values an individual sub-carrier may be modulated with is *reduced* to the finite set of values shown in Figure 2.9. This results in a signal structure that has less variance and will increase the level of ambiguity responses. This is shown in Figure 2.11, an ambiguity function generated using the same OFDM signal parameters as prior but modulated using DQPSK.

Figure 2.11: Showing the ambiguity function of an OFDM waveform with 1500 carriers and T_u of 1ms modulated with phase codes generated using DQPSK

2.3 The DAB Standard

With the basics of OFDM reviewed, its application in the Digital Audio Broadcasting standard will be investigated. This includes the extension of the signal described by Equation 2.13 to the definition used in the DAB standard. Furthermore, aspects of the standard including symbol allocation and the DAB mode will be covered. Important aspects surrounding the first symbols, the NS and the PRS, will also be reviewed in detail. This review is limited to a physical analysis of the DAB signal with specifics relating to modulation implementations covered in Chapter 5. Furthermore, signaling information, beyond the NS and PRS are out the scope of this investigation as implementation of the DAB standard itself is not within the scope of this investigation.

2.3.1 The Complete Signal

The DAB signal is an OFDM signal that is partially described by Equation 2.13. The shortcoming of Equation 2.13 is that it only defines a single symbol. This is an issue as the DAB standard defines a signal that is comprised of *multiple* symbols and frames (groups of consecutive symbols). This therefore motivates the adjustment of the equation such that it accounts for this. Before this is completed, the symbol structure will be reviewed.

At its most fundamental, the symbol begins with a single sub-carrier. K of these sub-carriers comprise a single symbol and occur in a single symbol time defined as the sum of the guard and integration period. Specific to the DAB standard is that the central-sub carrier is a null carrier, a carrier with zero amplitude. The signal description expands beyond that described in Equation 2.13 through the inclusion of L symbols occurring consecutively in time forming thereby a single DAB frame. For completeness, consecutive frames are included to form the DAB signal. Finally, the carrier waveform is also added with a carrier frequency of f_c. This is described by Equation 2.15. Notably, [1] and the DAB standard denote the guard interval as Δ but this investigation chooses to represent the guard interval as T_g.

$$s(t) = e^{2j\pi f_c t} \sum_{m=-\infty}^{\infty} \sum_{l=0}^{L} \sum_{k=\frac{-K}{2}}^{k=\frac{K}{2}} (\omega_{m,l,k})\,(a_{m,l,k})\, exp(\frac{j2\pi k(t-T_g)}{T_s})\, rect(\frac{t}{T_s}) \tag{2.15}$$

Figure 2.12 is a useful representation of a DAB frame. It denotes each carrier as a single block with each central null carrier denoted by a grey block. Furthermore K carriers are shown by a single row and form a single symbol and finally, multiple rows form L symbols and a single frame.

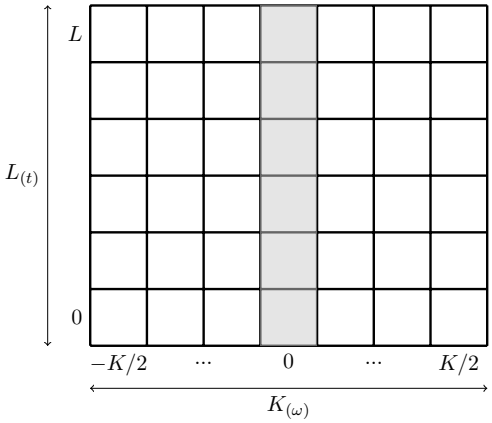

Figure 2.12: Showing a simplified spectrogram of a DAB signal with grey block indicating null central carriers

With the main signal fully defined, one can begin to look at the signaling information in the frame. These are allocated to the first two symbols of the DAB frame and occupy the first and second row if Figure 2.12. These symbols are defined in the DAB standard as members of the synchronisation channel [11]. They function as the mechanism by which receivers may detect and demodulate data within the transmitted frame. The first of these symbols is the NS while the second is the PRS.

2.3.2 Null Symbol

The first DAB symbol, $L = 0$ is defined as the as the Null Symbol. This symbol is defined to be 0 over period $[0, T_{null}]$ [11]. This signal as described by the DAB standard is used for course time synchronisation which gives a receiver an estimate of the starting position of a frame in a data stream [11].

2.3.3 Phase Reference Symbol

The next and final symbol in the synchronisation channel is the Phase Reference Symbol or PRS. This signal is fundamental to the processing of the frame itself as it performs two key functions. Firstly, it is used as the mechanism to perform fine time synchronisation [1]. This is the process of finding the exact starting index of the DAB frame. Secondly, it is the reference by which consecutive symbols in a frame may be demodulated. This symbol is *predefined* by formulae and lookup tables dependent on carrier numbers set out in the DAB standard. This is important as this means the receiver knows what signal it is looking for *a priori* and can therefore detect a frame corrupted by noise.

2.3.4 Data Carrying Symbols

As this investigation is primarily interested in the signal structure and synchronisation channel of the DAB standard, it deems it useful to make the same simplification used in [1]. That all other symbols, although further specified in the DAB standard, will be denoted as data carrying symbols.

2.3.5 DAB Mode

The main signal is described solely in terms of parameters such as the guard interval and integration period. This is intentional as it allowed for what are termed dab modes. These modes allow for the generation of signals following the same signal structure where parameter values change according to varying modes. Initial revisions of the DAB standard contained multiple modes for varying applications but subsequent revisions have resulted in a single remaining mode. It is termed DAB mode I and its parameters are shown in Table 2.1.

Parameter	Name	Value
L	Symbols	76
K	Carriers	15436 T
T_f	Frame time	196 608 T
T_{null}	Null period	2656 T
T_s	Symbol time	2552 T
T_u	Integration Period	2048 T
T_g	Guard interval	504 T
T	Fundamental period	$\frac{1}{2.048e6}$ Hz

Table 2.1: Showing a subset of the DAB mode I structure parameters

2.4 RadCom Systems

With underlying radar and communications principles discussed it is now possible to investigate the motivations for the development of a RadCom system. With the motivations clearly defined, a review of methods and platforms well suited to implementation of RadCom will be completed. Furthermore, methods and research that begin to integrate these traditionally separate systems will be reviewed. Finally, a brief comment on signal ambiguities will be made.

2.4.1 Motivation

The EM spectrum is fixed in size. With the growing demand for telecommunication and remote sensing applications it seems likely that in the future frequency bands traditionally assigned for radar applications may be auctioned off by the International Telecommunication Union for these applications [12]. Therefore the first motivation for investigating the development of a RadCom system is because the future may see increasingly narrow portions of the spectrum allocated solely for radar usage.

The increased demand for for telecommunications is finding application in the domain of smart mobility. Vehicles with multiple telecommunication links appear to be on the horizon [12]. This by implication means that they will by default have RF hardware and digital signal processing capabilities on board. While current autonomous driving research focuses on optical and lidar systems, in time, it is not impossible to imagine that these systems will begin to contend with diminishing returns while attempting to improving safety standards. These two points seem to imply that telecommunications is no longer in competition with radar applications but rather facilitates the integration of radar into

autonomous vehicles. This is because radar becomes an increasingly attractive option for integration into autonomous vehicles as a means to improve autonomous functionality. This therefore provides the motivation for dual purposing this communications hardware to additionally serve as radar hardware. This would allow for the integration of directly measured real world parameters (such as range and relative velocity) into autonomous driving systems providing improved functionality.

Merging radar and communications functionality provides an additional benefit. In the congested environment that are roads, radar transmissions from multiple vehicles may easily interfere and result in the reduced usability of automotive radar systems. This would introduce the motivation for some means of coordination (in time, frequency or both) between vehicles to prevent radar interference. This problem would be solved through the merging of the communications and radar system as communications traditionally manage physical medium access to prevent transmission collisions and the corresponding drop in data rate.

Finally it is worth observing that radars are not made equal. Using different portions of the spectrum one may obtain varying degrees of information about the environment [12]. As an example, operating in the TV VHF and UHF bands allow for radars to penetrate foliage while one may select to use another communication channel with higher bandwidth if one intends to conduct high resolution imaging. Lastly radar imaging in multiple bands provides additional information that may be used in automatic target recognition applications [12]. Therefore developing RadCom systems with dual functionality, allows for the leveraging of these characteristics for sensing applications.

2.4.2 Proposed Implementations

Motivation drives research and development. As such this area of research is still new resulting in multiple system configurations that remain interesting and open to investigation. The first of these configurations is the simplest and requires the use of the same hardware for both communications and radar applications. This specifically requires the hardware to operate either as a communications or radar system at any point in time. Therefore each function is allocated a slot of time to operate while requiring that the operation be completed by the end of its allocated slot. This is termed the time sharing approach [13].

Other approaches are more complex, but come with the advantage of allowing both radar and communications systems to operate at the same time. An example includes the beam sharing topology [13]. This requires the use of phased array antennas where radar and communications functionality are allocated to select portions of the array itself [13]. Where communications and radar functionality still operate independently between each sub-array. Instead of time sharing this is considered to be a space sharing approach.

The time and spacial sharing approaches arguably do not truly achieve full RadCom functionality as there is still resource distribution between radar and communications functionality. As such the final topology discussed is the signal sharing approach [13]. This proposes that instead of dividing hardware functionality in either time or space, one should rather integrate radar and communications functionality into a single waveform [13]. This approach allows for radar and communications to occur

at the same time, same space and the same frequency band.

2.4.3 Signal Design

The joint radar and communication waveform results in additional topology considerations that specifically surround waveform selection. [14] briefly covers research surrounding the investigation of this topic. These methodologies includes phase modulated continuous wave joint RadCom system combined with a direct sequence spread-spectrum technique and interleaved radar and communication signals within a single transmission (effectively creating a time domain multiplexing topology). Additional methodologies include the use of OFDM communication signal preambles while [14] finally goes on to investigate and demonstrate the viability of a FMCW chirp spread spectrum waveforms for RadCom implementation. This should convince the reader that there are multiple methodologies for RadCom implementation yet there is still space in the area of signal design for additional investigation.

2.4.4 Software Defined Radio

Of these signals, this investigation has placed importance on OFDM and it's suitability for both communications and radar applications. It is therefore deemed appropriate to review previous implementations of an OFDM SDR testbed, a hardware platform that has demonstrated its ability to facilitate OFDM applications. The first of which is the experimental set up for an OFDM based radar by [15] where it was demonstrated that the Ettus N210 with the XCVR2450 is a viable SDR platform.

Although a viable platform, challenges were faced surrounding isolation between the transmit and receive ports while using a single device [15]. Isolation between the transmit and receive ports is proportional to the distance separating them which led [15] to take advantage of N210s MIMO capability. This allowed [15] to increase the distance between transmit and receive by transmitting on one USRP and receiving on a second while connecting them via the MIMO cable.

Further challenges with the USRP are faced in other implementations. These primarily surround latency issues [16]. This issue is particular to radar applications as microseconds of unaccounted for delay introduce hundreds of meters error into a range measurement. Specifics surrounding delay complications are discussed in Chapter 6 and 7 but are primarily due to communication delays between the host device and the USRP under control [16].

2.4.5 Ambiguities

Recall that ambiguities are caused by aspects of a signal that *repeat*. This alongside the fact that communication signals *necessarily* require repeating components (to provide receivers with necessary information to detect, demodulate and decode a signal) poses an issue. Repeat in this case is not restricted to signals such as the PRS in the DAB standard but includes smaller time intervals, namely the guard interval. Although considered out of the scope of this report it is deemed worth stating that repeating time and frequency domain parameters will also cause ambiguities in both range and doppler as has been shown in the analysis of the DVBT standard [17].

Chapter 3

System Overview

'It's hard to see things when you're too close. Take a step back and look'

— *Bob Ross*

The following chapter aims to introduce the reader to the sub-systems that comprise the RadCom system. These subsystems are broadly defined as the Signal Generation Chain, Hardware Testbed, Radar Processing Chain and Communications Processing Chain with an overview of their relationships shown in the Figure 3.1. Combined, these systems allow for the design, customization and deployment of a fully functional demonstrator RadCom system. The Signal Generation Chain, as its name suggests, is responsible for the encoding of binary bitstreams onto OFDM waveforms specifically designed for both radar and communication applications. The Hardware Testbed is responsible for the transmission and receival of the waveforms previously generated. These received waveforms are processed by both the Communications Processing Chain resulting in the extraction of the initially encoded bit stream and the Radar Processing Chain resulting in the generation of a range Doppler plot.

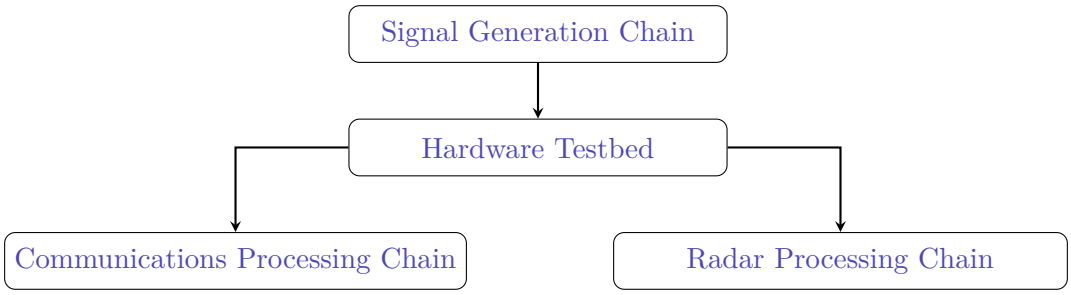

Figure 3.1: Block diagram showing a sub-system overview of the RadCom system

3.1 Signal Generation Overview

The first sub-system developed, the signal generation chain, was designed to generate RadCom waveforms. Using the DAB standards DAB mode structure as a scaffold allows for the generation of a highly configurable OFDM waveform with varying time and frequency domain parameters. This includes variation in integration periods, guard intervals and delays. The DAB mode defined in the DAB standard is extended to fully describe all aspects of the signal, barring the encoded bit stream.

In its complete functionality the chain allows for the conversion of custom bitstreams to phase

codes, which may be modulated onto the waveform (symbols and sub-carriers). These phase codes are modulated onto OFDM sub-carriers generated using time domain processing. This chain additionally allows for these waveforms to be stored as binary files for use in other sub-systems of the RadCom system.

3.2 Communication Processing Overview

Following the development of the signal generation chain was the generalisation of the previously developed DAB passive radar communications processing chain. The chain was specifically altered to allow for the generic post processing of any signal described by the generalised DAB mode structure. The original processing chain discussed in Section 3.2 was used as the basis for its development.

This functionality included the detection and extraction of OFDM signals generated using the signal generation chain. Beyond this extraction, was the demodulation of these waveforms resulting in the extraction of the encoded phases. An additional decoding stage was added onto the developed processing chain to allow for the conversion of phases to bitstreams.

3.3 Radar Processing Overview

With the generation and decoding implemented, the radar processing chain of the signal was investigated. This processing took two forms. These included ambiguity function generation using a frequency domain implementation and range-Doppler processing using a passive radar time domain implementation. These chains allowed for the post processing and analysis of generated signals and evaluation of real world/simulated radar performance of a given signal configuration.

This subsystem also covers topics such as file reading required to use the processing chain. Beyond this function are specifics surrounding the implementation of the radar processing chain. These include channel alignment procedures as well as pulse cancellation and clutter map subtraction techniques.

3.4 Hardware Testbed Overview

Finally, the sub-system connecting the signal generation, communication processing, and radar processing chain in the form of hardware testbed was developed. This involved the configuration of two Ettus N210's each using an SBX daughter board jointly operating as a full duplex transceiver using their MIMO capabilities. The testbed was designed to be configurable, allowing for the variation of signal parameters as well as hardware parameters. Coffee can antennas were used to transmit and receive the signal on two ports while a third port, terminated with a resistor, was sampled to measure the system feed-through.

Chapter 4

Signal Generation Chain

> 'We cannot solve our problems with the same thinking we used when we created them'
>
> — *Albert Einstein*

The RadCom signal is generated in three distinct phases using the DAB mode structure. First, the bit stream which one intends to transmit, is converted to a physical signal parameter, limited to complex phases within the scope of this investigation. This is denoted as Bit Encoding. It is followed by the generation and mapping of the complex phases onto each sub-carrier during Frame Generation. Finally the generated frame is appended with zeroes, denoted as Time insertion, and repeated. This procedure is shown in Figure 4.1 and was followed by writing the signal to a file and validating it to ensure it was generated correctly.

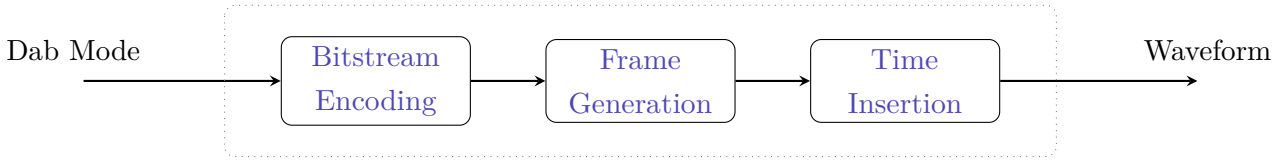

Figure 4.1: Block diagram showing an overview of signal generation process involving Bit Encoding, Frame Generation and Time Insertion

4.1 DAB Mode

The DAB mode structure is the fundamental description of the RadCom signal. Therefore the discussion surrounding the Signal Generation, Communications Processing and Radar Processing chains will begin with the review and alterations of the DAB mode. Chapters 5 and 6 will cover the importance of the structure with respect to each processing chain while its relevance to Signal Generation is discussed within the scope of this Chapter.

The DAB mode structure was altered to describe RadCom signal within the context of the developed processing chains. It does this by first defining all parameters relevant to the original DAB standard signal. Following this is the inclusion of additional parameters which will be discussed. This structure therefore includes the number of carriers K and the number of symbols L, the integration period T_u to name a few. For a a complete list of these parameters see Table 4.1.

4.1.1 The Generic Structure

The changes to the DAB mode structure when compared to its initial description in Section 2.3.5 include the inclusion of sampling rate parameters (F_s, F_{iq}), the carrier frequency (f_c), delay time (T_d) and frame repeat count (P). Additionally, the null time differs from the DAB standard as it has been set to the elementary units as the standard symbol time. This allows the signal generation chain to seamlessly integrate with the communications chain, radar chain and the hardware testbed. This is because signals intended for transmission are automatically resampled between processing and hardware sampling rates while received signals are resampled from hardware to processing chain rates. The additional parameters such as the carrier frequency and delay time are included to determine processing parameters such as PRTs and Doppler resolutions. The complete list of these parameters are shown in Table 4.1.

Parameter	Name	Description
K	OFDM carriers	The number of OFDM carriers in a single symbol
L	OFDM symbols	The number of symbols (including null and PRS) in a single frame
T_{null}	Null period	The length of the null symbol in elementary units
T_u	Integration Period	The length of the integration period in elementary units
T_g	Guard interval	The length of the guard interval in elementary units
T_s	Symbol period	The length of a single symbol in elementary units
T_d	Delay period	The length of a delay period in elementary units
F_{iq}	Hardware sampling rate	The sampling rate used by the physical hardware during TX/RX
F_s	Processing sampling rate	The processing chain sampling rate
T	Elementary time	The inverse of the processing chain sampling rate
f_c	Carrier Frequency	The carrier frequency of the RadCom waveform
P	Repeats	Number of times the frame is repeated

Table 4.1: Showing the expanded DAB mode structure including all parameters relevant to the RadCom system

Beyond integration of the DAB mode structure into the processing chains, the structure practically allows one to define a signal that may be pulsed or continuous in nature allowing one to seamlessly transition between the two modes of operation. This can be done by altering the delay parameter T_d between zero and non zero values. One is also able to directly control signal bandwidths by controlling the number of sub-carriers in a symbol in turn having direct implications for both communication data rates and radar range resolution.

Additional aspects of interest when designing a DAB mode for RadCom applications is that while transmitting, one is limited to transmit at finite power levels, governed either by hardware or national regulations. This has direct implications on signal performance as the power is necessarily divided between all the active sub-carriers. There are therefore design trade-offs that need to be made while selecting signal parameters. As an example: As one increases the bandwidth of a signal individual sub-carriers will be “allocated” less power. This, by extension, has direct implications on communications performance in the presence of poor SNR ratios. Finally it is also a notable design feature that one is

able to select the number of symbols and delay time in a frame and by extension the frame time for a given DAB mode. This has been a high level intuitive analysis on the DAB mode structure with the following subsections will attempting to quantify aspects of communications and radar performance.

4.1.2 Communications Performance Review

The reader should be convinced that the DAB mode structure is a useful abstraction to generalise signal processing. Beyond processing it also provides a useful method to quantify communication data rates. Using the DAB mode one may begin to quantify these rates by first determining the number of bits encoded onto a single carrier. From there one may expand the analysis to the sub-carriers in a single symbol, and finally to the data carrying symbols in a frame.

Therefore to begin, one may recall that the number of bits encoded in a single differential phase is m. Each of these m bits are mapped to the K carriers present in a single symbol. There are additionally L symbols in a given frame. Recall, as per the DAB standard, symbols one and two are not considered 'data carrying' symbols. The number of data carrying bits transmitted in any particular frame can therefore be described as follows:

$$B = mK(L-2) \tag{4.1}$$

Note that B is a number and not a *rate*. Therefore the next step is to generalise the description of the frame time, how long it takes for a frame to occur. Firstly, recall that the symbol time is comprised of the integration and guard interval: $T_s = T_g + T_u$. One should also recall that there are L symbols in a given frame. Notably, only $L-1$ are of length T_s as the first symbol, the NS is of length T_{null}. The final addition to the frame time is the inclusion of the delay time T_d. The frame time can therefore be stated to be:

$$T_f = T_{null} + T_s(L-1) + T_d \tag{4.2}$$

Dividing the number of data carrying bits in a particular frame by the time it takes for a frame to occur will result in the bit rate or bits per second (bps). This misses out on a single important reality. When using the waveform for radar functionality one may repeat transmissions. These P repeats needs to be accounted for in the bit rate. This can be done by dividing the frame bit rate by P. This can be stated as the following:

$$bps = \frac{B}{PT_f} = \frac{mK(L-2)}{P\left(T_{null} + T_s(L-1) + T_d\right)} \tag{4.3}$$

4.1.3 Radar Performance Reivew

With the bit rate of a DAB mode quantified one may also quantify the radar performance of the same mode. Again, using the DAB mode structure one may determine the expected performance characteristics described in Section 2.1. This quantification will be completed using radar parameters

including range resolution, Doppler resolution, as well as maximum range and Doppler bounds (for pulsed operation).

Firstly, recall that range resolution can be calculated using $\Delta R = \frac{c}{2BW}$. Therefore one needs to determine the bandwidth of a signal as controlled by the DAB mode structure. This can be done by multiplying the number of carriers, K, by their frequency separation Δf. Recall that the frequency separation is defined by the inverse of the integration T_u. Therefore the range resolution of a signal defined by the DAB mode can be defined as follows:

$$\Delta R = \frac{c}{2\,K\,T_u} \tag{4.4}$$

Furthermore, the Doppler resolution as stated in Section 2.2.5 is the inverse of the coherent integration time T. This is equivalent to the length of the waveform. Therefore the Doppler resolution can be stated as:

$$\Delta V = \frac{1}{T_f} \tag{4.5}$$

Discussed next are the parameters that effects range Doppler map processing. First of which is the maximum range. This is simply proportional to the PRT which in turn is simply the frame time. Therefore the maximum discernible range is defined as:

$$R_{max} = \frac{T_f\,c}{2} \tag{4.6}$$

Finally the maximum Doppler bound as a function of the DAB mode can be defined as follows:

$$V_{max} = \frac{c}{4\,f_c\,T_f} \tag{4.7}$$

4.2 Bitstream Encoding

Signal generation begins with Bit encoding. This is the process by which a bit stream is converted to a differential phase matrix. This is a matrix with a direct mapping back to the encoded bitstream which may be modulated onto individual RadCom carriers. This process begins with the definition of the bits to phase mapping. It then proceeds with slicing the bitsteam into sub streams corresponding to the number of bits encoded into a single phase. This is followed by the conversion of bits to phases and the reshaping and filling of the phases to symbols. The PRS is then prepended followed by the DQPSK computation. Once this computation is complete, the NS is prepended. This process is shown in Figure 4.2.

Figure 4.2: Showing the bit encoding procedure with the input as a DAB mode and bitstream while the output is a phase matrix

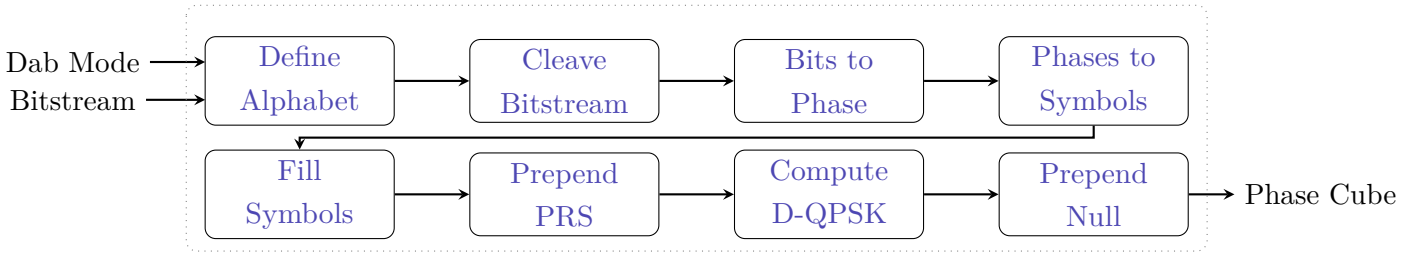

4.2.1 Define Alphabet

To begin the process of generating the phase matrix, one must first determine the number of bits mapped to each symbol. The fundamentals of phase shift keying are discussed in Subsection 2.2.4. The number of bits encoded in a single phase is therefore simply defined as m. This results in 2^m mappable positions on the complex plane. This value m is designed to be configurable allowing the user to select DBPSK, DQPSK and 8-DPSK. Within the scope of this investigation *only DQPSK has been fully implemented*. The alphabets (the phase bit mappings) are defined in Table 4.2.

Modulation Scheme	bts	Mapping
DBPSK	1	$[0:0\,,\,\pi:1]$
DQPSK	2	$[\frac{\pi}{4}:00\,,\,\frac{3\pi}{4}:01\,,\,\frac{5\pi}{4}:10\,,\,\frac{7\pi}{4}:11]$
8-DPSK	3	$[0:000\,,\,\frac{\pi}{8}:001\,,\,\frac{2\pi}{8}:010\,,\,\frac{3\pi}{8}:011\,,\,\frac{4\pi}{8}:100\,,\,\frac{5\pi}{8}:101\,,\,\frac{6\pi}{8}:110\,,\,\frac{7\pi}{8}:111]$

Table 4.2: Showing the mapping of bit to differential phase value according to differential modulation scheme

4.2.2 Cleave Bitstream

With the alphabet defined, the bit stream may be cleaved into a vector of $[]\times m$ bits. $[]$ indicates that the vector is of variable length and directly dependant on both the length of the bit stream and the value m. This vector will not necessarily be an integer multiple of m. Therefore *within* the cleave bitstream function, additional zeros are appended to the closest integer multiple of m. This adjusted bitstream is then finally cleaved into the variable length vector of size $[]\times m$ and is ready for the bits to be mapped to their corresponding complex phase value.

4.2.3 Bits to Phase

Using one of the mappings shown in Table 4.2, the $[]\times m$ vector will be converted to a vector of size $[]\times 1$. The m sets of bits are each converted to *single* phase. Note that these phases are the differential phases and are not the absolute phases that will be modulated onto individual sub-carriers.

4.2.4 Phases to Symbols

With the mapping of bits to phases completed, recall that zeros were appended to ensure there was an integer division number of phases. This does not imply that there are sufficient phases to be reshaped

into an integer number of symbols. Zero phases are therefore appended to the end of the phase vector $[] \times 1$ such that [] phases is exactly enough required to reshape an integer number of symbols. The result of this procedure is therefore a vector of phases of length $(L_r\, K) \times 1$ where L_r is a random number of symbols. This reshaped $L_r \times K$ array will be referred to as $\tilde{A}$, the array that carries the data carrying symbol information.

4.2.5 Prepend PRS

Recall the broader goal of this procedure. The signal generation chain modulates phases onto consecutive sub-carriers where the *difference* between these consecutive (symbol) sub-carrier phases determines the encoded bits. The DAB standard includes the PRS, which as the name suggests, is the reference by which the DQPSK is computed. The RadCom PRS leverages this predefined PRS through its alteration for the RadCom application.

Observing that the DAB PRS is centered around the null carrier provides a useful method by which to understand the generation of the altered PRS. The customised DAB mode structure defines the number of sub-carriers K. The processing chain then uses this value to generate the adjusted PRS such that the center most $\frac{K}{2}$ carriers above and below the null carrier are included. Therefore the customised PRS can be thought of as using a subset of the original DAB PRS sub-carriers and implies that the new DAB mode must have *at most* the same number of carriers as the original DAB mode I. This is therefore an adjusted PRS which is prepended to $\tilde{A}$ denoted as $\tilde{A}_{prs}$ which is now of size $(L_r + 1) \times K$.

4.2.6 Fill Symbols

As with the prior filling procedures, there is no guarantee that the number of symbols is the number of symbols required to form a frame. Simply put $(L_r + 1)$ is not equal to the DAB mode parameter L. Note that the parameter L *includes* the PRS and NS. Observe in Figure 4.2 that the NS is prepended *after* the computation of DQPSK. Therefore in order to ensure the number of symbols matches exactly with that required to generate a frame, the number of symbols needs to be increased to $L - 1$ such that when the NS is prepended the total number of symbols is L. In order to complete this task, $(L - 1) - (L_r + 1)$ symbols are appended to $\tilde{A}_{prs}$. The naming convention of this matrix remains unchanged even though its size has changed.

4.2.7 Compute D-QPSK

If one reviews the matrix $\tilde{A}_{prs}$, it should become apparent that it contains the differential phases not the absolute phases of individual sub-carriers. Therefore the task remains to compute the absolute phases. This is mathematically described in Equation 4.8:

$$D_l = \angle(L_l * L_{l-1}) \tag{4.8}$$

This mathematical procedure is implemented using Algorithm 2. The algorithm therefore calculates the absolute phases using the differential phases. Notably, the first symbol in this procedure, the PRS,

remains unchanged as the first symbol in the array.

inputs : Complex phase code matrix, $\tilde{A}_{prs}$
output : Complex differential phase matrix , A

begin
  $A[\,1\,,:] = \tilde{A}_{prs}[\,1\,,:]$
  for $(\,i = 2 : \text{SymbolsIn}(\tilde{\text{A}}_{\text{prs}})\,)$ **do**
    $A[\,i\,,:] = A[\,i\,,:] \odot \tilde{A}_{prs}[\,i-1\,,:]$
  end
end

Algorithm 2: Showing the generation of absolute phases to be modulated onto individual sub carriers

4.2.8 Prepend Null

Finally, with the absolute phases computed, the NS is prepended resulting in a matrix of size $L \times K$ and is denoted by A.

4.3 Frame Generation

Following the generation of the phase codes, frame generation is completed. This procedure is shown in Algorithm 3. Before discussing the procedure used to generate frames, the structure of the frame will be reviewed. This begins with its most basic elements, the set of K sub-carriers. These sub-carriers form a single symbol and are defined by their symbol time, the sum of the guard and integration interval. L symbols in turn form a continuous frame with no delay time appended. Finally, the delay time is appended with the complete frame then repeated.

This section will cover methodology used to generate the above components and compile them into frames. This will begin with the generation of the most basic element, the sub-carrier, progressively expanding the scope of consideration to include symbols and finally the frame. Importantly this procedure is agnostic towards signalling and data carrying information as this is the responsibility of Bitstream Encoding.

inputs : Phase code Matrix, A ; Carrier weight Matrix, W ;
OFDM carriers, K ; OFDM Symbols L ;
The dab mode, dabMode
output : Complex ofdm frame, F

begin
  for ($l = 1 : L$) **do**
    for ($k = -\frac{K}{2} : \frac{K}{2}$) **do**
      S_{sc} += genSC{ dabMode , k , $A[l, k]$, $W[l, k]$ }
    end
    $S_L[l, :] \leftarrow S_{sc}$
  end
  F = concat{ syms }
end

Algorithm 3: Showing time domain methodology for used to generate a RadCom frame

4.3.1 Sub-carrier Generation

The first procedure used to generate a frame is carrier generation. This is implemented in the time domain where each sub-carrier is independently generated using Equation 4.9 and is denoted by 'genSC' in Algorithim 3. To complete this procedure one requires three pieces of information. These include the *dabMode* (which includes T_u, T_g and T_s in elementary units T), the carrier number with respect to the baseband DC (k = 0) value and finally the symbol number l. Using these values one may first generate the correct sub-carrier and then modulate it with its respective frequency and phase weights $a_{l,k}$ and $\omega_{l,k}$ using the input phase and frequency matrices A and W. Square brackets have been used to indicate that the signal is discrete. The sub-carrier array is of size $1 \times T_s$ where T_s is in elementary units.

$$s_{sc}[n] = (a_{l,k})\,(\omega_{l,k})\,exp\left[\frac{j2\pi k(n - T_g)}{T_u}\right] \tag{4.9}$$

4.3.2 Symbol Generation

With the ability to generate a single sub-carrier, one may now approach symbol generation. This process, in practice, is the encapsulation of a repeated call of sub-carrier generation. It is shown by the inner most for loop in Algorithm 3, iteratively generating K sub-carriers centered around zero.

Therefore to generate a single symbol requires the use of phase and frequency weights corresponding to $A(l, :)$ and $W(l, :)$ where l is the symbol index. This procedure results in a matrix of size $1 \times T_s$ which is the iterative summation of the generated sub-carriers.

Upon review of this methodology one may observe that it may be improved. This is due to the time domain implementation of repeatedly creating arrays and summing sub-carriers. A significantly faster and more efficient methodology may be to generate a symbol in a single operation. This may be implemented using element wise multiplication of the phase and frequency weights. Padding this array with zeroes to be of size T_u, followed by computing the IFFT resulting in the complex envelope of an OFDM symbol with no guard interval.

4.3.3 Generate Frame

Generating a single frame follows a similar procedure to that of symbol generation as it requires the iterative generation of successive symbols. The processes differ due to the way in which the generated data is stored. This is because successive symbols are appended as matrix rows (This implementation facilitates symbol analysis). This therefore requires further processing once the $L \times T_s$ symbol matrix has been generated. This processing is the concatenation of the rows into a single $1 \times LT_s$ vector, the complex envelope of frame.

4.4 Time Insertion

At this point the complex envelope of the frame had been generated. This may be transmitted continuously achieving higher data rates thereby allowing it to operate as a pure communications signal. Alternatively, one may convert this continuous waveform into a pulsed waveform, allowing it to operate as both a communications and radar signal.

To do this a delay time, an array of zeros, was appended to the end of each frame. Therefore when transmitting continuously, waveform would be pulsed. The time period of these appended zeros was defined by the customised DAB mode parameter T_d.

The parameter T_d defines a single pulse. In practice a single pulse will not be transmitted, rather having multiple pulses transmitted consecutively. With the possibility of different pulse trains be transmitted consecutively the pulse repetition parameter P was defined. Thereby repeating the complex envelope P times. The output envelope of a single frame (containing multiple pulses and delay periods) is therefore of size $1 \times P(LT_s + T_d)$

4.5 Resample to Write

Although a utility and not shown in 4.1, the signal was then resampled from the processing chain sampling rate to the hardware sampling rate, cast to either a double, float or short and stored in a binary file such that it may be either read in to the demodulation chain or the SDR platform.

4.6 Validation

This section will validate the correct functionality of the Signal Generation Chain. It will begin with testing of the encoding and decoding of bit streams covered in Section 4.2. This encompasses the splitting of bit streams, reshaping and eventual computation of DQPSK and bit values.

Following this the generation of OFDM signal will be validated. This includes but is not limited to the time and frequency domain analysis of the generated waveforms. The generation of the altered PRS and insertion of delay times times will also be validated.

4.6.1 Bit Encoding

The first procedure to be validated was bit encoding functionality. The tests therefore aimed to validate that given a bitstream, it could be correctly converted and mapped to a matrix representing the absolute phases that could be modulated onto sub-carriers across consecutive symbols. Given this matrix, the phase codes must also be decoded and compared to the original bitstream. This comparison of the coded-decoded bit stream *must* be the same as the original stream for this subsystem to be considered functional.

Bit Mapping

To ensure the correct encoding of bitstreams, one is required to validate that bits are correctly mapped to their differential phases. The RadCom processing chain uses DQPSK while also laying the groundwork for other DPSK modulation schemes. Therefore the correct conversion of bitstreams to DBPSK, QPSK and 8-DPSK were validated. This mapping is demonstrated and validated in Figure 4.3. Recall that each technique allows for the modulation of an additional bit per phase with their mappings shown in Table 4.2. Therefore each modulation technique increases the number of possible positions on the complex plane. This will be relevant in further analysis of Figure 4.2.

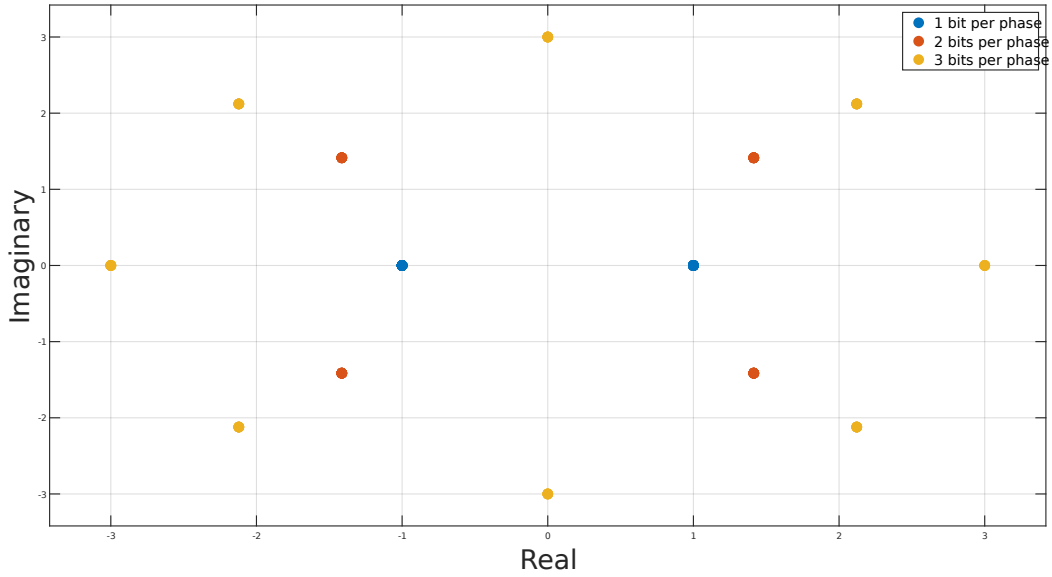

Figure 4.3: Showing the differential mapping for DBPSK (blue), DQPSK (red) and 8-DPSK (yellow) according to the values found in Table 4.2

Before further analysis is completed, the validation procedure will be covered. This began with the generation of random bitstream of length mLK. It was then iteratively reshaped into sub-bitstreams,

symbols and finally the frame. Following this, the differential phases were computed.

Given a long enough sequence one would expect every phase in the alphabets defined in Table 4.2 to occur. Figure 4.3 shows this with the complex values associated with a given differential phase plotted. For clarity, each complex value has been scaled by the number of bits encoded in each phase to differentiate the various mapping schemes.

$\frac{\pi}{4}$-DQPSK - Coding

With the bit to phase mapping validated, the following test was conducted using *only* DQPSK as a mapping technique. Therefore while using DQPSK one should expect alternating phases as shown in Figure 2.9 where a single symbol can either take on $[\pi, \frac{\pi}{2}, 0, \frac{-\pi}{2}]$ or $[\frac{3\pi}{4}, \frac{\pi}{4}, \frac{-\pi}{4}, \frac{-3\pi}{4}]$. After computing and plotting the absolute phase matrix (using previously generated differential phase matrix), one can see these alternating phases. This is shown in Figure 4.4 and validated the correct functionality of this stage of signal generation.

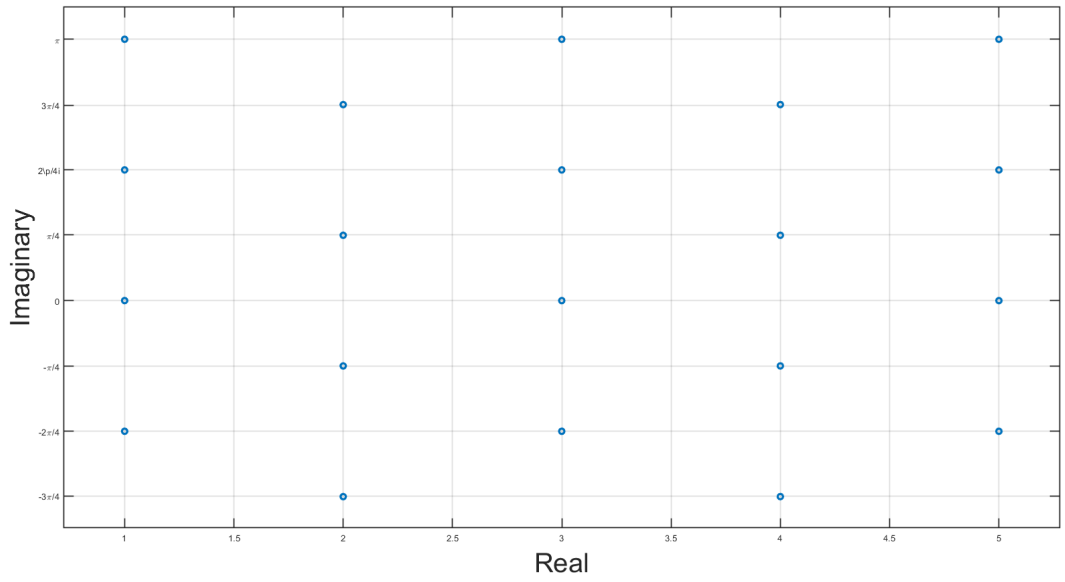

Figure 4.4: Showing consecutive OFDM symbol carrier phases alternating between two 2 absolute phase sets on a scatter plot

Frame Generation

It has been demonstrated that a bitstream may be coded into the phase matrix A. The inversion of this procedure has also been implemented in order to demonstrate the full coding-decoding functionality. In its completeness it demonstrated the ability to convert the absolute phases back to a bitstream. This procedure is not well suited to a succinct visual demonstration and leaves the opportunity for unnoticed errors to arise in edge cases. These cases particularly surround the last phase in a symbol and the last symbol in a frame. Therefore an alternate procedure to those used above was developed to test this functionality.

This involved the same conversion of bits to the previously mentioned phase matrix but with a small addition. In this case the *original* bitstream was stored as a reference to compare against the result of the decoding procedure. The inverse decoding procedure was computed by taking the phase matrix, computing the differential phases, reshaping, converting phases to bits and then reshaping again. The output of this procedure was a bitstream.

In order to verify that this bitstream matched the originally encoded stream, a mathematical operation was followed. The decoded bit stream and original bit stream were iteratively compared using a bitwise XNOR operation. The process followed is shown in Algorithm 4. If this operation produced a 0, meaning the bitstreams were different, an error counter was incremented. Once the two bit streams had been fully compared, the error counter was divided by the number of bits in a given bit stream. This resulted in a bit error rate or BER.

inputs : Reference bit stream, b_{ref}; Decoded bit stream, b_{decode}
output : Bit error rate, BER

error $\leftarrow 0$

i $\leftarrow 0$

begin
  while $i \leq$ length$\{b_{ref}\}$ **do**
    error += XNOR$\{b_{ref}[i], b_{decode}[i]\}$
    i++
  end
  $BER \leftarrow$ error $\div$ length$\{\mathrm{b_{ref}}\}$
end

Algorithm 4: Showing coding decoding test to determine BERs

When computing the coding-decoding BER the expected result should be zero as there is no point at which errors should be introduced. If the result is non-zero, it is an indication that the processing chain itself is not functioning correctly. The output of this validation test was a BER of 0, this therefore indicates that the bitstreams were *exactly* the same and that bit encoding was working correctly.

4.6.2 OFDM Generation

The following sets of tests are not exhaustive but were used as basic chain demonstrations and validations. These demonstrations attempted to display both time and frequency parameters of OFDM signals, and how they varied as DAB mode parameters such as the carrier number K and symbol number L varied. Furthermore, the customised PRS generation is also validated as this is the first instance it may be visualised.

Carrier Variation

Figure 4.5 demonstrates the effects of altering the number of sub-carriers in the DAB mode structure and by extension a single symbol. As the number of carriers increase in an OFDM signal the expected

bandwidth should increase. This is demonstrated in Figure 4.5 where multiple signals were generated using a sampling rate of 2.048 MHz and an integration time of 1 ms.

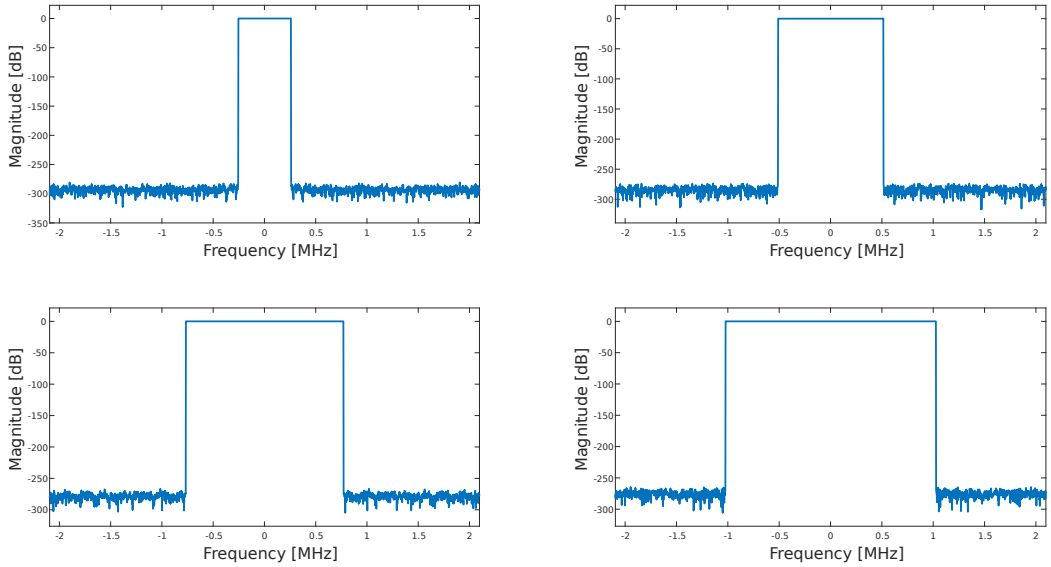

Figure 4.5: Showing the ability to generate variable bandwidth signal through alteration of the number of sub-carriers

The number of carriers, K, used in each signal was $500, 1000, 1500, 2000$ with actual bandwidths meeting the expected bandwidths of $0.5, 1, 1.5$ and 2 MHz. This validates that the chain can produce variable bandwidth signals.

Symbol Variation

Following the generation of single symbol carriers is the generation of *multiple* symbols. Visualised, this can be thought of as as a spectrogram, occurring in time and frequency. Given the ability to customize the number of symbols per frame, one would expect to see spectrograms of varying lengths but fixed bandwidths (given that K remains constant). Figure 4.6 shows this where $L \in [2, 5, 6, 10]$ and therefore validates the ability to generate frames with multiple symbols.

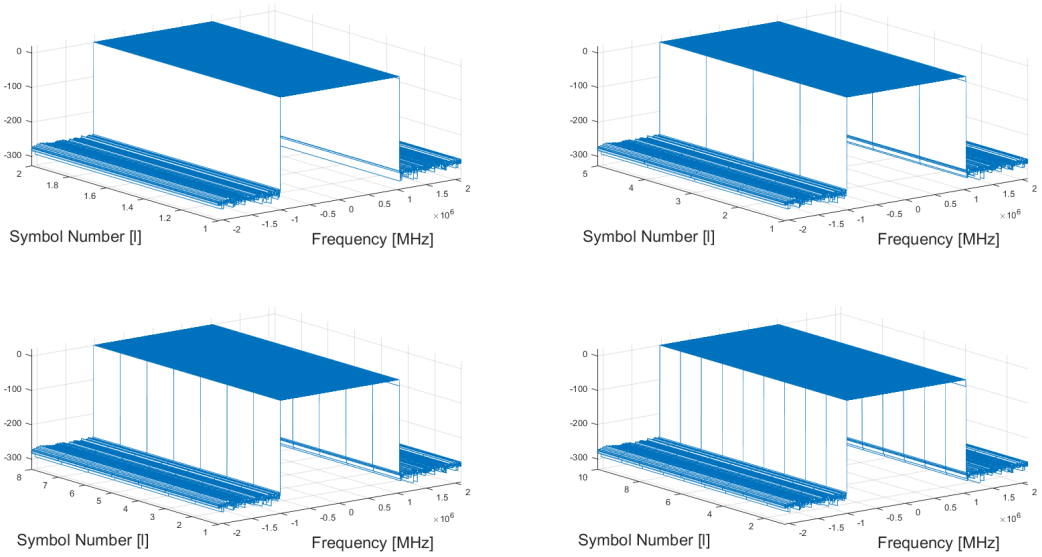

Figure 4.6: Showing the ability to generate variable symbol length signals through alteration of the number of symbols

Customized PRS Generation

With the ability to generate custom OFDM signals with varying K and L, the investigation turned back to the DAB standard. This is the first opportunity to validate the generation of the customized PRS as this is the first opportunity to visualise it. This procedure is shown in Figure 4.7 and involves the overlaying of the custom PRS over the standard DAB PRS. As one approaches the number of carriers used in the DAB standard ($L \to 1532$) one should expect the customized PRS and standard PRS have increasingly similar signal envelopes until such a point that they are the same. This is demonstrated in Figure 4.7 indicating the correct generation of the customized PRS.

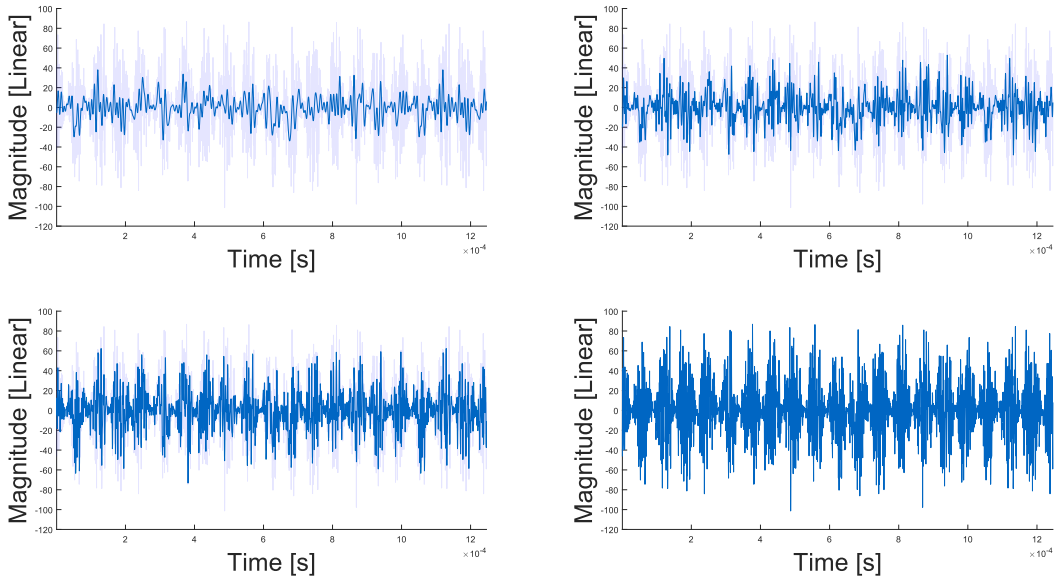

Figure 4.7: Showing the ability to correctly generate a customised PRS as the number of sub-carriers increase

4.6.3 Signal Generation

The final verification test conducted demonstrates the correct functionality of the time insertion procedure. This procedure inserts a delay time (after the generation of the frame envelope) and repeats the waveform. The parameters used to generate this waveform are shown in Table 4.3 and the resulting waveform is shown in Figure 4.8

Parameter	Value
K	1000
L	3
T_u	2048
T_g	504
T_d	5104
P	2

Table 4.3: Showing parameters used to complete the final verification procedure of signal generation

One may observe that the three symbols used to generate this waveform are allocated to the NS, PRS and a data carrying symbol. The first 2552 samples correspond to the NS while the 5104 samples between index 2552 and 7656 correspond to the PRS and data carrying symbol. This indicates the correct generation of frames complex envelope.

Furthermore, the last 5104 samples corresponding to the delay time indicate that the delay time has been inserted correctly . Notably, the delay period between the two frames was not considered as it is the combination of the NS and delay period and would therefore unnecessarily complicate the analysis. Finally, one may observe that there are two frame-delay signals as one would expect when considering the repeat parameter P. These measurements verify that the waveform is being correctly generated.

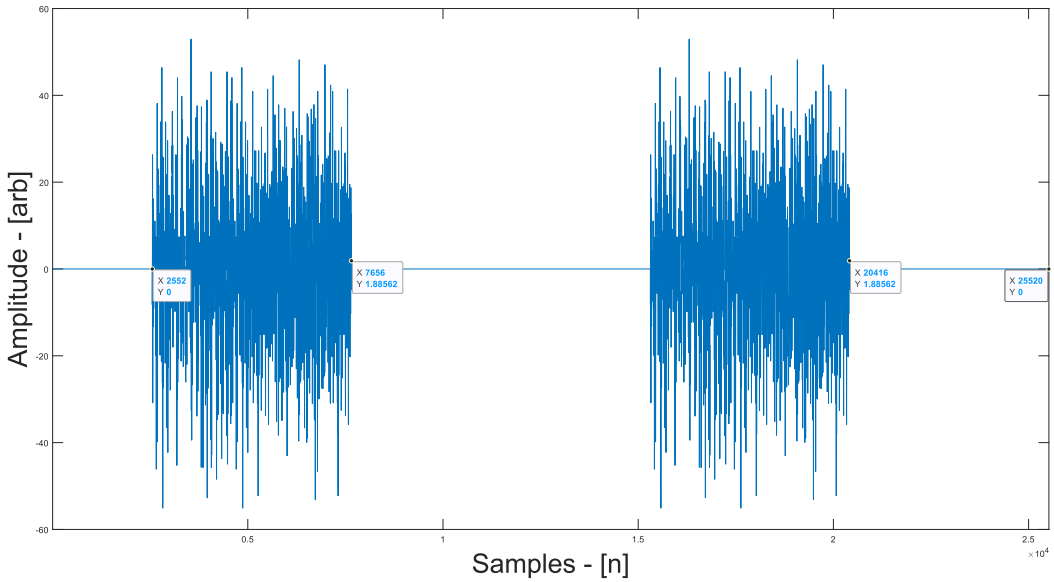

Figure 4.8: Showing a complete waveform generated using the signal generation chain

Chapter 5

Communications Processing Chain

> 'The successful among us delay gratification. The successful among us bargain with the future'
>
> — *Jordan B. Peterson*

The following chapter reviews a previously developed DAB processing chain intended for passive radar applications [1]. This will cover aspects of the chain relevant to the design of the RadCom system. This therefore includes a review of the functionality of the preprocessing and demodulation stages of the original chain. This is followed by a description of the alterations to the processing chain used to generalise its functionality and integrate it into the broader RadCom system. This includes the integration of the preprocessing chain, demodulation chain and the decoding chain as shown in Figure 5.1. Finally, the altered chains functionality will be validated.

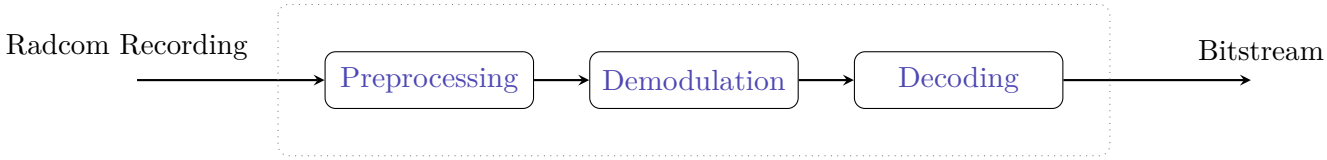

Figure 5.1: Block diagram showing an overview of communications processing chain

5.1 DAB Processing Chain Review

5.1.1 Preprocessing

The preprocssing chain aims to extract a frame as IQ data. With this in mind, during the initial development of passive radar processing chain it was observed that data would more likely be streamed through the chain. This introduces the possibility of multiple frames being extracted at once. Although the case, the preprocessing of stage of the DAB processing chain is designed to extract frames from prerecorded data [1]. This firstly requires the reading in of IQ data. This data is not guaranteed to be at the sampling rate required for demodulation and as such needed to be resampled. The resampled data may or may not contain a frame, therefore a PRS detection and by extension a fine time synchronisation procedure is implemented by the chain. With the exact beginning position of a frame determined, the frame could finally be extracted and passed into the demodulation processing chain. This procedure is shown in Figure 5.2. The remainder of this subsection provides the reader with additional information surrounding preproessing.

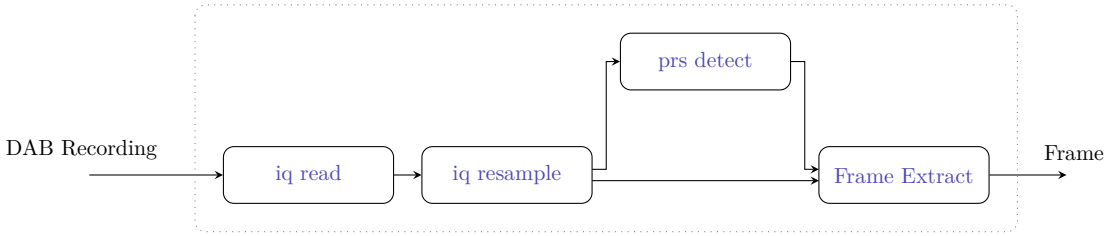

Figure 5.2: Showing a block diagram of the preprocessing stages of the DAB processing chain involving reading in data and the extraction of DAB frames

iq read

The first stage of preprocessing required the reading in of the IQ data from a binary file. Notably, the binary file contains *complex* data. As a binary file has no inherent way to store this data, standard practice in this processing chain is to store complex numbers as consecutively alternating real and complex numbers. Therefore when reading the prerecorded data the real and complex components may be extracted independently and summed together to form the recorded IQ data stream. Reading in data from a binary file additionally requires knowledge of the stored type to extract values correctly.

iq resample

This data stream will eventually be processed and demultiplex using an FFT. This places requirements on the data stream, particularly in terms of sampling rates. The orthogonal structure of the OFDM signal requires the sampling rate be exact. For a DAB signal this sampling rate is 2.048 MHz. Practical microwave systems will not necessarily use this during operation and as such there is no guarantee that the recorded data has been sampled at the processing chain sampling rate. Therefore the processing chain resamples the data from the microwave sampling rate, F_{iq}, to the processing chain sampling rate, F_s. This process requires a signal to be up-sampled by a factor P followed by a down-sampling of factor a factor Q such that $\frac{F_s}{F_{iq}} = \frac{P}{Q}$. This procedure should additionally incorporate an anti-aliasing filter.

prs detect

With the data read in and resampled, it is ready for further preprocessing. The detection of the PRS becomes the aim. This procedure will provide the exact index of the starting position of the frame. This procedure is important as a misalignment in the data will results in the signal being demodulated incorrectly. The methodology for the detection procedure is shown in Algorithm 5.

It begins with the input signal $x[n]$ and the PRS. Setting the signal index to zero ($n_0 \leftarrow 0$) allows one begin iterating through the data. At every index n_0 one extracts a single integration period worth of samples and is required to match filter it with the PRS. The peak value of this procedure is then compared to its average value. If the peak is larger than the mean scaled by a threshold constant, a signal is considered to be present.

In the case that the threshold is not met, the position index in incremented by T_a. Therefore the new index becomes $n_0 = n_0 + T_a$. Note that during the detection procedure the presence of the

guard interval will cause partial matching. The processing chain therefore constrains the step size T_a to $\frac{T_u}{2}$. This ensures that a small peak occurring in the second half the window would be guaranteed to occur in the following interval. This peak would also be guaranteed to be larger than the first and allows for setting of a more stringent γ threshold such that the guard interval does not cause a false detection.

inputs : A sampled DAB signal, $x[n]$; The PRS, $R[k]$
output : The exact index of the first PRS in $x[n]$
parameter : Threshold constant, $\gamma > 1$

begin
  $n_0 \leftarrow 0$
  while $(n_0 < T_f)$ **do**
    $X[k] \leftarrow \text{FFT}\{x[n_0 : n_0 + T_u]\}$
    $Y[k] \leftarrow R^*[k] \odot X[k]$
    $y[n] \leftarrow \text{iFFT}\{Y[k]\}$
    if $(\max|y[n]| > \gamma \cdot \text{mean}|y[n]|)$ **then**
      return $\text{argmax}|y[n]|$
    else
      $n_0 \leftarrow n_0 + T_a$
    end
  end
end

Algorithm 5: Showing frame detection and fine time synchronisation using the PRS

Frame Extract

Once the start index of the frame had been determined, one simply extracted the next 10 ms worth of samples which are stored passed to the demodulation chain for further processing. Note that frame extraction *does* extract the NS. Therefore the vector passed to the demodulation chain is of size $1 \times T_s\, L$.

Null Symbol Detection

Although not included in the preprocessing of RadCom signals, there is an additional means by which to estimate the beginning of the DAB frame. This requires the detection of the NS which is computationally less expensive than the detection of the PRS. This procedure requires one to estimate the power in a signal and compare it to a predefined threshold. When the power in the given set of samples drops *below* the predefined threshold, one estimates this as the position of the NS and then starts looking for the PRS. This procedure works as all other time periods in the DAB signal contain active carriers and therefore power. This implies that when there is less power in the given set of samples all that this could be in the NS.

5.1.2 Demodulation

Demodulation encompasses the process of DQPSK phase extraction. This is achieved using the procedures shown in Figure 5.3. These first split a DAB frame into its symbols using the symbols unpack functionality. These symbols are then demultiplexed into their sub-carriers and demapped into their corresponding DQPSK phases. The phases are deinterleaved and snapped to their corresponding differential phases. There is additionally an error correction procedure that remains unimplemented. The output of these procedures are the differential phases.

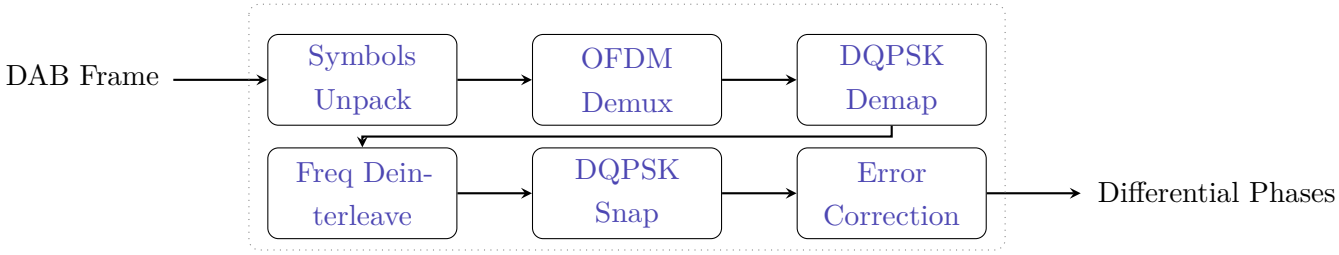

Figure 5.3: Block diagram showing an overview of the previously developed DAB demodulation processing chain

Symbols Unpack

This sub-block performed two functions. This includes splitting the frame into its individual symbols *and* removing both the NS and the guard interval from these symbols. This results in the conversion of the $1 \times T_s(L)$ to a $(L-1) \times T_u$ matrix at its output.

OFDM Demux

This procedure is responsible for the extraction of the signal sub-carriers. The $(L-1) \times T_u$ matrix is still in the *time domain*. This procedure is functionally the encapsulation of an the FFT. It takes and returns the FFT of the $L-1$ symbols.

DQPSK Demap

DQPSK Demap is responsible for the extraction of the previously modulated differential phases. This task is completed using Equation 5.1 where the differential phase between consecutive symbols is calculated using the complex division between consecutive symbol sub-carriers.

$$D_{l-1} = \angle\left(\frac{L_l}{L_{l-1}}\right) \tag{5.1}$$

Recall that the first symbol, the PRS is used in this procedure and is *not* a data carrying symbol. The output of this procedure is only the phases modulated onto data carrying symbols. As such the output is a matrix of size $(L-2) \times T_u$.

Freq Deinterleave

Freq Deinterleave takes in the differential phases and deinterleaves them according to map defined in the DAB standard while also returning only the used central sub-carriers. The output of this procedure is therefore a $(L-2) \times K$ matrix.

DQPSK Snap

This procedure snaps phases to their closest differential value. This is as in the presence of noise the demodulated phases will not correspond to an exact DQPSK value of $[\frac{\pi}{4}, \frac{3\pi}{4}, \frac{5\pi}{4}, \frac{7\pi}{4}]$ and rather occur in a noisy constellation. This procedure therefore snaps each phase in the constellation to the closest element in the set and returns it as a $(L-2) \times K$ matrix.

Error Correction

During the development of this processing chain, the error correction stages were considered out of the scope of development. As such no error correction was implemented and was simply included for completeness.

5.1.3 Remodulation

The remodulation stage of the processing chain is considered out of the scope of this investigation and will therefore not be covered in any detail. It is deemed sufficient to inform the reader that it exists and is able to convert differential phases into the perfect DAB signal.

5.2 Processing Chain Alterations

With the original chain reviewed, modifications are now discussed. These were implemented in the context of the broader design aims of this investigation. Therefore the modifications were designed to both allow for the generalised processing of a signal defined by a DAB mode structure and simplify the processing chain discussed in Subsection 5.1.2. This allows for the processing of any signal with varying parameters in both the time and frequency domain. Alterations to the DAB mode structure, PRS detection and demodulation of the original processing chain are therefore required. An additional Decoding stage has been incorporated into the broader processing chain. The complete processing structure implemented in this report is shown in Figure 5.1 comprising the cascaded preprocessing, demodulation and decoding chains.

5.2.1 DAB Mode Review

The unadjusted processing chain is designed to work using the DAB mode I structure introduced in Table 4.1 and fully defined in the ETSI DAB standard. But as covered in Signal Generation Chain, the signal structure has changed as a function of the newly described RadCom DAB mode. Limited changes therefore needed to be made to allow the processing chain to correctly process signals generated for RadCom applications. To understand the changes made to the chain one should be familiar with the alterations to the DAB mode as covered in Section 4.1. These changes include the addition of the

hardware and processing sampling rates (F_{iq}, F_s) and the delay time (T_d). Finally, it also includes the number of frame repeats (P).

5.2.2 Adjusted PRS Detect

The original processing chain was developed to operate with the unadjusted PRS. Observe two important points regarding Algorithm 5. Firstly, it defines a threshold upon which it considers the signal to be present. And secondly, this threshold is directly dependant on the output of the matched response of the IQ data and a PRS generated *within* the demodulation chain itself.

In order to generalise the functionality of the PRS detection, this procedure was generalised to function with a PRS that is a function of DAB mode. The generalised version of the PRS as defined in Subsection 4.6.2 is therefore generated using the DAB mode and passed into the PRS detect function for fine time alignment.

5.2.3 Interleaving Removal

Frequency interleaving is the technique used by the DAB standard to increase signal resiliency. As the scope of this investigation is limited to the basic design and demonstration of the RadCom system, designing an altered interleaving-deinterleaving technique for this sub-system is considered out of scope. Interleaving therefore returns only the active OFDM sub-carries.

5.2.4 Decoding

The previously developed processing chain did not incorporate a decoding procedure. Therefore a decoding stage to convert a set of phases to a bitstream was developed and incorporated into the broader chain. This is the inverse procedure to the encoding discussed in Subsection 4.2. This first reshapes the $(L-2) \times K$ snapped phase matrix into a single $1 \times (L-2)K$ vector. This vector is then mapped to its equivalent $1 \times (L-2)K$ vector of m bit sequences and returned as a single bitstream of length $(L-2)\,K\,m$.

5.3 Validation

With the original DAB processing chain altered, there is no guarantee that it still functions as intended. Therefore validation tests were run on the adjusted RadCom processing chain. This includes ensuring that both the preprocessing and demodulation stages of the processing chain were functioning correctly. Finally, the decoding stages of the processing chain were also be verified for correct functionality.

5.3.1 Preprocessing

These sets of tests aim to visually verify the functionality of the preprocessing chain. This was done using data generated from the signal generation chain. This therefore encompasses PRS detection and frame extraction. Particularly important to this test is the demonstration that the processing chain still works with the *adjusted* PRS and the altered frame size. The waveform parameters used to conduct preprocessing validation tests are shown in Table 8.2.

Parameter	Value
F_s	4.096 MHz
K	1000
L	5
T_u	2048
T_g	504
T_d	5104

Table 5.1: Showing DAB mode configuration used during the communications validation test

PRS Detection

Figure 5.4 demonstrates the PRS detection procedure. Specifically, the upper most sub-plot demonstrates the processing chains ability to generate the custom PRS while the second sub-plot displays the perfect data generated using the signal generation chain. Figure 5.4 demonstrates the ability to detect the PRS (and therefore the beginning of the RadCom frame). Frame extraction is therefore a question of threshold detection with the threshold setting a design decision.

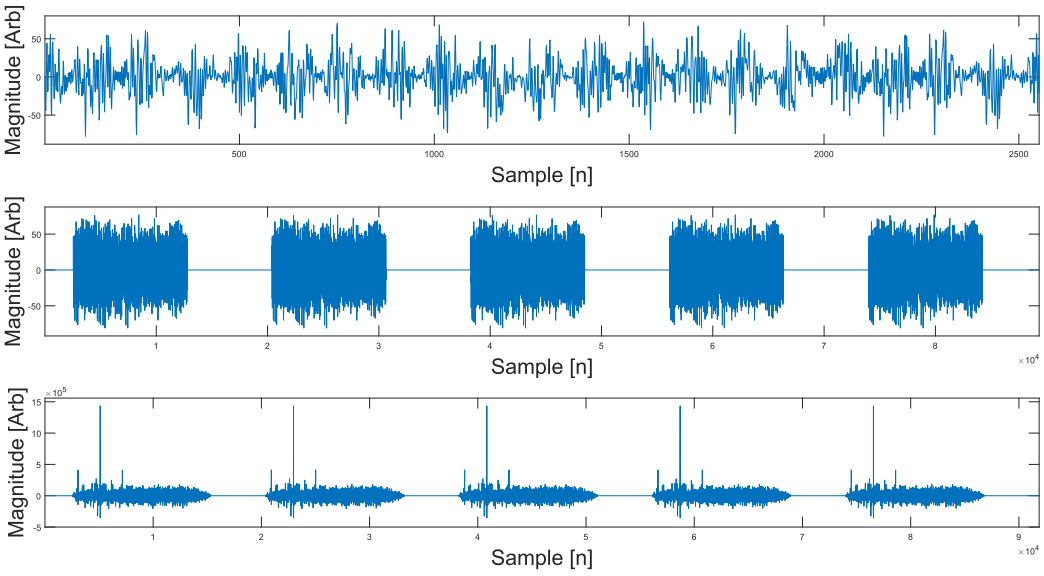

Figure 5.4: Showing multiple PRS detections in consecutive frames

Frame Extract

Following the detection of the frame, its correct extraction was validated. This test was completed as the length of the frame is now able to vary. The result of the extraction procedure is shown in Figure 5.5 and indicate that a variable length frame has been correctly extracted. This is as one is able to see both the NS, PRS and the three remaining data carrying symbols resulting in an expected total symbol count of 5.

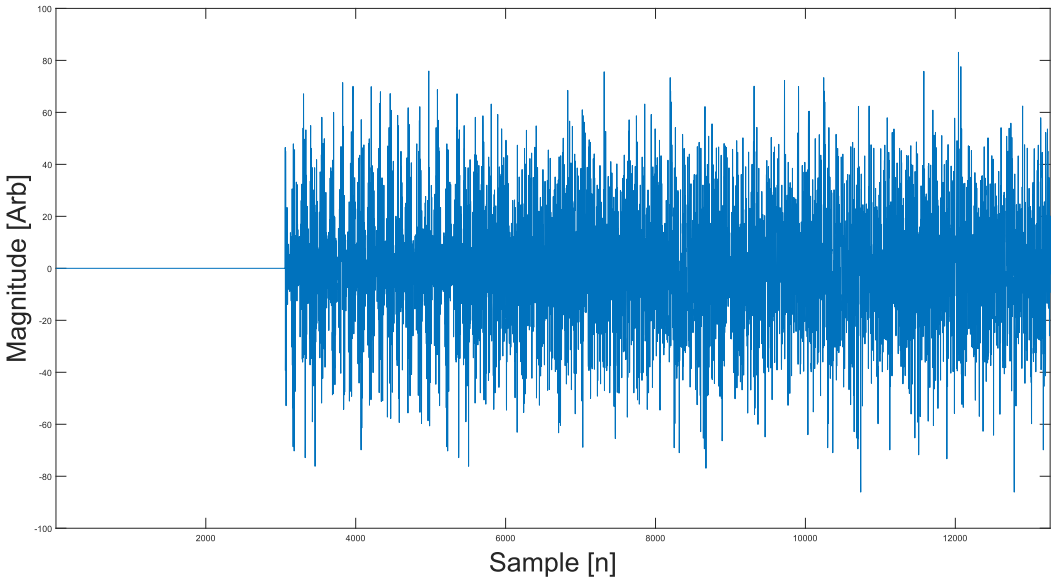

Figure 5.5: Showing the extraction of a single frame by the RadCom communications processing chain

5.3.2 Demodulation

With the frame extraction demonstrated, the altered demodulation stage of the processing chain was validated for correct functionality. This involved the demonstration of symbol unpacking, demultiplexing and demapping of the DAB mode shown in Table 8.2.

Symbols Unpack

Once the frame had been extracted from the data stream, unpacking was demonstrated for completeness with the output of this procedure shown in Figure 5.6. The Figure includes the PRS, followed by three data carrying symbols all of equal length (2048 samples) below it. Additionally, observe that the guard interval and NS have been removed (otherwise the resulting arrays would contain 2552 samples). This is the expected functionality and therefore validates the functionality of the unpacking procedure.

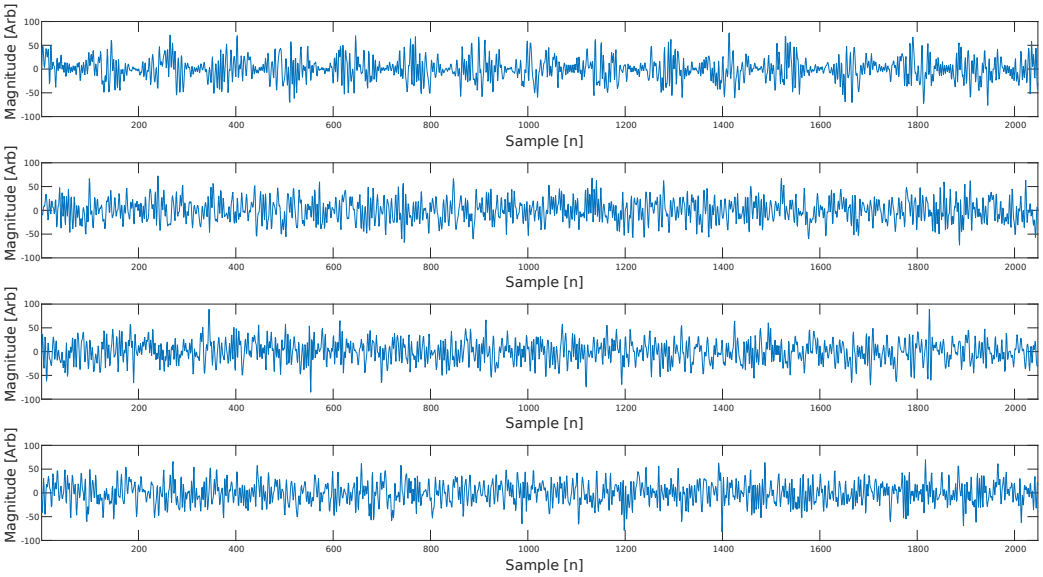

Figure 5.6: Showing the time domain unpacked symbols with 2048 samples, including the guard interval, PRS and three data carrying symbols

Symbols Demux

These symbols are demultiplexed following the unpacking procedure. The output of this procedure should be a smooth rect like function with a zeroed center and 1000 active sub-carriers. If this is not the output, it would indicate an error in one of the previous procedures, namely PRS detection, frame extraction or symbol unpacking. Figure 5.7 demonstrates the expected rect like function with the zeroed center. This therefore further indicates that the previous procedures during the demodulation are functioning correct.

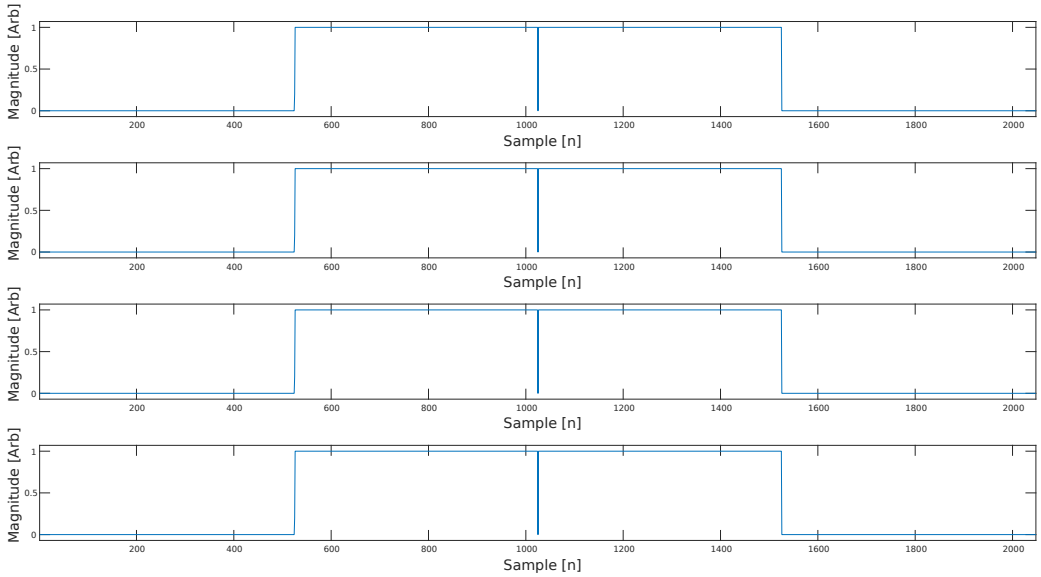

Figure 5.7: Showing the frequency domain unpacked symbols with 2048 samples, including the guard interval and three data carrying symbols

Symbols Demap

The demapping procedure successfully returns the differential phases between consecutive carriers. These take the expected differntial phase values of $[\,\frac{\pi}{4}, \frac{3\pi}{4}, \frac{5\pi}{4}, \frac{7\pi}{4}\,]$. Additionally, it has successfully removed the PRS and only returned the data carrying symbols.

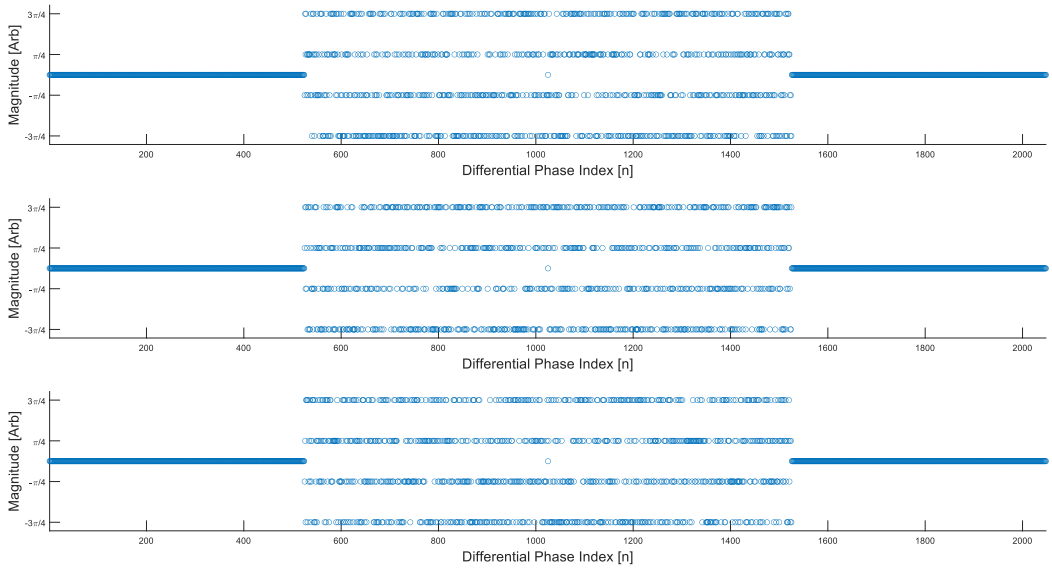

Figure 5.8: Showing the demapped phases from the demodulated frame

Symbols Deinterleave

The deinterleaving procedure successfully removes the unused and null sub-carriers and returns only the 1000 data-carrying differential phases of the sub-carriers.

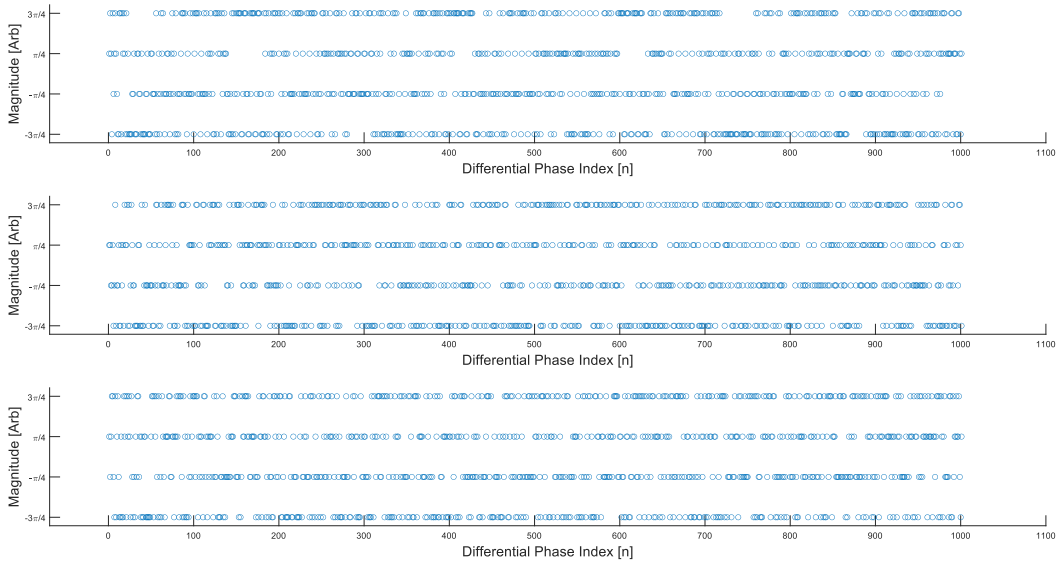

Figure 5.9: Showing the deinterleaved phases from the demodulated frame

Symbols Snap

The data used in this validation procedure is uncorrupted by noise and therefore there is no change between the demultiplexing and snapping procedure. Additionally, it remains unchanged when compared to its original development and has *already* been validated during its initial development. For these reasons testing is not completed within this stage of the investigation.

5.3.3 DAB Decoding

One has a $L-2\times K$ matrix of phase codes. In order to validate that the whole demodulation processing chain is working correctly, these phase codes need to be mapped and reshaped back into the bitstream that was initially encoded. This subsection therefore aims to decode the output of the demodulation procedure and compare it to the originally encoded bitstream. This allowed for the validation of both the decoding procedure and the complete cascaded preprocessing, demodulation and decoding procedures. A limitation of the validation procedures is the use of a single RadCom DAB mode. Therefore to validate the cascaded chains across *varying* DAB modes a looping cascaded validation test was developed. This involved varying all the DAB mode parameters and running multiple complete validation tests.

This required generating and processing waveforms using every possible combination of parameters shown in Table 5.2 while using a BER as the validation mechanism. On every iteration a new bitstream is generated and modulated onto the waveform while length of the bitstream was added to a

total bit counter. At the output the of processing chain the encoded and decoded streams are compared and the total number of differing bits added to an error counter. These counters are summed across multiple tests with the resulting BER being calculated. The BER across all the tests was determined to be zero. This validates that the complete chain, including the decoding stage, was working not only for a single DAB mode but for varying DAB modes.

Parameter	Name	Description
K	Carriers	$[500, 750, 1000]$
L	Symbols	$[3, 5, 8]$
T_u	Integration Period	$[1024, 2048, 4096]$
T_g	Guard Interval	$[0, 504]$
T_d	Delay Time	$[4096, 8192]$

Table 5.2: Showing the set of parameters used to conduct preprocessing, demodulation and decoding processing chain validation tests

Chapter 6

Radar Processing Chain

'The man who moves a mountain begins by carrying away small stones'
— *Confucius*

This chapter covers the implementation of ambiguity function generation and range Doppler map processing. Ambiguity function generation is limited to the frequency domain implementation previously discussed in subsection 6.1. Following the development of this analytical tool, time domain range Doppler processing is introduced using two distinct sub-processes. The first covers a time alignment procedure that aligns the surveillance and reference channel. This is required as this investigation implements passive range Doppler processing. The second and final sub-process includes the cross-correlation of the reference and surveillance channels, followed by an FFT'ing procedure resulting in the generation of the range Doppler map. These processes are additionally validated for correct functionality using FERS simulations and hardware loopback tests.

6.1 Ambiguity Function

The ambiguity function is not strictly required to meet the RadCom system specifications but is included for analysis purposes. This because it is a useful tool for analysing waveforms for radar applications as it provides one with the ability to understand and predict ambiguities that would occur on range Doppler maps. In order to generate the ambiguity function one is required to implement Equation 2.8.

The first requirement to generate the AF using Equation 2.8 is the complex envelopes $x(t)$. Using this envelope one may either generate the AF in the time or frequency domain by first additionally computing the matched filter $h(t)$. This investigation has taken the frequency domain approach. Therefore the computation of the *frequency domain* representation (the Fourier transform) of these complex envelopes was required. This is shown in Algorithm 6.

Recall that multiplying these two arrays together and taking the inverse Fourier transform is equivalent to time domain convolution. Therefore the computation of the delay response has been completed. Only the Doppler mismatch as described in Equation 2.8 remains to be implemented. The frequency domain implementation of AF generation provides a simple method for completing this task. This requires one to element-wise shift the H in the algorithm below which leverages the following Fourier transform property: $exp(j\omega_0 t)x(t) \leftrightarrow X(\omega - \omega_0)$. Computing the multiplication of the X and H with

these progressive shifts (as shown by the for loop in Algorithm 6), storing them, and taking the inverse Fourier transform will result in the generation of an AF.

inputs : Complex envelope, x;
Maximum Doppler bound shift v;
output : Ambiguity function , AF
begin
$X \leftarrow [\, zeros\{\, v \,\}\ \ FFT\{\, x \,\}\ \ zeros\{\, v \,\}\,]$
$H \leftarrow [\, zeros\{\, v \,\}\ \ FFT\{x_{*}\}_{\ zeros\{\, v \,\}}]$
while $(\, i\ \ in - v : v \,)$ **do**
$AF[i, :] \leftarrow X \odot circshift\{\, H \,, i \,\}$
end
$AF \leftarrow abs\{\, IFFT\{AF\}\,\}$
end

Algorithm 6: Showing the generation of a ambiguity function using a frequency domain processing

6.2 Range Doppler Map Processing

Range Doppler map generation, alongside ambiguity function generation, directly addresses the objectives of this investigation. It achieves this through the implementation of a passive processing technique. This therefore requires the use of two signals, the reference and a surveillance signal. These signals, used to generate a range Doppler map, must be aligned in time *before* range Doppler processing may be completed. This provides a clear separation in the processing stages, resulting a time alignment and range Doppler computation procedures. This division in shown in the Diagram 6.1. Finally, although range Doppler processing may be completed in the frequency domain, time domain processing has been selected as frequency domain processing has been implemented in the generation of the AF's.

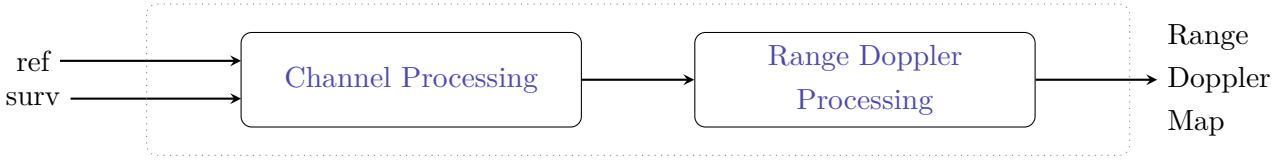

Figure 6.1: Showing passive range Doppler map generation using channel alignment and range Doppler procedures

6.2.1 Channel Processing

Channel processing encompasses three functions. These include channel alignment, transient removal and slow time slicing. The channel alignment procedure is important as it is implemented *in conjunction*

with both transient removal and slow time slicing. This is as one may face uncertain delays while using the SDR platform resulting in inconsistencies in transmission timing.

Channel Alignment

The uncertain delay problem is covered in detail in Chapter 7. This procedure accounts for the SDR platforms communication delays between a command to transmit and the actual transmission of a signal. This variable delay is introduced at every transmit command and therefore occurs in *every* slow time interval. This requires the processing stage to align every slow time interval. This procedure is shown in Algorithm 7.

inputs : Reference data, ref;
Surveillance data surv;
Matched PRS filter mf;
output : Reference data, ref;
Surveillance data, surv;

begin

$S_{slowSlice} \leftarrow \text{ref}[1 : PRT]$

$S_{slowResponse} \leftarrow S_{slowSlice} * mf$

$I \leftarrow \text{maxIndex}\{S_{slowResponse}\}$

$\text{ref} \leftarrow \text{ref}[I : end]$

$\text{surv} \leftarrow \text{surv}[I : end]$

end

Algorithm 7: Showing the channel alignment procedure implemented for every slow time slice due to the SDR uncertain delay problem

This procedure involves the alignment of the surveillance channel with respect to the reference channel using the PRS that is known *a priori*. Therefore the reference channel has its PRS aligned to the zero time position with previous additional samples discarded as these are attributed to the variable delay. This is done using convolution as show in Algorithm 7. The same number of samples are removed from the surveillance channel. In doing so the channels are independent of the transmit delays and aligned as both the surveillance and reference channel transmission occurred at the same time. This procedure is shown in Algorithm 7.

Transient Removal

With the procedure for channel alignment introduced, transient removal while maintaining channel alignment may be covered. The motivation for introducing transient removal is because some platforms may experience transient responses at the beginning of operation. This leads to the raising of range Doppler map noise floor. This procedure therefore requires incremental slow time steps through a data stream combined with the time alignment procedure. This is followed by discarding each step until a step threshold has been met, the remaining signal, with the transient removed, is then passed to the range Doppler processing operation.

Slow Time Slicing

With the two channels aligned and the transient response removed the final stage of range Doppler processing may be completed. This requires slow time slicing and storing the data as a matrix[1]. The data stream is split into a matrices of $N \times (PRT \times F_s)$ samples. As a useful visual, the result of this procedure is the first image shown in Figure 2.2.

This procedure follows the same logic as that described by Algorithm 7 but instead of removing slow time slices they are stored. Finally, recall that this investigation takes a passive approach to range Doppler processing and such both a reference and surveillance slow time matrix are created and stored for further processing. The procedure to generate these two matrices is shown in Algorithm 8.

inputs : Reference data, ref;
Surveillance data surv;
Matched filter mf;
Number of pulses, N;
output : Reference slow time slices, ref_{st};
$Surveillanceslowtimeslices, surv_{st}$;

begin
  while $(n < N)$ **do**
    ref ,surv $\leftarrow$ alignChannel$\{ref, surv, mf\}$
    $\text{ref}_{st}[n, :] \leftarrow \text{ref}[1 : PRT]$
    $\text{surv}_{st}[n, :] \leftarrow \text{surv}[1 : PRT]$
    ref $\leftarrow$ ref$[PRT : end]$
    surv $\leftarrow$ surv$[PRT : end]$
    n$\leftarrow n + 1$
  end
end

Algorithm 8: Showing methodology to slice reference and surveillance data into slow time matracies

6.2.2 Range Doppler Processing

Matching

Following the slicing of the data, matched filtering was completed. Although frequency domain processing would have decreased processing time, time domain processing was implemented as frequency domain processing was demonstrated in AF generation. This matching procedure followed an approach similar to that of standard pulsed processing through the implementation of a filter formed using time reversed conjugates of the reference channel slow time intervals. Prior to the convolution there were two matrices of size $N \times (PRT\, F_s)$ in size. After convolution, the resulting array would be

[1] In the context of a pulsed radar systems these slow time slices are considered to contain pulses. This terminology is maintained but within the context of the RadCom system pulses are considered identical to the non zero portion of the communications frame

$N \times (2\,PRT\,F_s + 1)$. The resulting matrix is therefore cut down to $N \times (PRT\,F_s)$ by removing the first $(PRT\,F_s + 1)$ samples. This allowed for the removal the additional sample's introduced during the time domain convolution.

Pulse Cancellation - Optional

Feed-through has been and will be discussed in subsections 2.4.4 and 7.2. Its effects may be reduced by re-configuring hardware but not fully removed. Therefore, to reduce its effects pulse cancellation was implemented within the radar processing chain. This involved iterating through $N + 1$ matched filter responses and storing the value of $P_N - P_{N-1}$ as the new slow time matrix.

Doppler FFT

With the matched filtering procedure completed (and pulse cancellation optionally applied), N slow time slices remain. These slices still contain unused Doppler phase information. Therefore as discussed in section 2.1.5 a FFT along the slow time dimension is computed. The output of this procedure is the completed range Doppler map.

Clutter Map Removal - Optional

These range Doppler maps will be limited to detecting static targets outside of the regions effected by feed-through. Pulse cancellation allows for improved detection performance of moving targets but does not improve detection performance of static targets within this region. Therefore an additional processing technique was developed for the processing chain.

clutter map removal involves imaging and computing the range Doppler map of an environment prior to the placement of a target. Once the static target had been imaged the clutter map can be subtracted from the computed range Doppler map which results in the increased detectability of the static target.

6.3 Validation

This section is intended to demonstrate and verify the radar processing chains ability to correctly generate range Doppler maps. The simulation was completed using FERS with the intention to demonstrate the correct range and Doppler offset determination. This validation procedure does not include the full demonstration of the channel processing functionality as usage of the testbed is out of the scope of this Chapter. A complete demonstration of the testbed and the channel alignment procedure are demonstrated in Chapter 7.

6.3.1 FERS Simulations

Simulations were completed using FERS, a simulator designed by [18] allowing for the simulation of complex radar environments. The simulator provides the ability to simulate an arbitrary number of transmitters and receivers which can transmit and receive both pulsed and continuous waveforms [18]. These waveforms may be generated externally and used within simulations, providing the ability to use RadCom signals generated by the Signal Generation Chain. Finally, the simulator additioanlly

allows for the placement, movement and selection of individual target RCSs.

This validation procedure is therefore divided into three sub-procedures. These include the design of the FERS simulation environment (encompassing the description of hardware and targets), the generation of the waveform for the simulation and finally, the processing of the data generated from the simulation.

The configuration of FERS itself can be quite involved and as such a high level overview of the simulation environment will be covered. This is not limited to but includes parameters such as sampling rates and transmission power. A complete overview of the simulated hardware parameters are shown in Table 6.1.

Parameter	Value
Sampling Rate	4.096 MHz
Transmission Power	0.01 W
Carrier Frequency	2.45 GHz
Tx Position	(0,0.05) m
RX Position	(0,-0.05) m

Table 6.1: Showing the simulation parameters used for the FERS simulation

With the simulated hardware configured the RadCom waveform could be designed and generated. The parameters for this waveform are shown in Table 6.2

Parameter	Value
F_{iq}	4.096 MHz
f_c	2.45 GHz
K	500
L	2
T_u	2048
T_g	504
T_d	5104

Table 6.2: Showing the waveform parameters used for the FERS simulation

As the simulated hardware and waveform had been configured and generated, a target was 'placed' in the simulation environment. This targets parameters are shown in Table 6.3.

Parameter	Value
Target Range	0.1 km
Target Velocity	6.67 ms^{-1}

Table 6.3: Showing the target range and velocity for the ??

To appreciate the simulation, notable aspects are discussed. The first is that the simulation makes use of two antennas, one for transmission and one for reception. These antennas are transmitting and receiving continuously, therefore from the instant the simulation begins they read/write to or from files. Notably, the transmit antenna operates continuously as delays in pulsed transmissions are incorporated into the waveform itself.

Range Doppler Map Validation

With the simulation parameters configured, the simulation was run. The resulting data was processed by the chain covered in section 6.2. The output range Doppler maps of the processing procedure are shown in Figure 6.2 and warrant further explanation as there some results that may not be immediately apparent.

The first sub-plot, the left most, demonstrates standard range Doppler map processing without the introduction of pulse cancellation. Although it is possible to see a faint target around the 100 m 6.67 ms^{-1} mark, at ±80 dB below the normalised peak it implies this response may not be visible in a real world test. The second sub-plot demonstrates the effect of pulse cancellation. The large zero Doppler response, due to feed-through, has effectively been removed with the resulting normalised peak at the 100 m 6.69 ms^{-1} position clearly visible. Finally, the third plot, the right most subplot, has thresholding applied to it such that all signals 30 dB below the max appear as a constant value. This is simply meant as a visual method to accentuate the presence of a target.

When comparing the target placed in the simulation to that shown in Figure 6.2 one can see that both range and Doppler match. This therefore validates that the radar processing chain is functioning correctly.

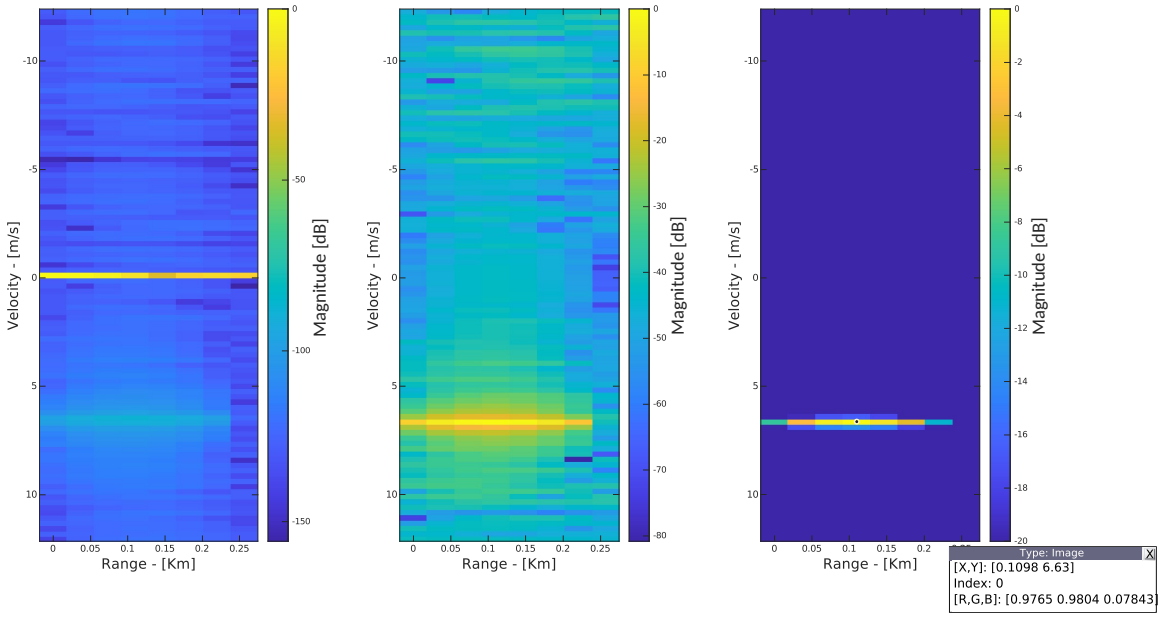

Figure 6.2: Showing the range Doppler map of the FERS simulation with a target at a range of 100 m and a velocity of 6.67ms^{-1}

Chapter 7

Hardware Testbed

> 'There will always be rocks in the road ahead of us. They will be stumbling blocks or stepping stones; it all depends on how you use them'
> — *Friedrich Nietzsche*

The testbed is fundamental to the demonstration of the RadCom system but faced inherent complications. This investigation addressed these complications surrounding isolation and timing motivating the final system configuration. This chapter will therefore begin by introducing the reader to the hardware used to operate the testbed while additionally demonstrating the complications of using the SDR platform. Once familiar with the hardware, system configuration and software will be reviewed. Validation tests demonstrating the correct transmit, receive and timing functionality are additionally included in this chapter.

7.1 Hardware Overview and Configuration

USRPs are the National Instruments Universal Software Radio Peripherals which are SDR platforms available for use in this investigation. Specifically, this investigation used the Ettus N210 as the selected SDR platform. These devices have a single transceiver card slot, a MIMO cable for shared references and communications and are capable of performing timed FPGA commands [19]. Using the SBX transceiver daughter board provides the Ettus with the respective frequency coverage and maximum analog bandwidth of 400 MHz - 4.4 GHz and 40 MHz. It has two antenna ports which are both able to operate as receivers while only a single port may transmit. These USRPs were used in conjunction with coffee can antennas with respective lengths and face radii of 15.5 cm and 5 cm which respectively are designed to operate at 2.4 GHz. These antennas provide a gain of 7.2 dBi and have a half power beamwidth of 72°. This hardware was configured as shown in Figure 7.1 for development and testing. Appendix C shows the actual hardware configuration used to conduct testing.

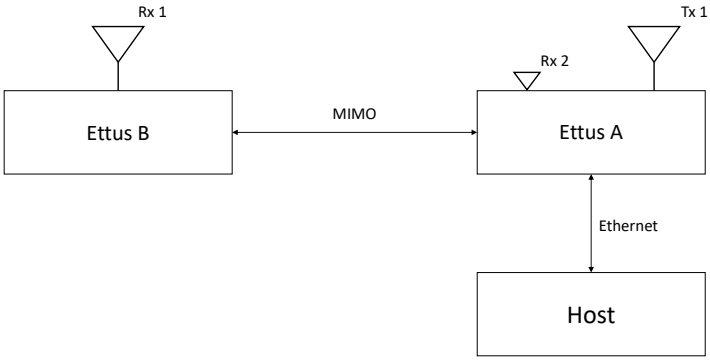

Figure 7.1: Showing the hardware configuration used to conduct demonstrations of the RadCom system

Two USRPs were used in this configuration: Ettus A and Ettus B. These were connected using a MIMO cable thereby allowing for the use of the same time reference for timed commands. Ettus B used a single receive port while Ettus A used two ports for transmission and receival. A host PC was additionally connected to Ettus A. This PC, via an ethernet cable, provided the USRPs with instructions, the waveform to transmit and additionally received and stored each receive datastream (from Rx 1 and Rx 2).

Coffee can antennas were connected to Tx 1 and Rx 1 allowing the testbed to transmit and receive waveforms while Rx 2 was terminated in a 50 Ω resistor. Rx 2 is denoted as a receive port because it is sampled during operation. This was to measure the isolation signal as a zero range reference signal and by extension allowed one to account for random delays. This is the same reference signal used by the radar processing chain.

7.1.1 Hardware Limitations

To motivate the selected hardware configuration it is useful to introduce the limitations of the Ettus N210, and therefore how the testbed configuration addresses them. These limitations surround port isolation, multi-usrp coherency and SDR communication delays.

Isolation

The Ettus N210 with an SBX daughter board as previously stated has two antenna ports. In the transceiver configuration, one for transmission and one for reception. While transmitting and receiving simultaneously, the receiver experiences feed-through. This is an issue as the received power is orders of magnitude less than the feed-through power and would therefore result in reduced radar performance.

This is the motivation for the use of the MIMO configuration shown in Figure 7.1. Feed-through is inversely proportional to distance, therefore increasing the distance between the transmit and receive antennas will reduce the feed-through level. The MIMO cable achieves this by allowing for transmission on Ettus A and receival on Ettus B thereby increasing the distance between the two ports.

As a demonstration, Figure 7.2 shows the isolation levels of the testbed configuration shown in Figure 7.1. The transmit level of Tx 1 was 30 dBm. Rx 2 on Ettus A has a feed through power level of

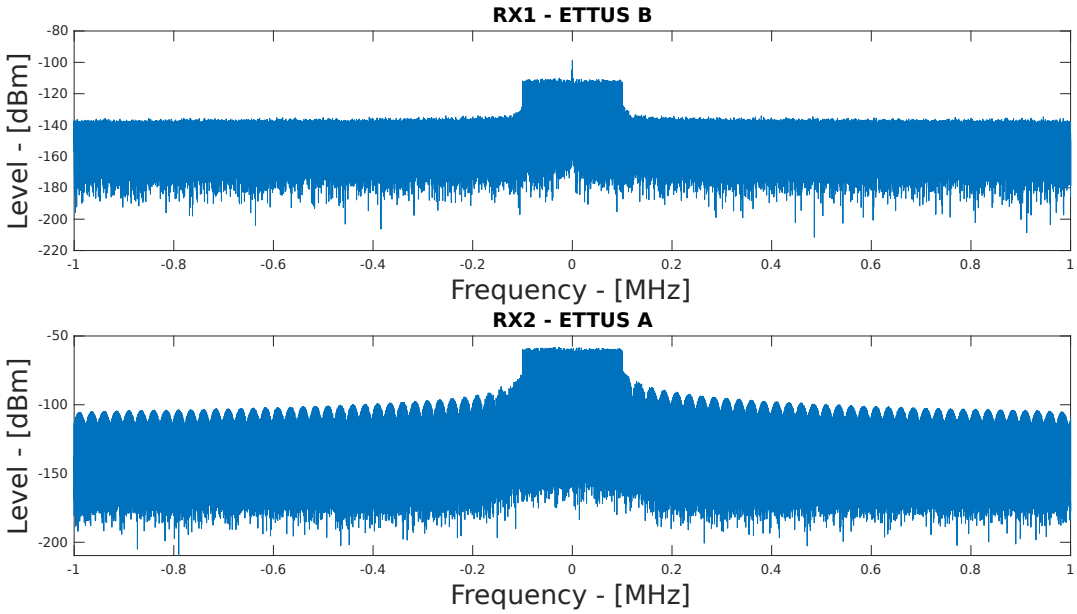

Figure 7.2: Showing the larger isolation level between an Rx 1 and Tx 1 versus the isolation level between Rx 2 and Tx 1

-60 dBm, resulting in the port having an isolation level of -90 dB. This is compared to Rx 1 on Ettus B with a feed-through power level of -110 dBm, giving it an additional 60 dB of isolation and a total isolation level of 150 dB.

Coherency

The use of the MIMO cable introduces a complication. Each device uses its own oscillator, implying that there is a non-coherent relationship between the transmitting and receiving USRPs. If one intends to use processing techniques such as coherent integration, one is therefore required to synchronize these two devices. This is a possible and implemented using the uhd c API.

Communication Delays

USRPs additionally face communication delays due to their requirement to communicate with the host PC. These communication delays encompass the transmission, propagation and processing delays introduced by both the PC and USRPs. These delays are uncertain and variable implying that delays before transmissions are also uncertain and variable.

While the communication delays occur, the USRPs still run their core processes. This poses a challenge as while Ettus A may wait to receive a signal to transmit, Ettus B would still record data. This would introduces additional samples into the recorded data stream that are *unaccounted for*.

The effects of these additional samples (introduced because of these delays) are demonstrated using range Doppler processing. If one completes a cabled loopback test, one should expect the emulated target to appear at a range corresponding to the time it takes for the signal to pass through the cable. The right sub-plot of Figure 7.3 demonstrates the radar processing chains operation without the adjustments for this random delay. With no adjustments no target is apparent. Using the processing

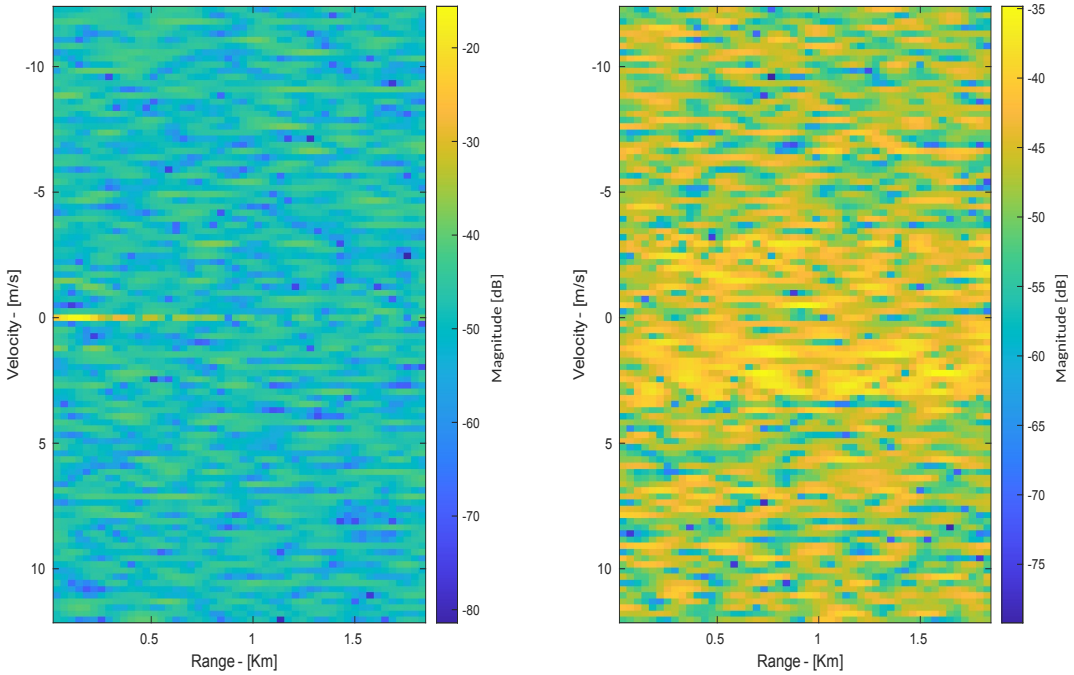

Figure 7.3: Showing the effect of communication delays accounted for (left) and unaccounted for (right) on a range Doppler plot

technique introduced in Subsection 6.2.1 accounts for this delay (through the removal of the unaccounted for additional samples) and allows for the generation of the left subplot.

7.1.2 Testbed Software Outline

The testbed as shown in Figure 7.1 was operated using software that performed multiple procedures. These are shown in Figure 7.4 and begin with the initialisation of communications between the two USRPs. With communications established, transmit and receive parameters were configured. Once configured, the transmit and receive threads were created and streaming began. This continued until a user interrupt was detected which halted streaming and joined all the threads. More detail on these procedures are covered below.

Initiate MIMO

The first procedure initialised MIMO communications using the MIMO cable as shown in Figure 7.1. This required the creation of two abstracted software USRP structures where Ettus A was configured as master and Ettus B as slave. In this configuration Ettus B reference time and clock source was the time and clock source of Ettus A.

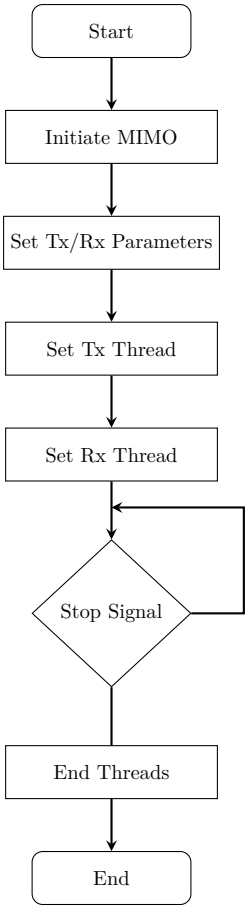

Figure 7.4: Showing the start up procedure followed by the two Ettus 210 during testing and validation

Set Tx/Rx Parameters

Following the successful initialisation of MIMO communications, the transmit and receiver parameters were set. These includes the following:

- **Tx Rate** - The transmission sample rate
- **Rx Rate** - The receival sample rate
- **Tx BW** - The transmission bandwidth
- **Rx BW** - The receival bandwidth
- **Tx args** - The transmitter Ettus A IP address
- **Rx args** - The receiving Ettus B IP address
- **Fc** - The carrier frequency
- **Type** - The data type to read and write to and from the binary files

Important to this procedure is the simultaneous setting of the carrier frequency on both devices. This was done using timed commands and enabled coherency between Ettus A and Ettus B.

Start Tx Thread

Following the configuration of the Tx parameters a Tx thread was created. This allowed the USRP to repeatedly transmit complex data from a binary file on the host device. Fundamental to this operation was the timed stream command. This forced the thread to wait until an internal time was met before beginning the operation. This allowed data to be moved into the transmit buffer *after* the timed command was set but *before* Ettus A began transmitting. This prevented transmissions beginning followed by buffer filling operations thereby preventing the introduction of additional (non-communicaiton) delays. This would otherwise introduce range errors into the radar measurements. This timed command additionally allowed for the transmit and receive thread to be set to begin at the same time.

Start Rx Thread

After setting the timed command for the Tx thread to begin, an Rx thread was created. This thread constantly moved data from the RX buffers to the host and stored it (as the predefined data type) in a

binary file. This thread was additionally provided a stream command with the *same* begin time as the transmit thread. This allowed for time synchronisation between transmission and receival. With this completed, transmission and receival began once the internal time threshold had passed.

Stop Signal

These threads ran continuously until the stop command was issued by the user. Upon detection of the command the transmission and receival were halted.

End Threads

The final procedure to conclude operations took the halted threads and joined them to the main thread. With this completed the program had concluded operation.

7.2 Validation

These validation tests were conducted in order to verify the correct functionality of the testbed. This included verifying that the testbed was able to correctly record and transmit known LFM and OFDM signals. Additionally, transmission and receival were performed simultaneously to verify that neither operation hindered the other. With these verification procedures completed field tests could then be conducted.

7.2.1 LFM Input

The first validation test verified the correct recording functionality of the testbed. This was completed through the transmission of a known LFM waveform through a variable attenuator into a receive port (Rx 1 shown in Figure 7.1). The LFM waveform with a sweep bandwidth of 200 MHz, sweep rate of 0.5 ms and a carrier frequency of 2.45GHz was generated using a Rhode & Schwartz SMF 100A. This signal was measured using Agilent FieldFox to verify that it was correctly generated. This is shown in Figure 7.5 and shows the expected 200 MHz bandwidth.

Figure 7.6 shows a sample of the generated recorded binary file (by the USRP testbed) in both time and frequency. The top subplot of Figure 7.6 demonstrates that the sweep time is 0.5 ms while the second subplot demonstrates that the signal bandwidth is 200 MHz. These are the expected results and therefore verify that the testbed is correctly recording signals.

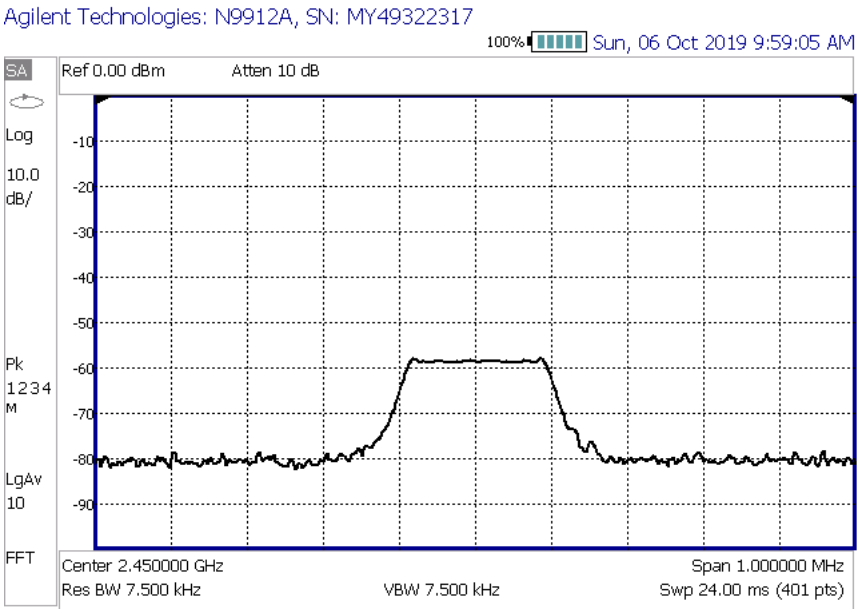

Figure 7.5: Showing the measure spectrum of an LFM output from the signal generator

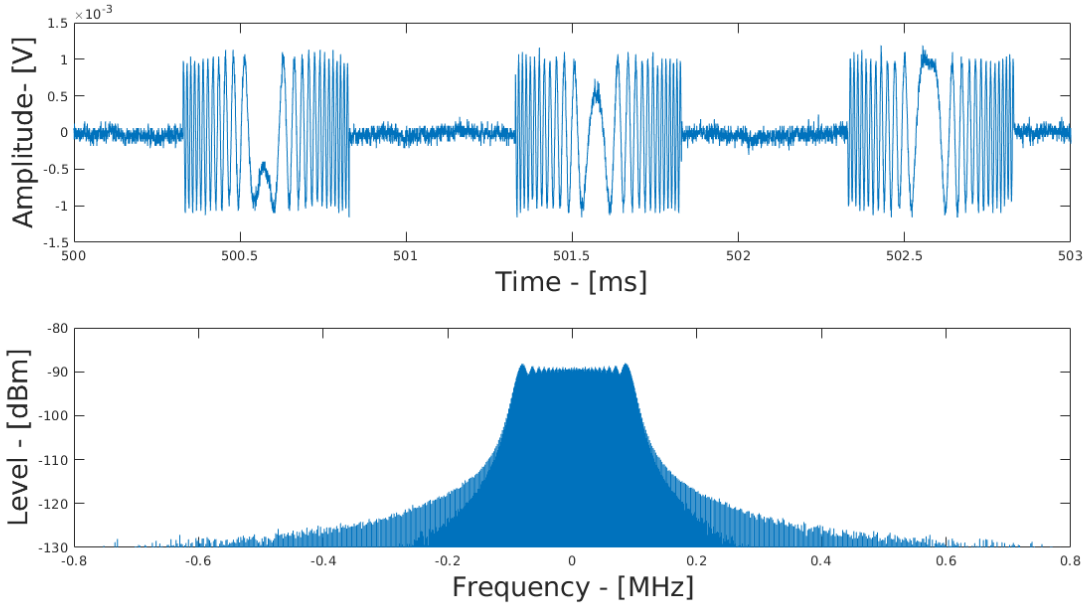

Figure 7.6: Showing the recorded time and frequency domain output LFM signal measured directly from the signal generator with a bandwidth of 200 MHz and sweep time of 0.5 ms

7.2.2 OFDM Output

Following the validation of the ability to record data, the ability to transmit data was tested. Using the Signal Generation Chain an OFDM signal was generated with the parameters shown in Table 7.1 for transmission. The single symbol used for the test is the PRS. The output of TX 1 was measured using the Agilent FieldFoxs max hold function, a function that allows the output to remain at the maximum recorded level. The output of this test is shown in Figure 7.7. The bandwidth of this signal was compared to the theoretical expected bandwidth. These two values were both 1.5 MHz and therefore validated the transmission functionality of the Ettus.

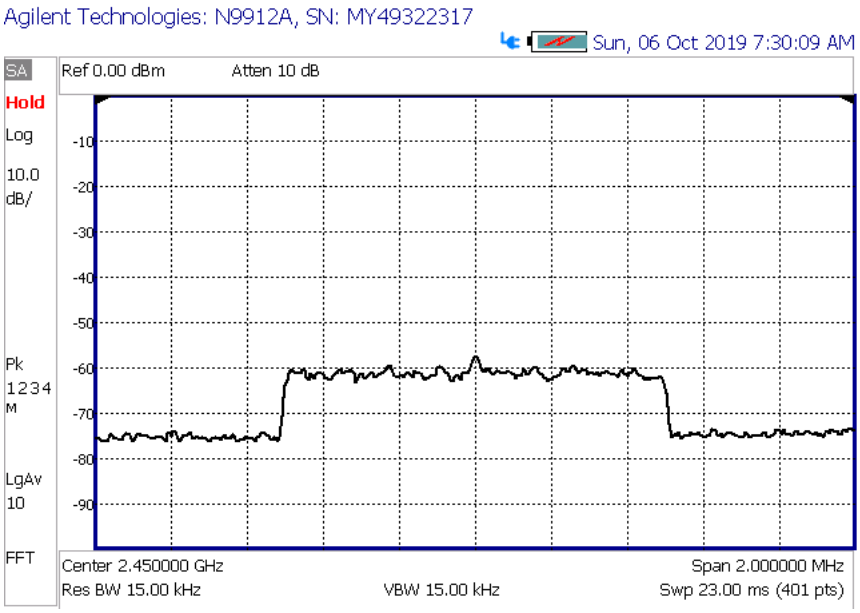

Figure 7.7: Showing measured spectrum of Tx 1 port of Ettus A while transmitting and OFDM signal with a bandwidth of 1.5 MHz

7.2.3 Direct Loopback

To validate the testbeds ability to correctly time transmission and reception (in conjunction with the radar processing chain), a direct loopback test through a variable attenuator was completed. In this configuration the path between the transmit and receive antenna was less than 0.5 m. Repeated transmissions through the path using the waveform parameters is described by Table 7.1.

Parameter	Value
F_{iq}	2.45e9
f_c	4.096e6
L	1
K	1500
T_u	2048
T_g	0
T_d	2048

Table 7.1: Showing RadCom DAB parameters used for direct path loopback test

Using these parameters one can determine a single range bin to be 30 m wide. Therefore the expected response should occur in the first range bin. This is where the maximum response occurs on the (normalised) range Doppler map generated using the Radar Processing Chain in Figure 7.8. This therefore validated the correct timing functionality of hardware testbed while also validating the channel alignment procedure developed in the Radar Processing Chain.

Figure 7.8: Validating the ability of the testbed to correctly generate a range Doppler map in a direct loop back configuration

7.2.4 Cabled Loopback

Using the signal parameters in Table 7.2 the ability to correctly determine range could also be validated. This was completed through the connection of a delay line of 100 m between the Tx 1 transmit and Rx 1 receive ports of the testbed.

Parameter	Value
F_{iq}	$2.45e9$
f_c	$2.048e6$
L	1
K	1500
T_u	2048
T_g	0
T_d	2048

Table 7.2: Showing system parameters used for delay path loopback test

The speed of light in this delay line is 83 % that in free space. Therefore although the cable is 100 m long, the actual time the signal will take to propagate from transmit to receive corresponds to a free space propagation distance of 120 m. One should therefore expect the response to occur in the 120 m range bin. Figure 7.9 shows this with the maximum normalised response occuring in the 120 m range bin therefore validating the correct channel timing and range determination functionality of the testbed.

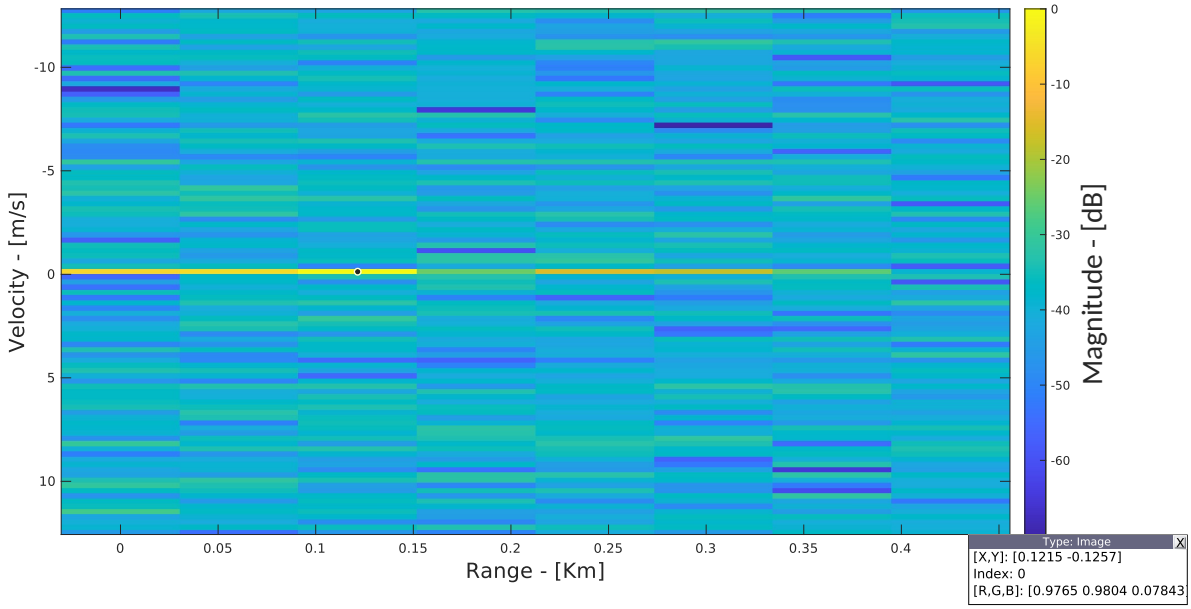

Figure 7.9: Showing range Doppler plot of the 100 m cabled loopback test with a target appearing at a range of 120 m

Chapter 8

System Integration Tests

> 'It ain't what you don't know that gets you into trouble. It's what You know for sure that just ain't so'
>
> — *Mark Twain*

In review, the signal processing sub-systems of the RadCom system have been developed and validated. Furthermore, the RadCom testbed was also tested and validated for correct functionality within the lab environment. With functionality demonstrated, field tests were conducted to demonstrate operability outside of the FERS and lab environments. These tests aimed to demonstrate the dual radar and communications functionality. This included a direct link communications test, a static range test and finally moving target tests.

8.1 Communications Demonstration

8.1.1 Method

The communications test faces complications in its experimental design. This is due to the presence of the previously discussed feed-through. As demonstrated in subsection 7.1.1, above certain transmission and receive gains, the feed-through signal is present at the receive port on Ettus B (of the setup shown in Figure 7.1). Therefore in order to conduct this test the transmit and receive gains were each set to 0 dB. A test waveform was transmitted prior to the communications demonstration to ensure there was no measured feed-through on Rx 1.

With no feed-through present, the transmit and receive antennas were pointed towards one another while separated by 2 m. Additionally to avoid the risk of excessive power being transmitted directly towards Rx 1, the transmit antenna was directed such that the signal was transmitted towards the receive antenna through a sidelobe.

With the hardware positioned and transmission levels set, the remaining parameters of the SDR platform were set. This included all parameters except those describing the baseband waveform. Therefore parameters such as the carrier frequency, sampling rates (transmit and receive) as well the transmit and receive bandwidth were set. These parameters are shown in Table 8.1.

Parameter	Symbol	Value
Tx Gain	-	0 dB
Rx Gain	-	0 dB
Tx Bandwidth	-	1.1 MHz
Rx Bandwidth	-	1.1 MHz
Sampling Rate	F_{iq}	5 MHz
Carrier Frequency	f_c	2.45 GHz
Read Type	-	Float
Write Type	-	Double

Table 8.1: Showing SDR platform parameters used during the direct link communications test

With the SDR platform configured, the waveform parameters were selected. The description of these waveforms are covered in Chapter 4 with a summary of their parameters shown in Table 8.2. To test this waveform, *at least two* symbols needed to be transmitted, the first and second were the PRS and a data carrying symbol respectively. Finally, the NS was not included in the waveform due to the inclusion of the delay time and the implementation of fine time synchronisation using the PRS.

Parameter	Value
F_s	4.96 MHz
K	500
L	2
T_u	2048
T_g	504
T_d	5104
P	1

Table 8.2: Showing dab mode configuration used during the direct link communications test

With the parameters set, the waveform was generated and resampled to the hardware sampling rate. This waveform was transmitted, received and stored. This received waveform was processed by the communications processing chain with the BER used to evaluate system performance.

8.1.2 Results

The first result shown in Figure 8.1 demonstrates the feed-through levels at Rx 1 and Rx 2. Rx 1, the port on which the communications test was conducted was demonstrated to have a feed-through level below the noise floor. This is compared to Rx 2 which was demonstrated to have a feed-through level of -80 dBm. Figure 8.2 shows the final communications test. The received feed-through level is still -80 dBm while the received signal level is -90 dbm.

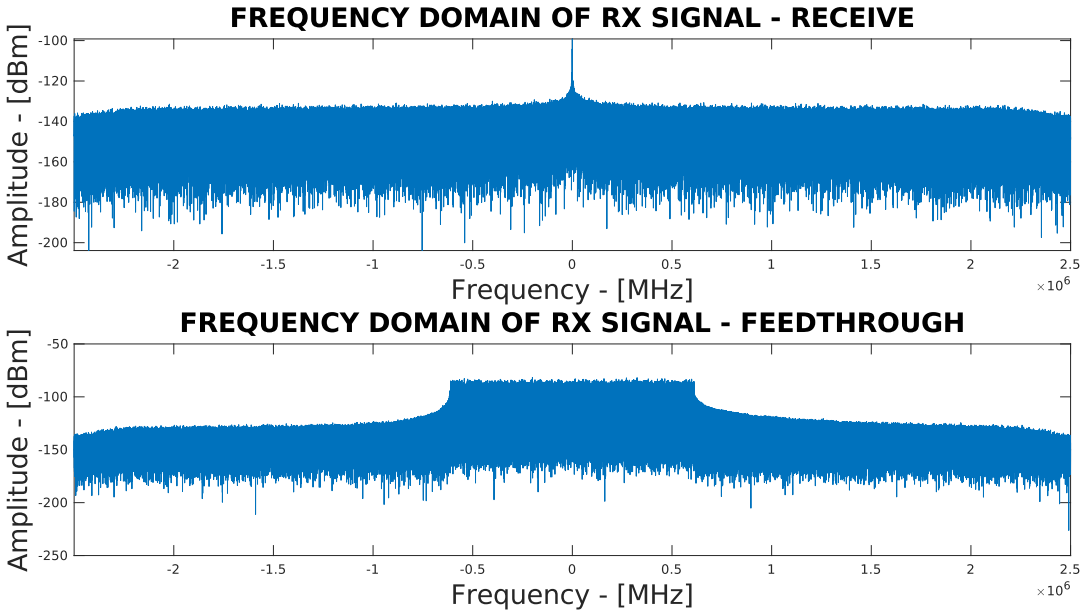

Figure 8.1: Showing received signal level at Rx 1 (top) and received feed-through level at Rx 2 (bottom) for the feed-through test

The calculated BER was 0% with the transient period removed while the BER was 0.7% with the transient period included. The BER was calculated using a single frame. This, using the parameters shown in Table 8.2, resulted in 1000 bits checked.

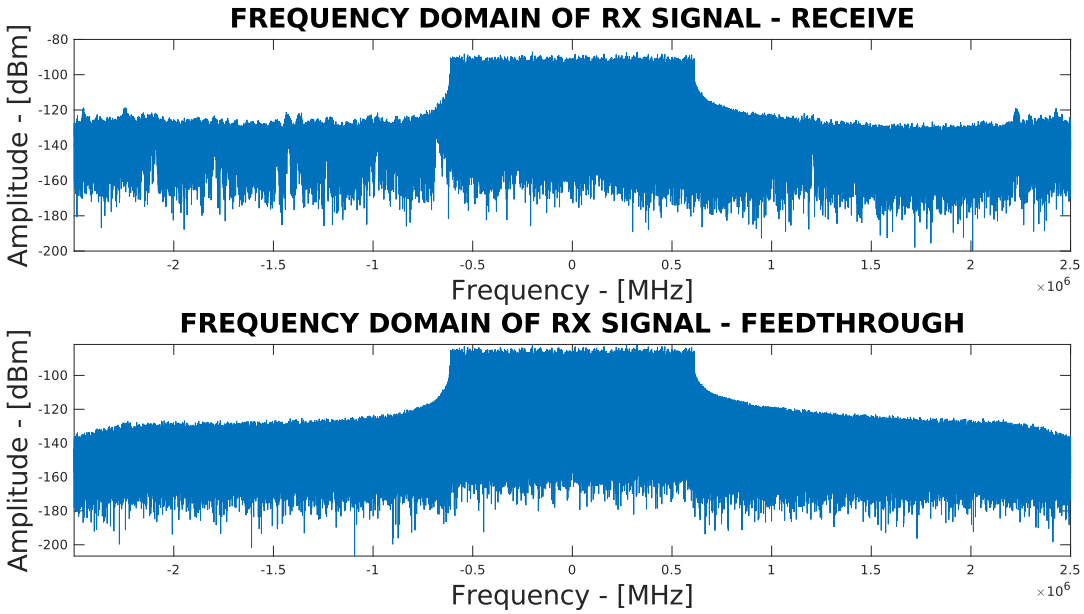

Figure 8.2: Showing received signal level at Rx 1 (top) and received feed-through level at Rx 2 (bottom) for the communications test

8.1.3 Discussion

These test results verify communications functionality of the RadCom system. This is as one may be sure that the demodulated bits are not a result of direct feed-through. This is because of the absence of a signal at Rx 1 as shown in Figure 8.1.

Furthermore, the BER rates are the expected results and demonstrate correct demodulation. The 0% BER with the transient removed is expected as this indicates the communications chain works correctly under high SNR conditions. Including the transient period results in the decrease of SNR. The expected result is an increase in the BER. This is exactly what occurs when considering the result of 0.7%.

8.2 Static Range Test

8.2.1 Method

The static range test used a Hyundai i20 with a trihedral corner reflector placed on the dashboard as the target. The test was run using the same waveform parameters shown in Table 8.2 and similar system parameters as those shown in Table 8.1. The only adjustment to these parameters is the transmit and receive gain. These were set to 30 and 20 dB. The bandwidth of this signal remained 1.5 MHz as higher data rates would result in dropped data. Two can antennas were used as the transmitter and receiver, Tx 1 and Rx 1 as shown in Figure 7.1. The antennas were fed with horizontal and vertical polarisations to increase their isolation. Rx 2 was terminated with a 50 Ω resistor and sampled, measuring the feed-through as an emulated reference channel.

With the system configured, two measurements were taken. The first was a reference clutter map measurement of the environment without a target present. The second was the range measurement with the target positioned 100 m away from the testbed. This range was selected as the testing environment was a residential road which was just over 100 m long. These measurements were stored and passed through the radar processing chain. When processing the recorded data, Rx 1 was surveillance channel while Rx 2 was considered the reference channel.

8.2.2 Results

The first result is the clutter map measurement and is shown Figure 8.3. The fist subplot demonstrates the normalised range Doppler clutter map with both channel synchronisation and transient removal applied. The second subplot implements the same procedure but additionally applies pulse cancellation. Finally, the third subplot is this same result but plotted with an adjusted dynamic range. These plots demonstrate the feed-through response and do not contain any apparent targets.

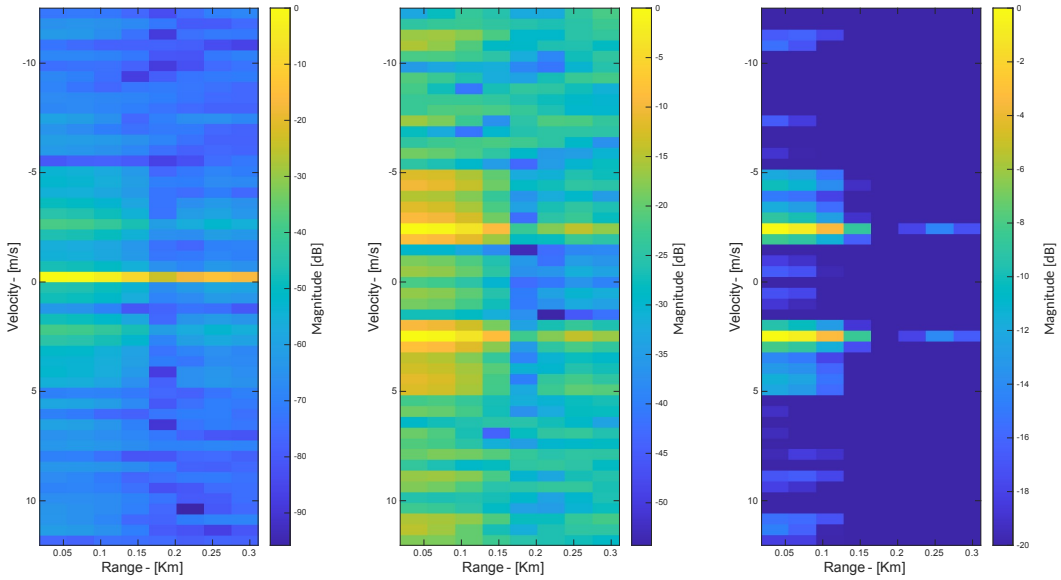

Figure 8.3: Showing a clutter map measurement of the environment where the first plot is a unadjusted range Doppler map, the second was generated using pulse cancellation and the third is the second with an adjusted dynamic range

The second result is the static range measurement of the target and is shown by Figure 8.4. The fist subplot demonstrates the normalised range Doppler map with no further processing. The second subplot demonstrates the range Doppler map with pulse cancellation applied. And finally, the third subplot demonstrates an adjusted dynamic range of the pulse cancelled range Doppler map. These plots demonstrate the feed-through response and do not appear to display a target at the 100 m range.

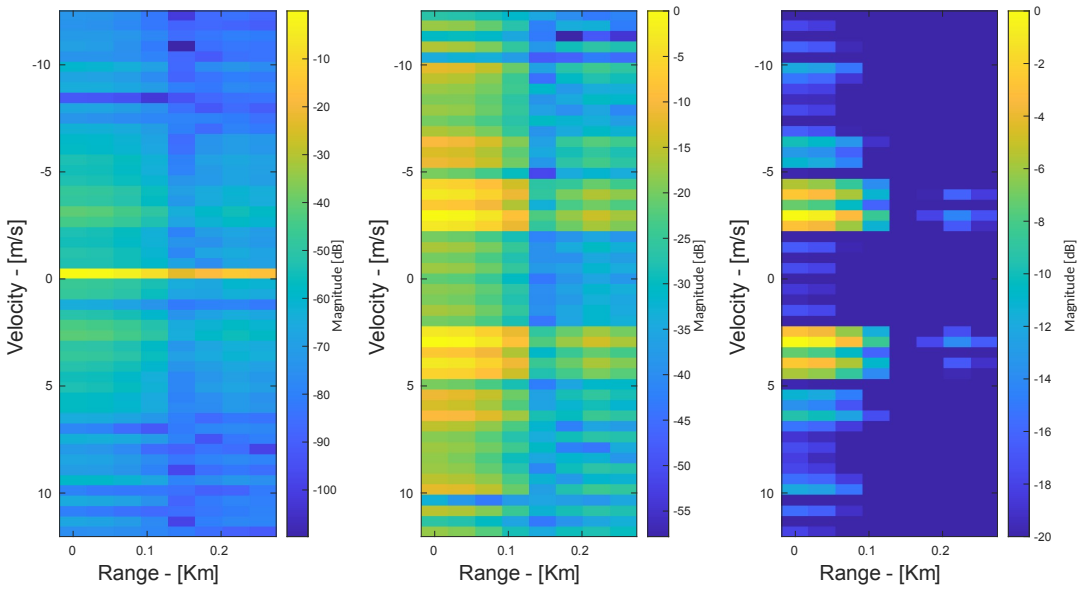

Figure 8.4: Showing range Doppler map measurement of the testing environment with a static corner reflector at 100 m where the first plot is a unadjusted range Doppler map, the second was generated using pulse cancellation and the third is the second with an adjusted dynamic range

The last result was generated using clutter map removal. This was completed through the subtraction of Figure 8.3 from Figure 8.4 without pulse cancellation applied. It demonstrates the presence of the target in the 109 m range bin once the clutter power had been removed.

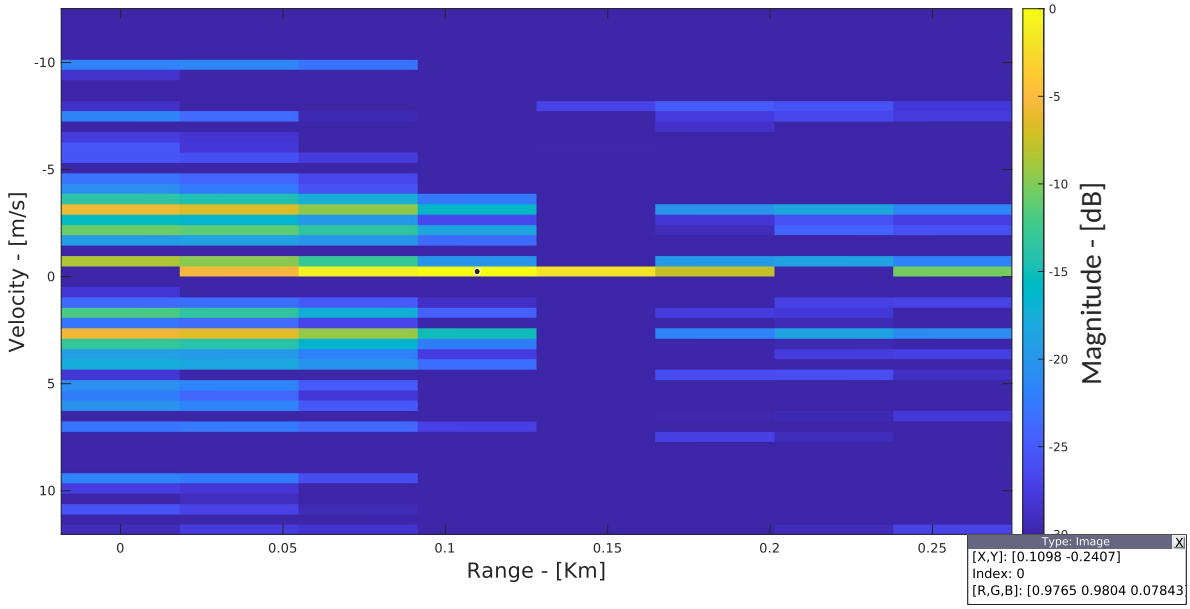

Figure 8.5: Showing the subtraction of the magnitude of the reference range Doppler map from the magnitude of the range Doppler map containing the corner reflector showing a target in the 109 m range bin

8.2.3 Discussion

The environment clutter map shown in Figure 8.3 is the expected result. It has a maximum response occurring in the 0 m range bin corresponding to the isolation and feed-through from the testbed. Additionally, when pulse cancellation is applied, as expected, there are no moving targets.

Figure 8.4 shows the response of the imaged environment with the target present at 100 m. The target is not identifiable on any of the subplots. This is expected as it is stationary and therefore the response is superimposed onto the feed-through response. Pulse cancellation is effective at removing stationary clutter and objects from a range Doppler map. For this reason pulse cancellation does not aid in the detection of the stationary target at 100 m. Other responses in this Figure are attributed to the imperfect removal of the feed-through response.

Figure 8.5 was generated using clutter map cancellation. Instead of removing stationary targets as done by pulse cancellation, this methodology removes the clutter power from the range Doppler map. With this power removed one would expect the target to appear at 100 m. This is exactly what occurs with a target response occurring in the expected 109 m range bin. The response was expected in this range bin as this is the closest range match with the actual target range of 100 m

8.3 Range Doppler Tests

8.3.1 Method

The same hardware and software setup used in Static Range Test was used to complete this test. An important difference between the two tests arise when considering the target. The first Doppler test involved the target positioned 30 m in front of the hardware and moved away from the hardware at a planned speed of 25 kmh^{-1}. The second Doppler test involved the target positioned 30 m in front of the hardware and moved away from the hardware at a planned speed of 20 kmh^{-1}. To validate the results generated by the range Doppler maps, GPS measurements, along with odometer measurements were taken.

8.3.2 Results

Figure 8.6 shows the result of the range Doppler test with the planned target velocity of 25 kmh^{-1} away from the testbed at a starting range of 30 m. The first subplot, shows the range Doppler map with additional processing while the second and third have pulse cancellation applied. The dynamic range on the third subplot was also adjusted to highlight the presence of the target.

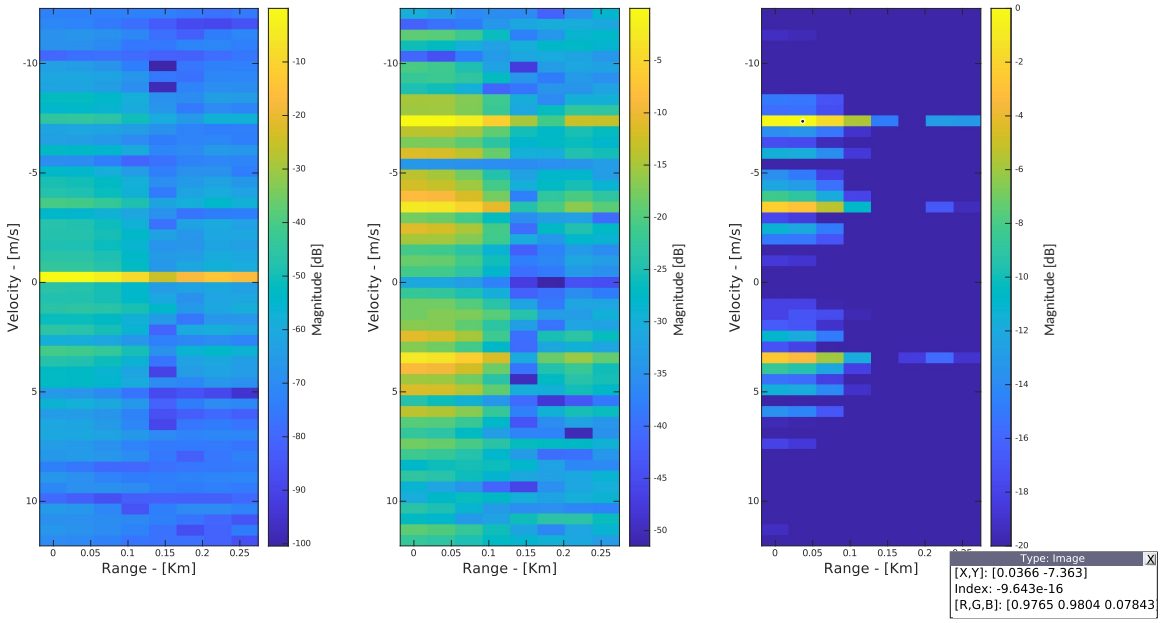

Figure 8.6: A range Doppler map showing a target travelling away from the testbed at a range of 30 m and with a measured velocity 7.4 ms^{-1}

The measured results of this test are shown in Table 8.3 with the target's true range being 30 m while the GPS and odometer velocities were 7.2 and 7.0 ms^{-1} respectively. This is compared to the measured range and velocity of 36 m and -7.4 ms^{-1} respectively.

Parameter	Value
GPS Average Velocity (ms^{-1})	7.2
GPS Average Velocity (kmh^{-1})	25.9
GPS measurements	10
Odometer Velocity (kmh^{-1})	25
Odometer Velocity (ms^{-1})	6.9
Range Bin (m)	30
True Range (m)	36

Table 8.3: Showing the true and recorded parameters of the range Doppler test with a target at a range of 30 m and measured velocity 7.4 ms^{-1}

Figure 8.7 shows the result of the range Doppler test where the target was travelling towards the testbed from a starting range of 100 m. The first subplot, shows the range Doppler map with additional processing while the second and third have pulse cancellation applied. The dynamic range on the third subplot was also adjusted to highlight the presence of the target.

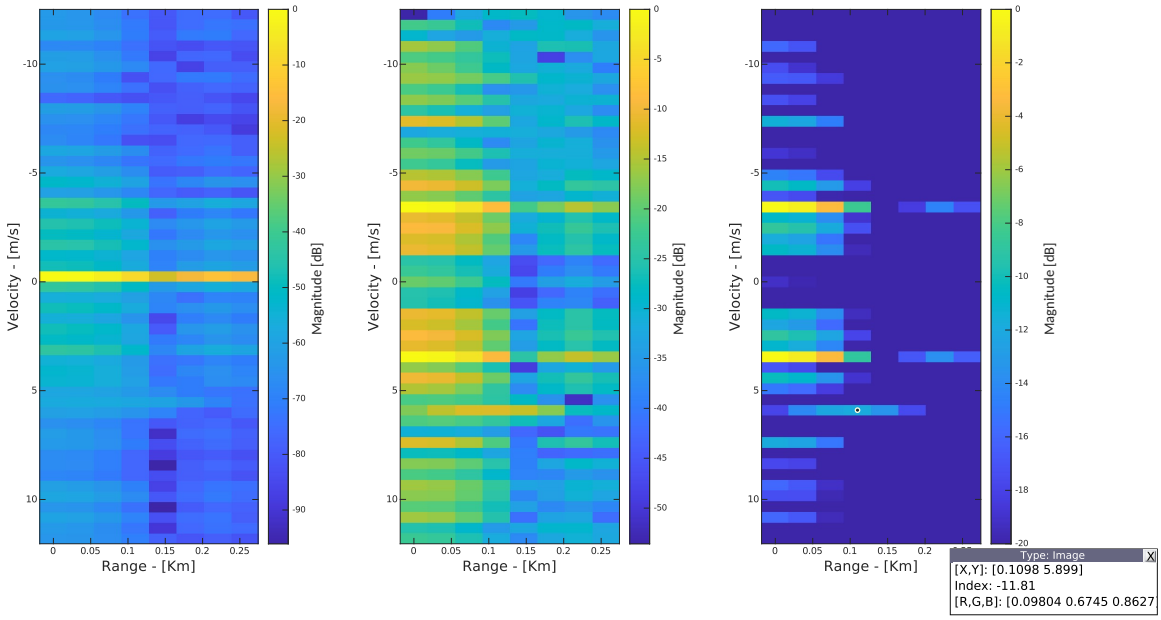

Figure 8.7: Of a range Doppler map showing a target travelling towards the testbed at a range of 100 m and measured velocity 5.9 ms^{-1}

The results of this test are shown in Table 8.4 with the target's true range being 100 m while the GPS and odometer velocities were 5.9 and 5.6 ms^{-1} respectively. This is compared to the measured range and velocity of 36 m and 5.9 ms^{-1} respectively.

Parameter	Value
GPS Average Velocity (ms^{-1})	5.9
GPS Average Velocity (kmh^{-1})	21.1
GPS measurements	13
Odometer Velocity (kmh^{-1})	20
Odometer Velocity (ms^{-1})	5.6
Range Bin (m)	100
True Range (m)	109

Table 8.4: Showing the true and recorded parameters of the range Doppler test with a target at a range of 100 m and measured velocity 5.90 ms^{-1} towards the testbed

8.3.3 Discussion

The first range Doppler test, shown in Figure 8.6 results in the expected range Doppler measurement. The range Doppler plot measurement of 7.4 ms^{-1} is similar to the respective GPS and odometer measurements of 7.2 ms^{-1} and 6.9 ms^{-1}. This therefore validates the Doppler measurement. This Figure has been normalised with maximum response occurring in the range Doppler bin of the target. The true range of 30 m matches this range bin of 36 m. One may also see additional responses around the $\pm 3\,ms^{-1}$, 0 m. These are attributed to the incomplete removal of the feed-through response (also seen in the static range test) while using the pulse cancellation processing technique.

The second range Doppler test shown if Figure 8.7 has an additional validation mechanism as it was simulated during the validation of the Radar Processing Chain. This is shown in Figure 6.1 with the simulated target having a respective range and velocity of 100 m and 6.7 ms^{-1}. Comparing these two Figures one may see they are similar and further validate the correct operation of the real world operation of the RadCom system. A notable difference between the two is the absence of feed-through in the simulated test versus the real world test. This can be attributed to the random noise power that is introduced in the real world tests.

Beyond the comparison of the real and simulated scenario one may also compare the calculated and recorded target parameters. Comparing the GPS and range measurements one may see that they agree with one another with the calculated GPS and odometer velocities respectively being 5.9, 5.9, 5.6 ms^{-1}. Furthermore, the true range of 100 m and the range bin measurement of 109 m agree.

Chapter 9

Conclusions and Recommendations

> 'In soloing – as in other activities – it is far easier to start something than it is to finish it'
>
> — *Amelia Earhart*

9.1 Conclusion

In the context of the design and demonstration of a RadCom system conclusions will be drawn. This requires a review of each sub-system while considering the corresponding objectives and requirements. Therefore each processing chain, the hardware testbed and system integration test results will be reviewed.

The first objective of this investigation was the generalisation of the DAB standards physical signal for use in RadCom applications. The adjusted DAB mode structure provides a method to design this signal through the alteration of its time and frequency domain parameters. Furthermore, it allows for the quantification of both radar and communications performance using parameters such as range resolution and bit rates. This sub-system component therefore satisfies the requirement for the RadCom signal to have customizable radar and communications performance.

The signal generation chain, using the RadCom DAB mode, provides the system with two specific functionalities. The first is the ability to generate an OFDM signal while the second introduces the ability to encode bitstreams onto OFDM wavefroms using DQPSK. This allows the system to encode bitstreams onto a waveform and therefore use the RadCom waveform for communications applications. This successfully addresses the bitstream encoding requirement and investigation objective of developing a RadCom signal.

An additional objective of this investigation was to refactor a previously developed DAB passive radar processing chain for generalised use in offline RadCom applications. This investigation demonstrated the altered chains ability to use the DAB mode structure to both demodulate and decode DAB based RadCom waveforms into the encoded bitstreams. The communications processing chain therefore successfully met this objective as set out by this investigation requiring demodulation and decoding functionality.

Radar functionality was also required of the RadCom system. This was successfully demonstrated using the developed radar processing chain through the use of both simulated and recorded integration test

data. This was achieved through the development of the additional pulse cancellation and clutter map subtraction techniques. This therefore fulfilled the radar functionality requirement and met the object of developing a processing chain able to generate range Doppler maps for generalised RadCom applications.

The hardware testbed was developed to perform system integration tests. This sub-system successfully demonstrated its ability to transmit and receive echos in both the controlled lab environment and during the system integration tests. Furthermore, through the post-processing of this data, bitstreams were successfully decoded and target ranges and velocities correctly determined. This subsystem therefore contributed to the final objective of demonstrating a functional RadCom system.

These subsystems, when cascaded, complete the design and demonstration of the RadCom system. They provide the ability to generate and encode bitstreams onto OFDM waveforms, thereby forming RadCom signals. These waveforms were also demonstrated for use in both radar and communications applications. This investigation therefore set out and met all it objectives.

9.2 Recommendations

This investigation was limited to the basic design and demonstration of a RadCom system. This leaves space for further testing and development of system performance and system functionality. Therefore future work may address the following aspects of the designed RadCom system that include:

- The refactoring of signal generation chain to implement frequency domain signal generation thereby increasing generation speeds and moving the system closer to online processing capabilities
- The refactoring of the radar processing chain to frequency domain processing thereby increasing processing speeds additionally bringing the system closer to online processing capabilities
- The use of a different radar platform to allow for the simplification of hardware configuration, reduction in feed-through and improvement of timing performance
- The simultaneous demonstration radar and communications functionality in a single system integration test.
- The development of a signal remodulation chain to allow for communal radar applications
- The robust mapping of system performance as a function of DAB mode parameters

Bibliography

[1] C. Tilbury, "Dab processing chain for passive radar applications," University of Cape Town, Electrical Engineering, Tech. Rep., 11 2020.

[2] M. A. Richards, J. Scheer, W. A. Holm, and W. L. Melvin, "Principles of modern radar," 2010.

[3] "Ieee standard for radar definitions," *IEEE Std 686-2017 (Revision of IEEE Std 686-2008)*, pp. 1–54, 2017.

[4] H. Kuschel and D. O'Hagan, "Passive radar from history to future," in *11th International Radar Symposium*, 2010, pp. 1–4.

[5] D. Koks, "How to create and manipulate radar range-doppler plots," Defence science and technology organisation Edinburgh (Australia), Tech. Rep., 2014.

[6] G. Turin, "An introduction to matched filters," *IRE transactions on Information theory*, vol. 6, no. 3, pp. 311–329, 1960.

[7] F. Le Chevalier, O. Krasnov, F. Deudon, and S. Bidon, "Clutter suppression for moving targets detection with wideband radar," 08 2011.

[8] S. B. Weinstein, "The history of orthogonal frequency-division multiplexing [history of communications]," *IEEE Communications Magazine*, vol. 47, no. 11, pp. 26–35, 2009.

[9] "Digital phase modulation: Bpsk, qpsk, dqpsk: Radio frequency modulation: Electronics textbook." [Online]. Available: https://www.allaboutcircuits.com/textbook/radio-frequency-analysis-design/radio-frequency-modulation/digital-phase-modulation-bpsk-qpsk-dqpsk/

[10] N. Levanon and E. Mozeson, *Radar signals*. John Wiley & Sons, 2004.

[11] EN ETSI, "300 401 Ver. 1.4.1: Radio Broadcasting Systems," *Digital Audio Broadcasting (DAB) to mobile, portable and fixed receivers*, Jan. 2006.

[12] A. Mishra, "Pre-study on dual-purpose telecommunication and radar system."

[13] S. Quan, W. Qian, J. Guq, and V. Zhang, "Radar-communication integration: An overview," in *The 7th IEEE/International Conference on Advanced Infocomm Technology*, 2014, pp. 98–103.

[14] S. Dwivedi, A. N. Barreto, P. Sen, and G. Fettweis, "Target detection in joint frequency modulated continuous wave (fmcw) radar-communication system," in *2019 16th International Symposium on Wireless Communication Systems (ISWCS)*, 2019, pp. 277–282.

[15] M. Fuhr, M. Braun, C. Sturmz, L. Reichardtz, and F. K. Jondral, "An sdr-based experimental setup for ofdm-based radar," in *Proceedings of the 7th Karlsruhe Workshop on Software Radio*, 2012, p. 176.

[16] N. B. Truong, Y.-J. Suh, and C. Yu, "Latency analysis in gnu radio/usrp-based software radio platforms," in *IEEE Military Communications Conference*. IEEE, 2013, pp. 305–310.

[17] S. Paine, S. Schonken, D. O'Hagan, and C. Schupbach, "Comparison of different range-doppler processing techniques for ofdm based dvb-t2 passive radar," *UNPUBLISHED*.

[18] M. Brooker, "The design and implementation of a simulator for multistatic radar systems," Ph.D. dissertation, 2008.

[19] *USRP Hardware Driver and USRP Manual*, Ettus Research, 1 2021, version: 4.1.0.0-231-g5f5bb7921.

Appendix A

Ethics Approval

Application for Approval of Ethics in Research (EiR) Projects
Faculty of Engineering and the Built Environment, University of Cape Town

ETHICS APPLICATION FORM

Please Note:
Any person planning to undertake research in the Faculty of Engineering and the Built Environment (EBE) at the University of Cape Town is required to complete this form **before** collecting or analysing data. The objective of submitting this application *prior* to embarking on research is to ensure that the highest ethical standards in research, conducted under the auspices of the EBE Faculty, are met. Please ensure that you have read, and understood the **EBE Ethics in Research Handbook** (available from the UCT EBE, Research Ethics website) prior to completing this application form: http://www.ebe.uct.ac.za/ebe/research/ethics1

APPLICANT'S DETAILS		
Name of principal researcher, student or external applicant		Grant Norrie
Department		Electrical Engineering
Preferred email address of applicant:		NRRGRA002@myuct.ac.za
If Student	Your Degree: e.g., MSc, PhD, etc.	MSc
	Credit Value of Research: e.g., 60/120/180/360 etc.	120
	Name of Supervisor (if supervised):	Stephen Paine
If this is a researchcontract, indicate the source of funding/sponsorship		N/A
Project Title		A demonstration of a DAB based RadCom system

I hereby undertake to carry out my research in such a way that:

- there is no apparent legal objection to the nature or the method of research; and
- the research will not compromise staff or students or the other responsibilities of the University;
- the stated objective will be achieved, and the findings will have a high degree of validity;
- limitations and alternative interpretations will be considered;
- the findings could be subject to peer review and publicly available; and
- I will comply with the conventions of copyright and avoid any practice that would constitute plagiarism.

APPLICATION BY	Full name	Signature	Date
Principal Researcher/ Student/External applicant	Grant Norrie		2021/04/23
SUPPORTED BY	Full name	Signature	Date
Supervisor (where applicable)	Stephen Paine		26/04/2021

APPROVED BY	Full name	Signature	Date
HOD (or delegated nominee) Final authority for all applicants who have answered NO to all questions in Section 1; and for all Undergraduate research (Including Honours).	Amit Mishra	Amit	23-6-21
Chair: Faculty EIR Committee For applicants other than undergraduate students who have answered YES to any of the questions in Section 1.			

Page **1** of **1**

Appendix B

Matched Filter Derivation

The derivation of the matched filter begins with the assumption that one has received a waveform $x(t)$. This signal may contain either white noise ,$n(t)$ or white noise and a signal $s(t)$. Notably, white noise has a power density $\frac{N_0}{2}$. The total noise power at the output of the filter $H(j2\pi f)$ is defined as follows: $\frac{N_0}{2}\int_{-\inf}^{\inf}\left|H(j2\pi f)\right|^2 df$. This is the summation of the power density at the output of the filter.

One may observe that the input signal spectrum may be described as $S(j2\pi f)$. The output of the filter with the same transfer function $H(j2\pi f)$ results in a spectrum described as $S(j2\pi f)H(j2\pi f)$. The inverse Fourier transform of this output spectrum is defined as $y(t) = \int_{-\inf}^{\inf} S(j2\pi f)H(j2\pi f)e^{2\pi ft}df$.

The SNR at the output of the filter is the ratio of the output signal power to the output noise power. This can be restated as the ratio of the square of the time domain signal $\int_{-\inf}^{\inf} S(j2\pi f)H(j2\pi f)e^{2\pi ft}df$ and the frequency noise power.

$$SNR = \frac{2(\int_{-\inf}^{\inf} S(j2\pi f)H(j2\pi f)e^{2\pi ft}df)^2}{N_0\int_{-\inf}^{\inf}\left|H(j2\pi f)\right|^2 df\}}$$

If one considers $H(j2\pi f)$ as $f(x)$ and $S(j2\pi f)e^{2\pi ft}$ as $g(x)$ and then uses the Schwartz inequality described as follows:

$$\left|\int f(x)g(x)dx\right|^2 \leq \int\left|f(x)\right|^2 dx\int\left|g(x)\right|^2 dx$$

A substitution results in $SNR < \frac{2}{N_0}\int_{\inf}^{inf}\left|S(j2\pi f)\right|^2 df$. Noticing that $\left|S(j2\pi f)\right|^2$ is the energy density spectrum one may therefore recognize that the integral of this term is the total energy E in $s(t)$. This results in the SNR being described as follows: $SNR < \frac{N_0E}{2}$.

By inspection it may be observed that the Schwartz inequality holds when $H(j2\pi f)$ is equal to $kS^*(j2\pi f)e^{-j2\pi ft}$. Therefore to maximise the SNR, the filter should be matched to $s(t)$.

Appendix C

Hardware Configuration

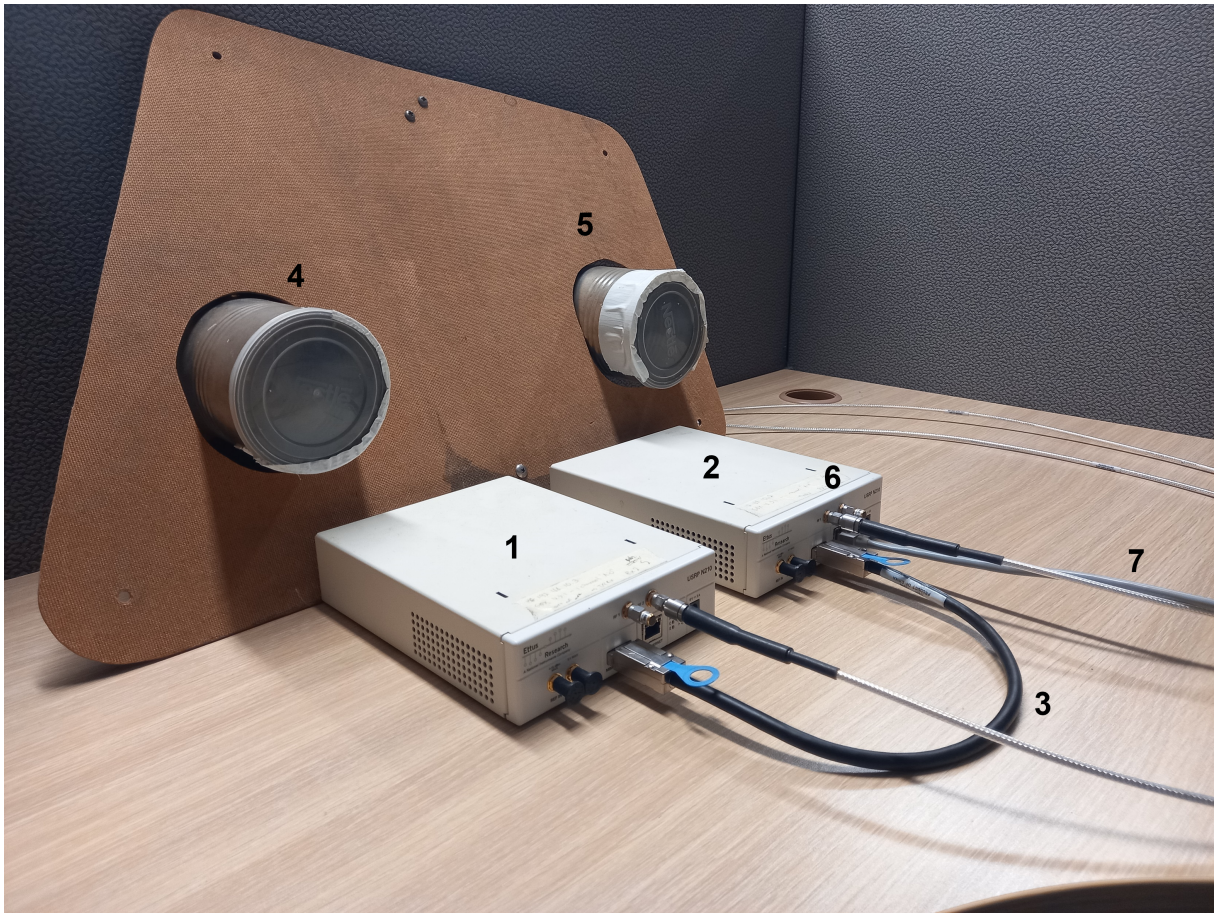

1. Ettus B acting only as a receiver
2. Ettus A acting as both a receiver and transmitter
3. MIMO cable alloing for communcations and synchronisation between devices
4. Transmitting antenna
5. Receiving antenna
6. 50 Ohm terminated reference
7. Ethernet to host